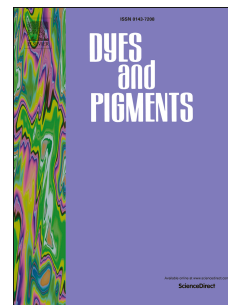


# Journal Pre-proof

$\beta$ -Maleimide substituted *meso*-arylporphyrins: Synthesis, transformations, physico-chemical and antitumor properties

Valentina A. Ol'shevskaya, Viktoriya M. Alpatova, Alexandra S. Radchenko, Alla A. Ramonova, Albina S. Petrova, Victor V. Tatarskiy, Andrei V. Zaitsev, Elena G. Kononova, Nikolay S. Ikonnikov, Alexey A. Kostyukov, Anton E. Egorov, Mikhail M. Moisenovich, Vladimir A. Kuzmin, Natalya A. Bragina, Alexander A. Shtil



PII: S0143-7208(19)31290-2

DOI: <https://doi.org/10.1016/j.dyepig.2019.107760>

Reference: DYPI 107760

To appear in: *Dyes and Pigments*

Received Date: 4 June 2019

Revised Date: 22 July 2019

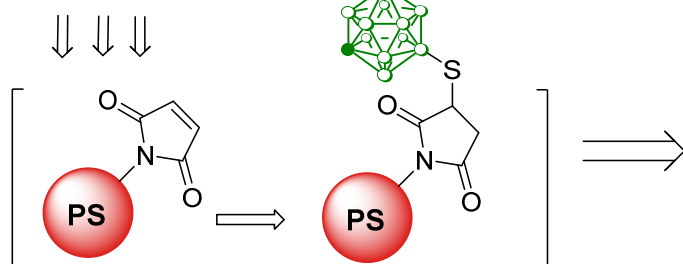
Accepted Date: 28 July 2019

Please cite this article as: Ol'shevskaya VA, Alpatova VM, Radchenko AS, Ramonova AA, Petrova AS, Tatarskiy VV, Zaitsev AV, Kononova EG, Ikonnikov NS, Kostyukov AA, Egorov AE, Moisenovich MM, Kuzmin VA, Bragina NA, Shtil AA,  $\beta$ -Maleimide substituted *meso*-arylporphyrins: Synthesis, transformations, physico-chemical and antitumor properties, *Dyes and Pigments* (2019), doi: <https://doi.org/10.1016/j.dyepig.2019.107760>.

This is a PDF file of an article that has undergone enhancements after acceptance, such as the addition of a cover page and metadata, and formatting for readability, but it is not yet the definitive version of record. This version will undergo additional copyediting, typesetting and review before it is published in its final form, but we are providing this version to give early visibility of the article. Please note that, during the production process, errors may be discovered which could affect the content, and all legal disclaimers that apply to the journal pertain.

© 2019 Published by Elsevier Ltd.

Synthesis



Study of

Quantum yields of:  
- fluorescence  
- singlet oxygen  
Localization  
 $O_2$  generation  
Photodamage  
Cell death

Journal Pre-proof

**$\beta$ -Maleimide substituted *meso*-arylporphyrins: Synthesis, transformations,  
physico-chemical and antitumor properties**

Valentina A. Ol'shevskaya<sup>a</sup>, Viktoriya M. Alpatova<sup>a,b</sup>, Alexandra S. Radchenko<sup>c</sup>, Alla A. Ramonova<sup>d</sup>, Albina S. Petrova<sup>e</sup>, Victor V. Tatarskiy<sup>f,g,h</sup>, Andrei V. Zaitsev<sup>a</sup>, Elena G. Kononova<sup>a</sup>, Nikolay S. Ikonnikov<sup>a</sup>, Alexey A. Kostyukov<sup>c</sup>, Anton E. Egorov<sup>c</sup>, Mikhail M. Moisenovich<sup>d</sup>, Vladimir A. Kuzmin<sup>c</sup>, Natalya A. Bragina<sup>b</sup>, Alexander A. Shtil<sup>f,g</sup>

<sup>a</sup>*A.N.Nesmeyanov Institute of Organoelement Compounds, Russian Academy of Sciences, 119991 Moscow, Russian Federation*

<sup>b</sup>*MIREA - Russian Technological University, M.V. Lomonosov Institute of Fine Chemical Technologies, 119571 Moscow, Russian Federation*

<sup>c</sup>*Emanuel Institute of Biochemical Physics, Russian Academy of Sciences, 119334 Moscow, Russian Federation*

<sup>d</sup>*Department of Biology, Moscow State University, 119991 Moscow, Russian Federation*

<sup>e</sup>*RUDN University, 117198 Moscow, Russian Federation*

<sup>f</sup>*Blokhin National Medical Research Center of Oncology, 115478 Moscow, Russian Federation*

<sup>g</sup>*Institute of Gene Biology, Russian Academy of Sciences, 119334 Moscow, Russian Federation*

<sup>h</sup>*National University of Science and Technology "MISIS", 119991 Moscow, Russian Federation*

**Highlights**

1. A panel of new  $\beta$ -maleimide-substituted *meso*-arylporphyrins was synthesized.
2. Reactivity of porphyrin maleimides towards S-nucleophiles was studied.
3. Flash photolysis showed the ability of new compounds to generate ROS.
4. Complexes with albumin were determined for maleimide and succinimide porphyrins.
5. Selected compounds induced rapid photonecrosis in colon carcinoma cells.

**Abstract**

The maleimide moiety is widely used in drug design. To explore the properties of maleimide containing photosensitizers we obtained a series of new  $\beta$ -maleimide functionalized *meso*-arylporphyrins through acylation of  $\beta$ -amino group in porphyrins with maleic anhydride followed by condensation of maleic acid monoamides. The selective reactivity of porphyrin maleimides toward thiols was demonstrated using mercaptocarboranes and cysteine. New derivatives retained the ability of tetrapyrrolic macrocyclic compounds to absorb light in visible spectral region and to generate triplet states and reactive oxygen species upon photoactivation. Importantly, illumination of cells loaded with a cell permeable 2-{3-[(*o*-carboran-1'-yl)thio]pyrrolidine-2,5-dione-1-yl}-5,10,15,20-tetraphenylporphyrin triggered rapid (within the initial minutes) generation of superoxide anion radical concomitantly with a decrease of mitochondrial membrane potential and then the loss of the plasma membrane integrity and cell death. Thus, the maleimide-substituted porphyrins represent a new chemotype of polyfunctionalized compounds for an in-depth investigation as photosensitizers in cancer and beyond.

**Key words:** porphyrins, maleimides, carboranes, fluorescence, singlet oxygen, phototoxicity.

## 1. Introduction

During the last few decades porphyrins and their analogues have attracted significant interest due to their exploration in various fields such as dyes for photovoltaic solar cells [1,2], chemical sensors [3,4], molecular electronic components [5], non-linear optic materials [6,7], catalysts [8], nanomaterials [9,10], and as photosensitizers in photodynamic therapy (PDT) of cancer and other diseases [11-14]. Progress in antitumor PDT is associated with advances in the design of non-toxic efficacious photosensitizers capable of providing the maximum therapeutic effect while sparing the surrounding non-malignant tissues.

Among the tetrapyrrolic macrocyclic systems, the tetraarylporphyrins are of great importance as a source of new photosensitizers due to their availability and diversity of structurally functionalized, highly potent derivatives. The aryl substituted porphyrins are the synthetic analogues of natural porphyrins and chlorins. Derivatives of arylporphyrins and their metal complexes are of practical use in the creation of a variety of anticancer drugs, including the agents for PDT. Furthermore, porphyrins are basic compounds for the preparation of chlorins and bacteriochlorins that are used for a deeper tumor photodamage due to a stronger absorption in the visible and near-infrared region [15]. Therefore, the design of new porphyrins with particular structural fragments is of considerable importance since it gives to the porphyrin system new specific properties and extends the areas of application.

To improve PDT efficiency of photosensitizers a number of approaches have been developed to conjugate the photosensitizer with another structural moiety using a covalent bond [16-20]. A considerable attention has been paid to the conjugates of porphyrins with proteins and peptides [21]. The advantage of such conjugates is that they make it possible to overcome the low water solubility of tetrapyrrolic compounds and reduce their aggregation. Selective conjugation of porphyrins to peptides is based on thiol-targeting reactions. Modification of porphyrins with functionalities capable of reacting with cysteine thiol groups is a useful strategy for regioselective delivery of the photosensitizer to target cells [17].

Bioconjugation via the maleimide moiety has emerged as an excellent approach for a variety of applications, in particular, therapeutic antibody-drug conjugates [22-25], structural investigations of complex cellular compartments [26] and design of targeted delivery systems [27]. The maleimide-substituted porphyrin derivatives are of significant interest. The maleimide units represent the substrates for thiol Michael addition reactions [28]. The presence of two *cis*-oriented carbonyl groups in the maleimide structure makes its electron-deficient double bond extremely reactive towards cysteine thiol groups of proteins at physiological pH, with the formation of relatively stable succinimidyl thioether bonds. Commonly the Michael addition process provides a high selectivity, high yields of products, good reaction rates, insensitivity to

oxygen or water, and a compatibility with various thiol structures. Moreover, the thiol group displays a higher nucleophilicity compared to the hydroxyl and amino groups at physiological pH, thereby reacting preferentially with the double bond of maleimide. A series of porphyrin-maleimide derivatives have been used for the preparation of efficient cell penetrating peptide-porphyrin conjugates which are suitable for use in targeted PDT. The regiospecific bioconjugation of maleimide porphyrins to the peptide backbone can improve the selectivity and broaden the spectra of therapeutic applications [17, 29].

In this study we describe a new panel of  $\beta$ -maleimide-substituted porphyrins. A variety of synthetic approaches have been developed to synthesize  $\beta$ -substituted porphyrins [30-34]. The  $\beta$ -substituents can shift the electronic absorption bands to the near infrared region; these systems may find use in PDT [33] and elsewhere [35]. There is available information on the improved antitumor properties of tetrapyrrole photosensitizers containing boron polyhedra in PDT as compared with their non-boronated analogs [34,36,37]. Considering our long-term interest in boronated porphyrins as antitumor agents we report the synthesis, characterization of  $\beta$ -maleimide-substituted porphyrins and their reactivity towards S-nucleophiles including mercaptocarboranes. Among the series of new derivatives, the boron containing 2-{3-[(*o*-carboran-1'-yl)thio]pyrrolidine-2,5-dione-1-yl}-5,10,15,20-tetraphenylporphyrin demonstrated good properties in vitro and in cell based test systems, suggesting its potential as an antitumor photosensitizer.

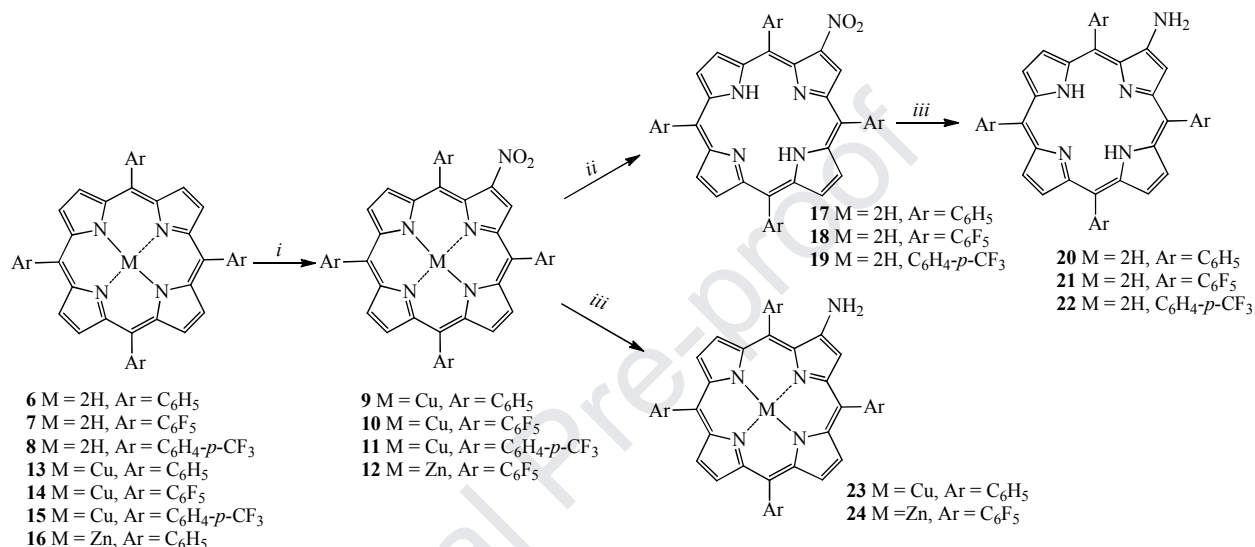
## 2. Results and Discussion

### 2.1. Synthesis

$\beta$ -Maleimide-substituted porphyrins **1-5** were synthesized using *meso*-arylporphyrins **6-8** [38,39] as starting compounds. For their preparation we exploited the availability of  $\beta$ -nitro-substituted porphyrins which can be easily synthesized in a good yield by the regioselective nitration of corresponding porphyrin copper complexes with copper(II) nitrate [40]. We tried to obtain 2-nitro-derivatives of porphyrins **6-8** on the basis of metal-free derivatives, using an excess of copper nitrate in CH<sub>2</sub>Cl<sub>2</sub>/acetic acid/acetic anhydride mixture, suggesting the *in situ* formation of a copper complexes followed by simultaneous nitration under reflux. As a result for all porphyrins the desired products were obtained but the yields of copper(II) 2-nitroporphyrinates were dependent on the *meso*-substituent in the porphyrin macrocycle. In the case of porphyrins **6, 8** the 2-nitro-substituted copper complexes were obtained in ~ 45-50% yields while for pentafluorophenyl substituted porphyrin **7** the yield of desired product was almost quantitative (97%). In this regard, copper(II) 2-nitroporphyrinates **9-11** were obtained in a good yield (81-98%) by nitration of the corresponding porphyrin copper complexes with copper(II) nitrate at room temperature in CH<sub>2</sub>Cl<sub>2</sub>/acetic acid/acetic anhydride mixture.

Demetallation of 2-nitroporphyrinates **9-11** was readily proceeded according to [41] in  $\text{H}_2\text{SO}_4/\text{CF}_3\text{COOH}$  (1:1) system affording the free base 2-nitroporphyrins **17-19** in 83-90% yield.

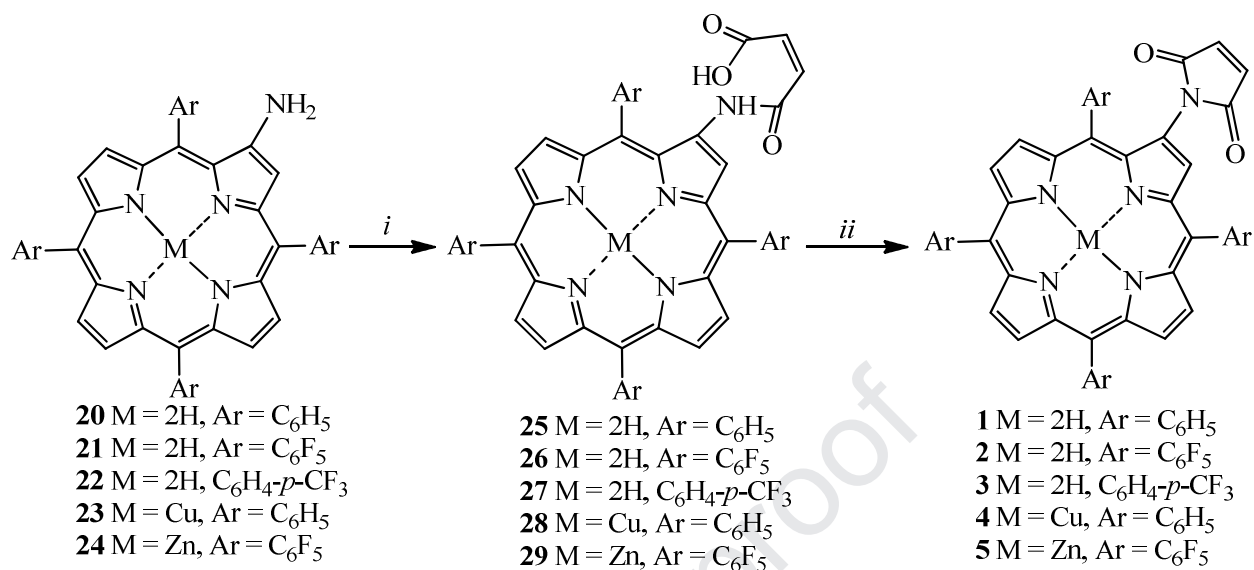
The derivatives **17-19** are considered the key compounds for the synthesis of 2-aminoporphyrins. The most efficient protocols to transform  $\text{NO}_2$  group into the amino group are based on reduction with  $\text{SnCl}_2\text{-HCl}$  or  $\text{NaBH}_4\text{-Pd/C}$  [42, 43]. All 2-nitro-substituted porphyrins **9, 12, 17-19** were smoothly reduced with  $\text{NaBH}_4$  and  $\text{Pd/C}$  [43] in  $\text{CH}_2\text{Cl}_2$  -  $\text{MeOH}$  to afford the expected aminoporphyrins **20-24** in 71-79% yields as starting compounds for maleimide cycle formation.



Scheme 1. Synthesis of 2-aminotetraarylporphyrins (i)  $\text{Cu}(\text{NO}_3)_2 \cdot 3\text{H}_2\text{O}$ ,  $\text{CH}_2\text{Cl}_2$ ,  $\text{AcOH}$ ,  $\text{Ac}_2\text{O}$ ; (ii)  $\text{CF}_3\text{COOH}/\text{H}_2\text{SO}_4$  (1:1), r.t.; (iii)  $\text{NaBH}_4$ ,  $\text{Pd/C}$  in  $\text{CH}_2\text{Cl}_2$  -  $\text{MeOH}$ , Ar, r.t.

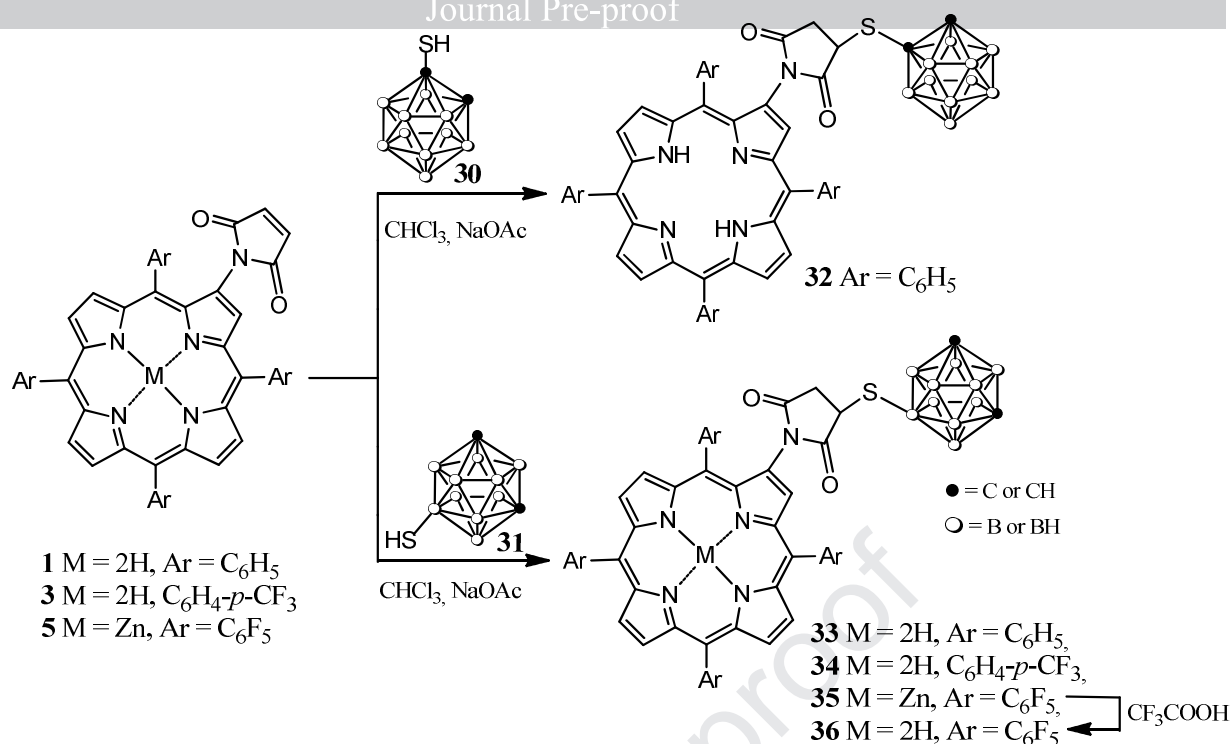
The synthetic strategy to obtain new  $\beta$ -pyrrole maleimide derivatives involved acylation of  $\beta$ -amino groups with maleic anhydride (Scheme 2). These reactions produced porphyrin conjugates **25-29** containing the substituted maleic acid monoamides. Acylation of porphyrins **20, 21, 23** with maleic anhydride was carried out in  $\text{AcOH}$  for 50h at room temperature; the corresponding monoamides were obtained in 20-82 % yields. These results demonstrated that the product yields are dependent on the *meso*-substituents in the porphyrin macrocycle; the lowest yield was obtained for **21** that contains pentafluorophenyl substituents. To increase the yield of maleic acid monoamide for **21**, we used the reaction of its zinc complex **24** with maleic anhydride in  $\text{MeCN}$  under reflux. In this case the yield of the target product was 69% after column chromatography on  $\text{SiO}_2$ . The same reaction conditions ( $\text{MeCN}$ , reflux) were used for acylation of porphyrin **22** with maleic anhydride; porphyrin **27** was obtained in a good yield. The use of  $\text{MeCN}$  instead of acetic acid for acylation is more convenient since the reaction time is significantly reduced. However,  $\text{MeCN}$  as a solvent is not suitable for acylation of **20, 22, 23** since these porphyrins are insoluble in  $\text{MeCN}$ .

The subsequent thermal cyclization of porphyrin maleamic acids **25-29** was performed at 110 °C in Ac<sub>2</sub>O in the presence of NaOAc producing the corresponding 2-maleimide-substituted porphyrins **1-5** in 61-77% yields.

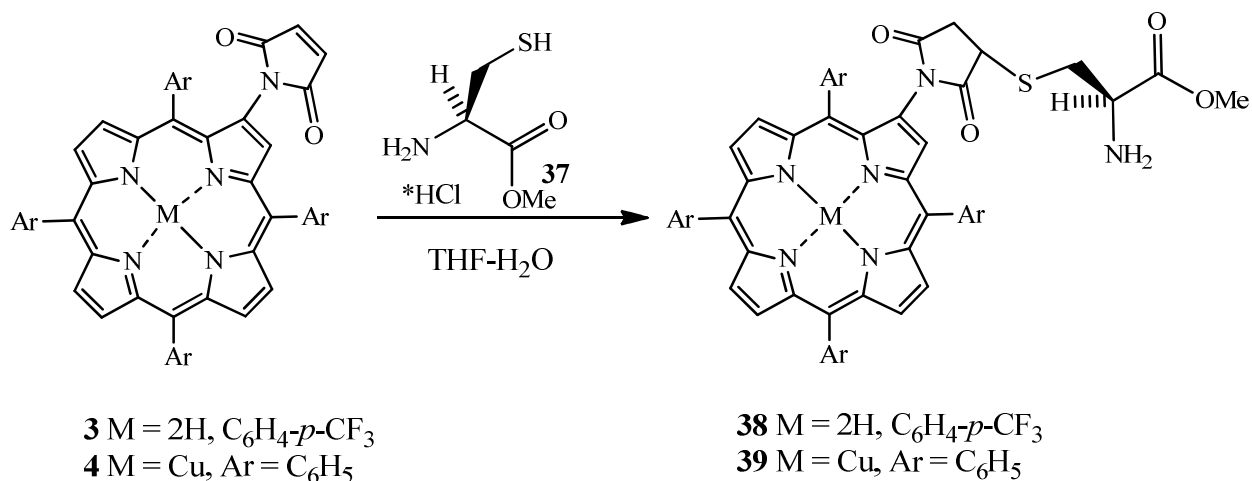


Scheme 2. Synthesis of 2-maleimide-substituted porphyrins: (i) for **20**, **21**, **23**: maleic anhydride, HOAc, r.t.; for **22**, **24**: maleic anhydride, MeCN, reflux; (ii) NaOAc, Ac<sub>2</sub>O, 110 °C.

Substituted maleimides are a unique class of compounds used in chemical and biological studies due to the activated double bond suitable for chemical transformations of different types. Substituted maleimides can behave as dipolarophiles in the reaction of 1,3-dipolar cycloaddition or as dienophiles in the Diels–Alder reaction, as well as acceptors in the Michael reaction with O-, N- and S-nucleophiles. Since we were interested in the reactivity of prepared maleimides with S-nucleophiles, we studied the Michael addition reaction of 1-mercapto-*o*-carborane **30** [44] and 9-mercapto-*m*-carborane **31** [45] with porphyrins **1**, **3** and **5**.

Scheme 3. Synthesis of carborane-substituted porphyrins **32-36**.

Functionalization of the maleimide double bond in **1**, **3**, **5** with carboranes **30**, **31** was performed in boiling CHCl<sub>3</sub> in the presence of NaOAc affording the corresponding carborane succinimidyl thioethers **32-35** in a good yield. Free base porphyrin **36** was obtained by the removal of Zn from coordination sphere of porphyrin **35** under the action of trifluoroacetic acid (Scheme 3). Since the maleimide is by far the most suitable functional group to be coupled to a cysteine residue because the coupling reaction is highly specific and efficient [28], we demonstrated the ability of maleimides **3**, **4** to form conjugates with cysteine **37**. Reactions were carried out in a THF-H<sub>2</sub>O system at room temperature in argon to produce **38**, **39** in a quantitative yield (Scheme 4). Of note, it is necessary to remove oxygen from solvents otherwise the disulfide bond in the formed cystine would prevent the reaction with maleimides.

Scheme 4. Synthesis of cysteine-substituted porphyrins **38**, **39**.

Compounds **38**, **39** contain functional amino and ester groups suitable for further functionalization including their use in peptide synthesis. The structures of all newly prepared compounds were identified by IR and  $^1\text{H}$ ,  $^{11}\text{B}$ ,  $^{11}\text{B}\{^1\text{H}\}$ ,  $^{19}\text{F}$  NMR spectroscopies and mass spectrometry. (See *Experimental and Supporting Information* Figure S1-13 for details).

## 2.2. Physico-chemical properties

### 2.2.1. UV-visible absorption spectra

The absorption spectra of the new compounds in DMSO solutions are shown in Figure 1A. Spectra were normalized [0; 1] to their respective  $Q_{X10}$  maxima ( $Q_{Y00}$  for **5**). Spectra for **1-3**, **32**, **34** are characteristic of metal free porphyrins [46, 47] showing the intense Soret bands around  $\lambda=420$  nm and four Q-bands of lower intensities at longer wavelengths. For **5** containing  $\text{Zn}^{2+}$ , the spectra showed three Q-bands and the Soret band was slightly red-shifted (4 nm) (Table 1). The major Q-bands for all the compounds were located at  $\lambda=516$  nm with exception of **5** ( $\lambda=554$  nm) and **2** ( $\lambda=508$  nm). Introduction of the pentafluorophenyl group (porphyrin **2**) led to a 7-10 nm blue shift of all the bands.  $\text{Zn}^{2+}$  derivative **5** displayed a 10 nm red shift and less number of Q-bands with significant red-shift relative to the metal free **2**.

### 2.2.2. Fluorescence spectra

The emission spectra of porphyrins **1-3**, **5**, **32**, **34** were normalized to the respective  $Q^*_{X00}$  (**1**, **32**, **3**, **34**) or  $Q^*_{X01}$  (**5**, **2**), the maxima are shown in Figure 1B. All the spectra demonstrated  $Q^*_{X00}$  and  $Q^*_{X01}$  emission bands typical of porphyrins [46, 47] (see Table 1 for the band positions). Trifluoromethyl-substituted porphyrins **3** and **34** showed a 8 nm red shift of  $Q^*_{X00}$  bands relative to the 2-maleimide-substituted porphyrin **1**. No correlation was found between the substituent in porphyrins **2**, **5**, **32**, **34** and the red shift of  $Q^*_{X00}$  bands. Similar to the absorption spectra, all the bands in the fluorescence spectra of the pentafluorophenyl substituted porphyrin **2** are blue-shifted by 13 nm relative to maleimideporphyrin **1**, and the band intensities were inversed. The pentafluorophenyl-substituted porphyrin **5** ( $\text{Zn}^{2+}$  complex) displayed fluorescence bands which values are significantly blue-shifted ( $\lambda=598$  nm and  $\lambda=650$  nm) compared to other zinc containing porphyrins ( $\sim \lambda=650$  nm and  $\lambda=715$  nm) [48,49].

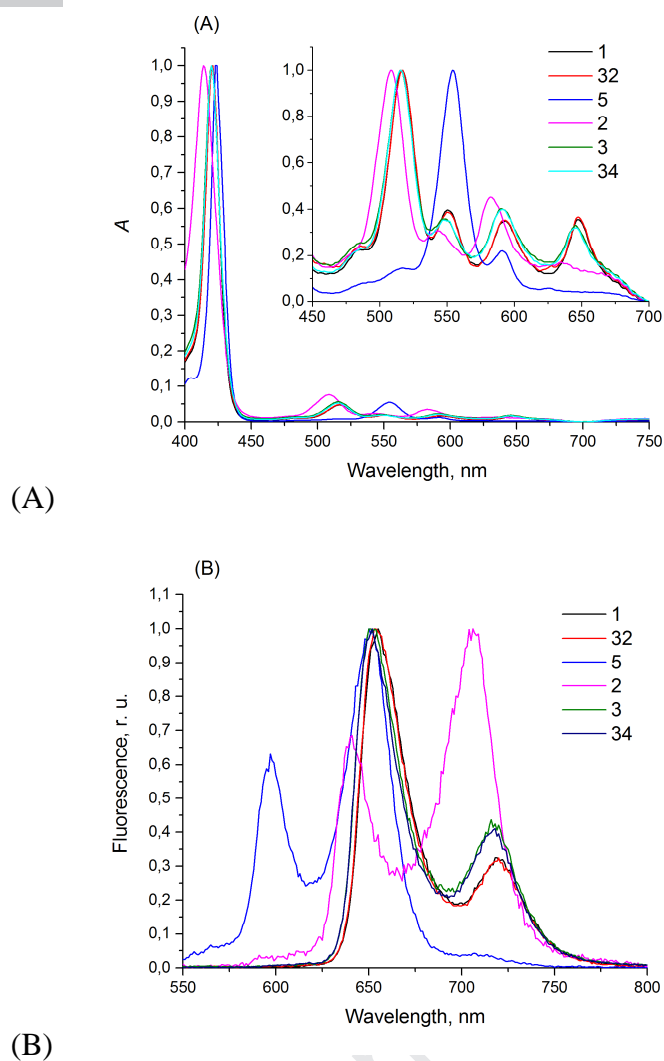


**Figure 1.** Normalized absorption (A) and fluorescence (B) spectra of the porphyrin derivatives and zoomed Q-bands in the 450-700 nm region. See *Experimental* for details.

**Table 1.** UV–visible absorption and fluorescence data in DMSO solution.

Porphyrin	$\lambda_{\max}$ , nm		
	Soret band	Q bands	Emission
<b>1</b>	420	<b>516</b> , 551, 594, 647	<b>653</b> , 718
<b>32</b>	421	<b>516</b> , 550, 593, 648	<b>653</b> , 718
<b>5</b>	424	517, <b>554</b> , 593, -	598, <b>650</b>
<b>2</b>	414	<b>508</b> , 543, 583, 635	640, <b>706</b>
<b>3</b>	420	<b>516</b> , 549, 590, 645	<b>650</b> , 715
<b>34</b>	420	<b>516</b> , 548, 592, 646	<b>650</b> , 715

The most intensive peaks are marked in bold. Standard deviation  $\pm 1$  nm.

## 2.2.3. Fluorescence lifetimes and quantum yields, singlet oxygen quantum yields

Fluorescence lifetimes and quantum yields in DMSO (measured relative to rhodamine 6G) for all tested porphyrin derivatives are summarized in Table 2 and Figure 2. Values of quantum yields of fluorescence varied from 0.04 for **34** to 0.01 for Zn<sup>2+</sup>-containing **5**. The decay curves fit to single-exponential functions with  $\chi^2 < 1.6$  except for **5** that required a two-exponential fit. The short decay time for **5** indicates that Zn<sup>2+</sup> conferred a shorter lifetime of S<sub>1</sub> state [50]. The pentafluorophenyl-substituted **2** had the longest lifetime  $\tau_f = 10.52$  ns and an average quantum yield of fluorescence ( $\sim 0.01$ ). Boronated derivatives had average values  $\tau_f \sim 8-9$  ns and the highest  $\phi_f$  (0.03-0.04). Values of  $\phi_f$  and  $\tau_f$  for Zn<sup>2+</sup> derivative **5** were the lowest in the series corroborating the published data [50].

Fluorescence, being dependent largely on the inner  $\pi$ -electron system of the macrocycle, is unlikely to be affected by periphery substituents that do not distort the macrocycle's planarity. In general, the quantum yields of fluorescence should be  $\sim 0.1$  in the free tetraphenylporphyrin (TPP) and  $\sim 0.04$  for a zinc-TPP in an organic solvent [50-52]. In fact, the obtained values for investigated porphyrins are lower than for TPP. This difference can be explained by influence of the maleimide group on the central macrocyclic  $\pi$  system. However, the ratio of values  $\phi_f$  and  $\tau_f$  of Zn<sup>2+</sup> containing **5** ( $\phi_f = 0.01$ ,  $\tau_f = 1.37$  ns) to its free base analog **2** ( $\phi_f = 0.02$ ,  $\tau_f = 10.52$  ns) are in good agreement with the reference data.

**Table 2.** Fluorescence quantum yields and lifetimes, and quantum yield of singlet oxygen generation in DMSO.

Compound	$\phi_f(\text{DMSO})^{a,c}$	$\tau_f(\text{DMSO}), \text{ns}$	$\phi^1\text{O}_2(\text{DMSO})^b$
<b>1</b>	0.03	$8.20 \pm 0.01$	0.69
<b>32</b>	0.03	$8.39 \pm 0.02$	0.81
<b>5</b>	0.01	$1.37 \pm 0.01$	0.77
<b>2</b>	0.02	$10.52 \pm 0.02$	0.92
<b>3</b>	0.03	$8.73 \pm 0.05$	0.70
<b>34</b>	0.04	$9.08 \pm 0.08$	0.91

<sup>a,b</sup>Reproducibility  $\pm 10\%$ . <sup>c</sup>The optical density was matched for tested compounds and reference at the excitation wavelengths (see *Experimental*).

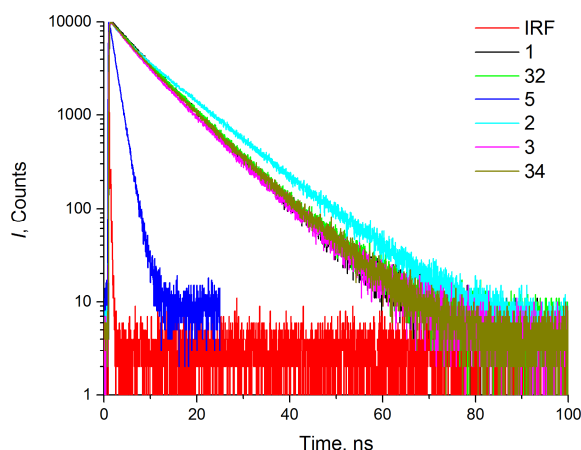


**Figure 2.** Time course of fluorescence decay of porphyrins in DMSO.

#### 2.2.4. Triplet states of new porphyrin derivatives

The flash photolysis was used to investigate the ability of the new compounds to generate ROS upon photoactivation. Excitation by the visible light (400–510 nm or 480–560 nm) in the oxygen free organic solvents (ethanol, propanol-1, DMSO) induced a short-lived triplet state of porphyrins. Differential absorption spectra of the triplet states (see Figure 3 for **32** as an example) showed the absorption bands at 440–510 nm and 540–750 nm and bleaching of S- and Q- bands. Spectra were recorded after a single pulsed photoexcitation (480–560 nm, 80 J). The kinetics decay of the triplet states followed a first-order law  $\Delta A = \Delta A_0 \times \exp(-t/\tau_T)$ , where  $\Delta A$  is the triplet-triplet absorption at a given time,  $\Delta A_0$  is triplet-triplet absorption immediately after light illumination,  $t$  is time. The triplet lifetime is  $\tau_T = 1/k_T$ , where  $k_T$  is the constant of the triplet state kinetics decay. Lifetimes of the triplet states for **1-3**, **5**, **32** and **34** varied insignificantly within a low millisecond range.

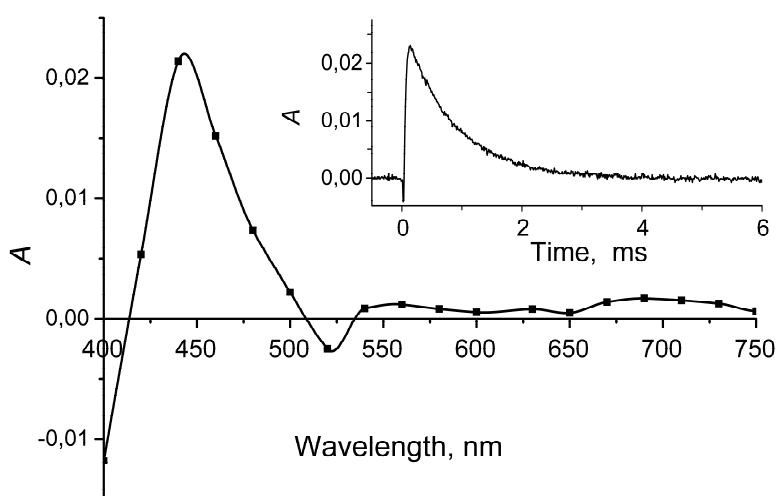


**Figure 3.** Transient triplet-triplet absorption spectrum of **32** (2  $\mu\text{M}$ ) in propanol-1 (200  $\mu\text{s}$  after flash) and the kinetic trace of triplet at 440 nm.

Quenching of the triplet states for **1-3**, **5**, **32** and **34** by oxygen leads to the formation of the singlet oxygen (see Figure S14 for  $^1\text{O}_2$  phosphorescence spectra; rose bengal (RB) is a reference compound). Measurements of quantum yields of the singlet oxygen were carried out at high concentrations of oxygen in solutions; all the porphyrin triplets transferred energy to the singlet oxygen. Quantum yields in the solutions are presented in Table 2. All the new compounds showed a significant quantum yield of the singlet oxygen (0.69-0.92). Thus, the quantum yields of singlet oxygen and the triplet state of porphyrin derivatives were almost coincident, making these compounds perspective as photosensitizers for PDT.

#### 2.2.5. Stable complexes with HSA

We were interested whether **1-3**, **5**, **32**, **34** can form complexes with HSA, a major drug carrier in the body. Figure S15 shows the absorption spectra depending on HSA concentrations (**32** as an example). The equilibrium dissociation constants (calculated by formula 4, see *Experimental*) are shown in Table 3. Compounds **1** and **2** showed the biggest affinity to HSA. Introduction of the carborane or  $\text{CF}_3$  substituents, as well as  $\text{Zn}^{2+}$ , somewhat weakened the ability of drug-albumin complex formation, most probably due to a steric hindrance [53].

**Table 3.** Dissociation constants ( $K_d$ ) of porphyrin-HSA complexes.

Compound	$K_d \times 10^6, \text{M}$
<b>1</b>	$0.83 \pm 0.25$
<b>2</b>	$1.10 \pm 0.34$
<b>3</b>	$2.09 \pm 0.73$
<b>5</b>	$4.14 \pm 1.76$
<b>32</b>	$3.39 \pm 0.96$
<b>34</b>	$1.84 \pm 0.52$

Altogether, testing in several cell free systems demonstrated that our new maleimide-substituted porphyrins largely retained the characteristics suitable for PDT. All tested derivatives fluoresced in the visible spectral region that makes them convenient for detection in the cells. Most importantly, peripheral moieties or metal ion in the coordination sphere of the tetrapyrrolic macrocycle did not seriously alter the ability to generate ROS upon light activation and form stable complexes with albumin. Therefore we set out to investigate these compounds in cell based assays and evaluate their relevance as candidates for antitumor PDT.

### 2.3. Biological properties

#### 2.3.1. Dark and light toxicity

We tested dark cytotoxicity of **1-3**, **5**, **32** and **34** by treating HCT116 human colon carcinoma cell line with each of these compounds (up to 50  $\mu\text{M}$ ) for 72 h followed by an MTT-test. No discernible cell growth inhibition or death was registered (data not shown). Next, we monitored intracellular accumulation of **1-3**, **5**, **32** and **34**. The HCT116 cells were loaded with 5  $\mu\text{M}$  of each compound for 24 h, washed with cold saline and immediately analyzed by flow cytometry. Figure S16 shows the histograms of cell associated fluorescence after excitation at 405 nm and emission at 710 nm and 780 nm. The most pronounced accumulation was detected for **32**.

Next, we evaluated light activated cell death after loading the HCT116 cells with **1-3**, **5**, **32** and **34** (0-50  $\mu\text{M}$  each, 24 h at 37 $^{\circ}\text{C}$ , 5%  $\text{CO}_2$ ) and illumination with a 420 nm laser. Cell viability was assessed by an MTT test 2 h post illumination. Data in Table 4 showed that **32** was the most potent photosensitizer:  $\text{IC}_{50}$  was in a low micromolar range of concentrations. Also, we illuminated cells with a 650 nm laser (Figure 1A; 5  $\text{J}/\text{cm}^2$ ) after the same loading. Only **32** triggered a pronounced death whereas **1-3**, **5** and **34** were inert. At 30  $\text{J}/\text{cm}^2$  compound **5** was slightly active (not shown). Together, based on the appropriate physico-chemical characteristics in cell free systems, the lack of dark cytotoxicity, good cell permeability and a potent phototoxicity, we selected **32** for further experiments as a candidate antitumor photosensitizer.

**Table 4.** Phototoxicity of porphyrins **1-3**, **5**, **32**, **34**.

Compound	$\text{IC}_{50}$ , $\mu\text{M}$
<b>1</b>	13.2
<b>2</b>	32.6
<b>3</b>	>50
<b>5</b>	7.8
<b>32</b>	1.1
<b>34</b>	>50

The HCT116 cells were loaded with 5  $\mu\text{M}$  of each compound for 24 h, washed with saline, illuminated with a 420 nm laser (1.5  $\text{J}/\text{cm}^2$ ) and incubated in a fresh medium supplemented with the MTT reagent for 2 h at 37 $^{\circ}\text{C}$ , 5%  $\text{CO}_2$ .  $\text{IC}_{50}$  values are mean of 3 independent measurements with a <10% error. See *Experimental* for details.

### 2.3.2. Intracellular distribution

Cells were exposed to 5  $\mu\text{M}$  **32** for 24 h at 37 $^{\circ}\text{C}$ , 5%  $\text{CO}_2$  to achieve maximum accumulation (see Figure S16). Figure 4 demonstrates that **32** can be visualized in the cytoplasm of HCT116 cells. No co-localization with lysosomes, mitochondria, endosomes or nuclei was detectable using the respective fluorescent probes. Similar patterns of intracellular localization were observed for **1-3** and **34** (Figure S17) indicating that new maleimideporphyrins and succinimideporphyrins are distributed across the organelle-free cytoplasm.

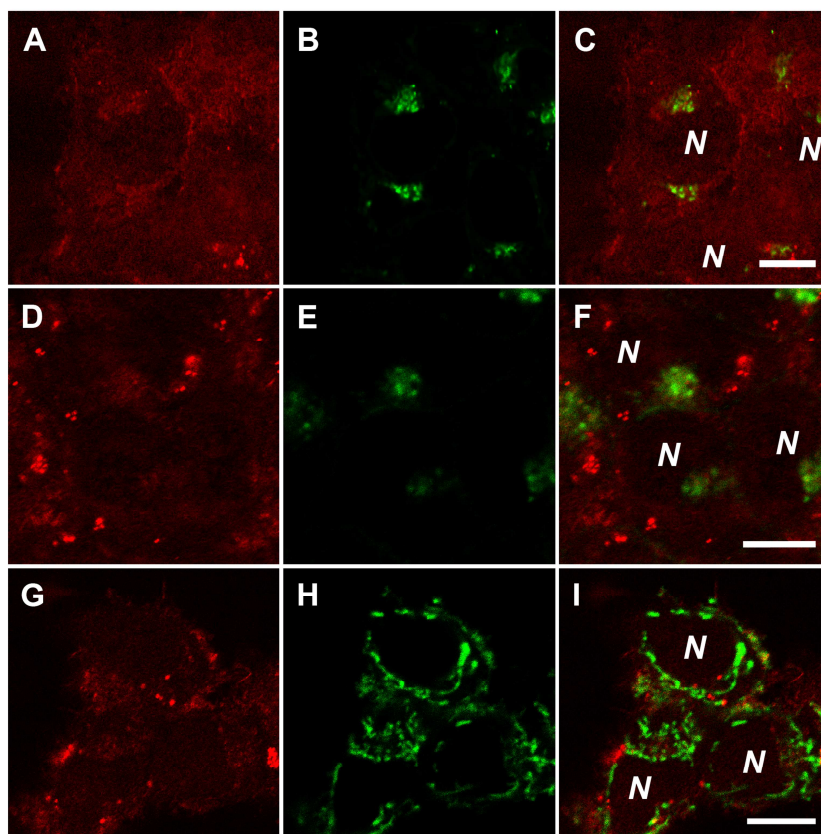


**Figure 4.** Cytoplasmic localization of compound **32** in HCT116 cells.

Cells were exposed to 1  $\mu\text{M}$  **32** for 1 h at 37 $^{\circ}\text{C}$ , 5%  $\text{CO}_2$ , washed and visualized by a confocal laser scanning microscopy. *A, D, G*: autofluorescence of **32**, *B*: LysoTracker Green DND-26, *E*: transferrin-FITC, *H*: MitoTracker Green FM; *C*: merge of *A* and *B*; *F*: merge of *D* and *E*; *I*: merge of *G* and *H*. N: nuclei. Bar, 10  $\mu\text{m}$ .

### 2.3.3. Lethal cell photodamage upon photoactivation of **32**.

To evaluate the perspective of **32** as an antitumor photosensitizer we investigated the events that lead to death of cells loaded with this compound. We were interested whether ROS generation by **32** detectable in a cell free system (Table 2), translates into intracellular free oxygen burst upon illumination of cells loaded with this compound. In so doing we used the MitoSOX Red probe for intracellular visualization of  $\text{O}_2^-$  and the MitoTrackerCMXRos Red

dye sensitive to mitochondrial transmembrane electric potential. As expected, in intact HCT116 cells MitoSOX Red fluorescence was localized largely to mitochondria (Figure 5A-C). However, illumination of cells loaded with **32** led to an instant (by 30 sec) increase of MitoSOX Red fluorescence whereas MitoTrackerCMXRos Red fluorescence decreased (Figure 5D,E). Merged images (Figure 5F) showed that, in illuminated cells, MitoSOX Red fluorescence was no longer attributable to viable (that is, maintaining their membrane potential) mitochondria. To simultaneously monitor mitochondrial damage and cell death, the DNA intercalating agent propidium iodide (PI) was added to the cell culture prior to illumination. PI staining is a hallmark of the loss of plasma membrane integrity [34,54]. The mitochondrial membrane potential dropped dramatically within the initial 1-2 min post illumination (Figure 6A-D). This effect was paralleled by increased cell permeability for PI. As shown in Figure 6E, F, PI alone did not affect the morphology of non-illuminated cells that remained PI-negative over the time of experiment. In contrast, as soon as 5 min post illumination PI entered individual cells; by 10 min the dye was clearly detectable in the nuclei and perinuclear areas (Figure 6G,H). Thus, ROS generation coincident with the drop of the mitochondrial membrane potential preceded the influx of PI into illuminated cells. Together with data in Figure 4, these results indicated that, although **32** lacks a specifically mitochondrial accumulation, the intracellular oxidative burst upon light activation can damage mitochondria and probably other membrane organelles. Most importantly, the plasma membrane permeability for PI indicates a non-repairable cell photodamage.

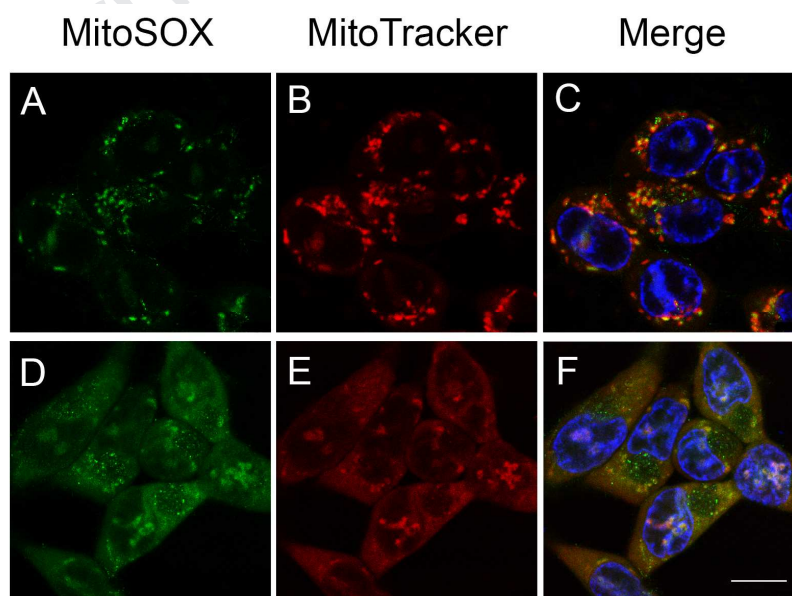


**Figure 5.** Detection of  $O_2^-$  in HCT116 cells.

Cells were loaded with 5  $\mu$ M **32** for 24 h at 37<sup>0</sup>C, 5% CO<sub>2</sub> prior to laser confocal microscopy. A-C: no light; D-F: 30 sec after photoactivation. Shown are intracellular distribution of  $O_2^-$  sensor MitoSOX Red (green; excitation 488/emission 510-600 nm); nuclear dye Hoechst 33342 (blue; excitation 405/emission 415-480 nm); mitochondrial probe MitoTracker Red CMXRos (red; excitation 543/emission 560-620 nm). Bar, 10  $\mu$ m.

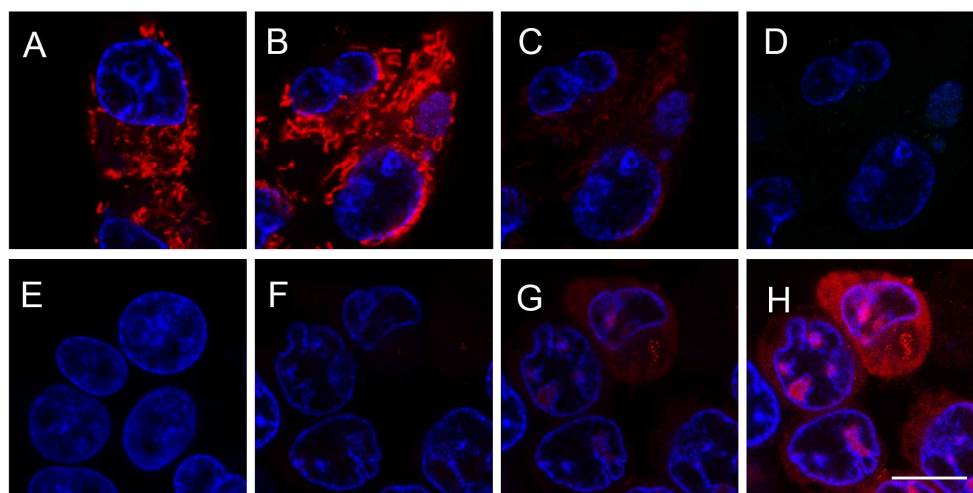


**Figure 6.** Rapid photodamage of HCT116 cells loaded with porphyrin **32**.

*A-D*: cells were loaded with MitoTracker Green FM (1  $\mu$ M) for 30 min in the absence (*A*) or presence of 5  $\mu$ M **32** (*B-D*) followed by washing with saline. *A,B*: no light; *C, D*: 1 min or 2 min, respectively, after illumination with a 405 nm laser. *E-H*: cells were given 10  $\mu$ g/ml PI for 10 min prior to imaging. *E*, no **32**, *F-H*: cells loaded with 5  $\mu$ M **32** and then either left in the dark (*F*) or illuminated with a 405 nm laser and photographed 5 min (*G*) or 10 min (*H*) post illumination. In each image: cells were counterstained with DAPI (blue). Bar, 10  $\mu$ m.

Overall, aiming at conjugation of a biologically active moiety to the known photoactivatable scaffold, we synthesized and characterized a new series of  $\beta$ -functionalized maleimide-substituted *meso*-arylporphyrins. The maleimide units were highly specific for thiols through the Michael addition. New compounds can be used for porphyrin-driven, site-selective modifications of cysteine residues in proteins. Recently these residues have been shown to be important for covalent but reversible binding to and potent inhibition of the enzyme critical for cell division [54; see also 28 for recent review].

Along with the maleimide moiety, our new porphyrin derivatives carried diverse *meso*-aryl substituents including fluorine groups, metal centers ( $\text{Zn}^{2+}$ ,  $\text{Cu}^{2+}$ ) in the coordination sphere of the tetrapyrrolic macrocycle, as well as succinimide units in  $\beta$ -position of macrocycle functionalized with the boron polyhedron (carborane cage) or cysteine. The resulting compounds represented bulky structures decorated with individual chemical groups for a variety of biological functions. Multifunctionality of new compounds re-iterates the suitability of the tetrapyrrolic macrocycle as a versatile core in medicinal chemistry.

Importantly, in aqueous and/or organic solutions the substituents did not alter a major biomedical property of porphyrins, that is, the ability to generate ROS upon light activation. Furthermore, the selected compounds formed stable complexes with the carrier protein albumin in a physiological buffer. Nevertheless, the behavior of individual new derivatives in cell culture

varied. Although all porphyrins tested in cell-based assays were non-toxic in the dark within as long as 72 h, their differential intracellular accumulation and phototoxicity made not each compound therapeutically perspective. Compound 2-{3-[(*o*-carboran-1'-yl)thio]pyrrolidine-2,5-dione-1-yl}-5,10,15,20-tetraphenylporphyrin (**32**) demonstrated reasonably good photochemical properties *in vitro*. Furthermore, the carborane moiety did not seriously alter the **32**:HSA binding, corroborating our experimental and *in silico* findings with other monocarboranyl substituted tetrapyrrolic photosensitizers [53]. Together with a high intracellular uptake, **32** can be considered a lead in the series.

Most importantly, **32** was the most potent in sensitizing HCT116 colon carcinoma cells to light. A burst of ROS and a drop of mitochondrial membrane potential occurred within the initial minutes post cell illumination. These events preceded rapid (by 10 min) loss of the plasma membrane integrity followed by a dramatically decreased reduction of the MTT reagent by mitochondrial dehydrogenases. This mode of cell death is reminiscent of the previously reported fast photonecrosis triggered by illumination of cells loaded with the monocarboranyl- or polyfluorinated tetracarboranylchlorins [14,34]. Still, **32** differed from these photosensitizers in the patterns of intracellular distribution. Boronation of chlorin e6 amide conferred its localization in the membrane organelles and the ability to traverse across the artificial membranes [34]. However, the carborane containing **32** accumulated in the organelle-free cytoplasm rather than in the organelles. Thus, the carborane cage alone does not necessarily render the compound affine to biomembranes. Nevertheless, an extensive ROS generation by photoactivated cytoplasmic **32** was sufficient to quickly trigger irreversible damage of the vital compartments such as mitochondria and the plasma membrane.

### Conclusion

This study analyzed the synthesis and properties of novel porphyrins functionalized with the maleimide substituent at the  $\beta$ -position of the macrocycle. The maleimide units readily interacted with mercaptocarboranes and cysteine via Michael addition reactions; no catalyst was needed for these transformations. The new chemotype is particularly pertinent to the development of anticancer agents with manifold activities, the photosensitizers and beyond. In particular, the maleimide moiety can be useful in the design of protein kinase inhibitors via selective targeting of the cysteine residues. Individual new compounds demonstrated a remarkable ability to produce singlet oxygen (quantum yields > 70%). The peripheral substituents provided no steric hindrance for the formation of stable complexes with serum albumin, a major biological carrier. The cell permeable 2-{3-[(*o*-carboran-1'-yl)thio]pyrrolidine-2,5-dione-1-yl}-5,10,15,20-tetraphenylporphyrin was virtually non-toxic in the dark whereas rapid generation of superoxide anion radical and a necrotic death were observed after

illumination of tumor cells loaded with this compound. Overall, the new chemotype is perspective for an in-depth investigation as a source of multifunctional anticancer drug candidates.

### 3. Experimental

#### 3.1. Synthesis

##### 3.1.1. General information

Reagents were from Sigma-Aldrich unless specified otherwise. All reactions were performed in an atmosphere of dry argon. The starting free base porphyrins, 5,10,15,20-tetraphenylporphyrin (**6**) [38], 5,10,15,20-tetrakis(pentafluorophenyl)porphyrin (**7**) [39] and 5,10,15,20-tetrakis[4-(trifluoromethyl)phenyl]porphyrin (**8**) [38] were prepared according to published procedures. All solvents were dried as recommended in standard protocols. Chemical shifts ( $\delta$ ) were referenced to the residual solvent peak ( $\text{CDCl}_3$  and  $(\text{CD}_3)_2\text{CO}$ ,  $^1\text{H}$ : 7.26 ppm and 2.05, respectively) for  $^1\text{H}$ , external  $\text{BF}_3 \cdot \text{OEt}_2$  for  $^{11}\text{B}$  and external  $\text{CFCl}_3$  for  $^{19}\text{F}$ . IR spectra were recorded on a Bruker FTIR spectrometer Tensor 37 in KBr tablets. Merck silica gel L 0.040–0.080 mesh was used for column chromatography. The identities of new compounds were verified by TLC on Sorbfil and Kieselgel 60 F254 (Merck) plates. The UV-Vis spectra were measured on a spectrophotometer Carl Zeis Specord M 40 in  $\text{CH}_2\text{Cl}_2$ . MALDI mass spectra for carborane-substituted porphyrins were recorded on a Bruker autoflex speed time-of-flight (TOF) mass obtained mass spectrometer (Bruker Daltonics Inc., Germany) equipped with a solid-state ultraviolet (UV) laser of 355 nm (1 kHz repetition rate, 1000 shots for each spectrum) and operated in positive reflectron mode. MALDI mass spectra were recorded by using stainless-steel targets (MTP 384 ground steel; Bruker Daltonics Inc., Germany) containing 384 cells for the deposition of the analyte mixed with matrix; the most intense peaks were given for each compound. The APCI mass-spectra were registered on the Finnigan LCQ Advantage tandem dynamic mass-spectrometer (USA), equipped by octapole ion trap mass analyzer with the Surveyor MS pump and the nitrogen generator Schmidlin-Lab (Germany). Nitrogen 70/10 served as a sheath and auxiliary gas. The flow rate of acetonitrile was 350  $\mu\text{l}/\text{min}$ . The temperature of the vaporizer was 400  $^\circ\text{C}$ . The temperature of the heated capillary was 150  $^\circ\text{C}$ , the electric potential between the needle and the counter electrode 6.0 kV. Samples (100  $\mu\text{M}$  in acetonitrile solution) were introduced into the ion source through the Reodyne injector with 5  $\mu\text{l}$  loop. Acetonitrile (Merck) was used for gradient analysis. For data collection the *X Calibur* version 1.3 was used.

##### 3.1.2. General procedures for preparation of copper(II) complexes of porphyrins.

A solution of  $\text{Cu}(\text{OAc})_2 \cdot \text{H}_2\text{O}$  (4.6 mmol) in methanol (10 mL) was added to a solution of corresponding porphyrin (1.15 mmol) in methylene chloride (50 mL). The resulting mixture was

stirred for 1.5 h at room temperature with TLC monitoring (CHCl<sub>3</sub>–hexane 1:2). Then the reaction mixture was poured into water and extracted with methylene chloride. The organic layer was dried over Na<sub>2</sub>SO<sub>4</sub>, and the solvent was removed under reduced pressure. The residue was used in the reactions without purification.

5,10,15,20-(tetraphenylporphyrinato)copper(II) (**13**) [56] (757 mg, yield 97%). UV-Vis (CH<sub>2</sub>Cl<sub>2</sub>) λ<sub>max</sub>, (εx10<sup>-3</sup>) nm: 414 (611), 539 (29). APCI-MS Found: [M]<sup>+</sup> 676.16; 'C<sub>44</sub>H<sub>28</sub>CuN<sub>4</sub>' requires [M]<sup>+</sup> 676.26.

5,10,15,20-{*tetrakis*[4-(trifluoromethyl)phenyl]porphyrinato}copper (II) (**15**) [57] (1080 mg, yield 99 %). UV-Vis (CH<sub>2</sub>Cl<sub>2</sub>) λ<sub>max</sub>, (εx10<sup>-3</sup>) nm: 416 (60.2), 544 (2.40). APCI-MS Found: [M]<sup>+</sup> 948.11; 'C<sub>48</sub>H<sub>24</sub>CuF<sub>12</sub>N<sub>4</sub>' requires [M]<sup>+</sup> 948.26.

### 3.1.3. General procedures for nitration of porphyrin copper(II) and zinc(II) complexes.

To a solution of corresponding porphyrin copper complex (1.13 mmol) in methylene chloride (90 mL) Cu(NO<sub>3</sub>)<sub>2</sub>·3 H<sub>2</sub>O (2.30 mmol) in the mixture of acetic acid (5 mL) and acetic anhydride (2 mL) was added, and reaction mixture was stirred for 3 h at room temperature, with TLC monitoring (CHCl<sub>3</sub>–hexane 1:2). After completion the reaction the solution was washed with water (200 mL), then with Na<sub>2</sub>CO<sub>3</sub> solution, the organic phase was separated and dried over Na<sub>2</sub>SO<sub>4</sub>. After removal of the solvent under reduced pressure, the residue was purified by column chromatography on silica gel using a CH<sub>2</sub>Cl<sub>2</sub>–hexane system (3:7).

2-Nitro-5,10,15,20-(tetraphenylporphyrinato)copper(II) (**9**) [58] (798 mg, yield 98%). UV-vis (CH<sub>2</sub>Cl<sub>2</sub>): λ<sub>max</sub>, nm (εx10<sup>-3</sup>) 423 (94), 548 (6.9), 592 (4.5). IR (KBr) ν<sub>max</sub>, cm<sup>-1</sup>: 3435 (NH), 2922 (CH), 1524 (NO<sub>2</sub>), 1342 (NO<sub>2</sub>). MALDI-MS Found: [M]<sup>+</sup> 721.15; 'C<sub>44</sub>H<sub>27</sub>CuN<sub>5</sub>O<sub>2</sub>' requires [M]<sup>+</sup> 721.26.

2-Nitro-5,10,15,20-*tetrakis*(pentafluorophenyl)porphyrinato)copper(II) (**10**) was obtained under reflux for 4h, [41] (1186 mg, yield 97%). UV-vis (CH<sub>2</sub>Cl<sub>2</sub>): λ<sub>max</sub>, nm (εx10<sup>-3</sup>) 416 (225), 543(18), 588 (16.2). IR (KBr) ν<sub>max</sub>, cm<sup>-1</sup>: 3435 (NH), 2956 (CH), 1520 (NO<sub>2</sub>), 1493 (CF), 1293 (CF), 1339 (NO<sub>2</sub>). APCI-MS Found: [M]<sup>+</sup> 1081.74; 'C<sub>44</sub>H<sub>7</sub>CuF<sub>20</sub>N<sub>5</sub>O<sub>2</sub>' requires [M]<sup>+</sup> 1081.07.

{2-Nitro-5,10,15,20-*tetrakis*[4-(trifluoromethyl)phenyl]porphyrinato}copper (II) (**11**) [57] (909 mg, yield 81%). UV-vis (CH<sub>2</sub>Cl<sub>2</sub>): λ<sub>max</sub>, nm (εx10<sup>-3</sup>) 418 (112), 547 (11.8), 590 (8.67). MS IR (KBr) ν<sub>max</sub>, cm<sup>-1</sup>: 3389 (NH), 1527 (NO<sub>2</sub>), 1326 (CF). APCI-MS Found: [M]<sup>+</sup> 993.89; 'C<sub>48</sub>H<sub>23</sub>CuF<sub>12</sub>N<sub>5</sub>O<sub>2</sub>' requires [M]<sup>+</sup> 993.26.

[2-Nitro-5,10,15,20- *tetrakis*(pentafluorophenyl)porphyrinato]zinc(II) (**12**) [59].

To a solution of 5,10,15,20-tetraphenylporphyrinporphyrin zinc complex (**16**) [60] 500 mg (0.48 mmmol) in methylene chloride (50 mL) Cu(NO<sub>3</sub>)<sub>2</sub>·3 H<sub>2</sub>O (200 mg, 0.84 mmol) in the mixture of acetic acid (5 mL) and acetic anhydride (2 mL) was added, and reaction mixture was stirred for 1,5 h under reflux, with TLC monitoring (CHCl<sub>3</sub>–hexane 1:1). After the reaction was

complete the solution was washed with water (100 mL), then with Na<sub>2</sub>CO<sub>3</sub> solution, the organic phase was separated and dried over Na<sub>2</sub>SO<sub>4</sub>. After removal of the solvent under reduced pressure, the residue was purified by column chromatography on silica gel using a methylene chloride-hexane system (4:6). Yield 500 mg (96%). UV-Vis (CH<sub>2</sub>Cl<sub>2</sub>)  $\lambda_{\max}$ , ( $\epsilon \times 10^{-3}$ ) nm: 426 (243), 558 (19.4), 603 (14.0). IR (KBr)  $\nu_{\max}$ , cm<sup>-1</sup>: 3392 (NH), 1521 (NO<sub>2</sub>), 1501 (CF), 1337 (NO<sub>2</sub>), 1286 (CF). <sup>1</sup>H NMR,  $\delta_{\text{H}}$  (CDCl<sub>3</sub>, 400 MHz), ppm: 8.94 (m, 6H,  $\beta$ -H), 9.26 (s, 1H,  $\beta$ -H). <sup>19</sup>F NMR,  $\delta_{\text{F}}$  (CDCl<sub>3</sub>, 376 MHz), ppm: -136.5 (d, 2F,  $J = 16.5$  Hz), -136.8 (d, 4F,  $J = 22.0$  Hz), -137.5 (d, 2F,  $J = 16.5$  Hz), -150.5 (t, 1F,  $J = 22.0$  Hz), -150.7 (t, 1F,  $J = 22.00$  Hz), -151.3 (t, 2F,  $J = 19.3$  Hz), -160.9 (t, 2F,  $J = 16.5$  Hz), -161.3 (t, 4F,  $J = 19.3$  Hz), -161.7 (t, 2F,  $J = 19.3$  Hz). APCI-MS Found: [M]<sup>+</sup> 1082.98; 'C<sub>44</sub>H<sub>7</sub>F<sub>20</sub>N<sub>5</sub>O<sub>2</sub>Zn' requires [M]<sup>+</sup> 1082.91.

#### 3.1.4. General procedure of demetallation of copper complexes (9-11).

To the corresponding copper (II) complex of 2-nitroporphyrin (0.5 mmol) concentrated H<sub>2</sub>SO<sub>4</sub> (5 mL) and CF<sub>3</sub>COOH (5 mL) were added and the reaction was stirred for 3 h at room temperature. After the demetallation (TLC monitoring, CHCl<sub>3</sub>-hexane 1:2), the mixture was poured into water, extracted with CH<sub>2</sub>Cl<sub>2</sub> (50 mL), washed with a saturated solution of NaHCO<sub>3</sub> and water. The organic layer was dried over anhydrous Na<sub>2</sub>SO<sub>4</sub>. After removal of the solvent under reduced pressure, the residue was purified by column chromatography on silica gel using CH<sub>2</sub>Cl<sub>2</sub>-hexane system (1:1) as an eluent.

2-Nitro-5,10,15,20-tetraphenylporphyrin (**17**) (287 mg, yield 87%). UV-Vis (CH<sub>2</sub>Cl<sub>2</sub>)  $\lambda_{\max}$ , ( $\epsilon \times 10^{-3}$ ) nm: 425 (200), 527 (14.5), 568 (4.1), 604 (4.1), 651 (8.3). IR (KBr)  $\nu_{\max}$ , cm<sup>-1</sup>: 3327 (NH), 1523 (NO<sub>2</sub>), 1347 (NO<sub>2</sub>). <sup>1</sup>H NMR,  $\delta_{\text{H}}$  (CDCl<sub>3</sub>, 400 MHz), ppm: -2.50 (br s, 2H, NH), 7.82 (m, 12 H, Ph), 8.28 (m, 6 H, Ph), 8.36 (dd, 2H,  $J = 7.9, 1.2$  Hz, Ph), 8.80 (d, 1H,  $J = 4.6$  Hz,  $\beta$ -H), 8.82 (d, 1H,  $J = 4.6$  Hz,  $\beta$ -H), 8.99 (d, 2H,  $J = 4.9$  Hz,  $\beta$ -H), 9.04 (d, 1H,  $J = 5.2$  Hz,  $\beta$ -H), 9.12 (d, 1H,  $J = 5.2$  Hz,  $\beta$ -H), 9.16 (s, 1H,  $\beta$ -H). MALDI-MS Found: [M]<sup>+</sup> 659.23; 'C<sub>44</sub>H<sub>29</sub>N<sub>5</sub>O<sub>2</sub>' requires [M]<sup>+</sup> 659.73.

2-Nitro-5,10,15,20-tetrakis(pentafluorophenyl)porphyrin (**18**) [41] (459 mg, yield 90%). UV-Vis (CH<sub>2</sub>Cl<sub>2</sub>)  $\lambda_{\max}$ , ( $\epsilon \times 10^{-3}$ ) nm: 420 (100), 516 (7.71), 557 (3.10), 591 (3.86), 656 (2.29). IR (KBr)  $\nu_{\max}$ , cm<sup>-1</sup>: 3334 (NH), 1522 (NO<sub>2</sub>), 1360 (NO<sub>2</sub>), 1499 (CF), 1201 (CF). <sup>1</sup>H NMR,  $\delta_{\text{H}}$  (CDCl<sub>3</sub>, 400 MHz), ppm: -2.79 (s, 2H, NH), 8.83 (dd, 2H,  $J = 7.2, 4.8$  Hz,  $\beta$ -H), 9.06 (m, 4H,  $J = 5.7$  Hz,  $\beta$ -H), 9.19 (s, 1H,  $\beta$ -H). <sup>19</sup>F NMR,  $\delta_{\text{F}}$  (CDCl<sub>3</sub>, 376 MHz), ppm: -136.1 (dd, 2F,  $J = 21.6, 6.5$  Hz), -136.4 (dd, 4F,  $J = 22.7, 6.5$  Hz), -137.2 (dd, 2F,  $J = 21.6$  Hz,  $J = 6.5$  Hz), -149.4 (m, 1F,  $J = 20.6$  Hz), -149.6 (m, 1F,  $J = 20.6$  Hz), -150.3 (m, 2F), -160.3 (m, 2F,  $J = 20.6, 6.5$  Hz), -160.7 (m, 4F,  $J = 19.5, 4.3$  Hz), -161.1 (td, 2F,  $J = 20.6, 5.4$  Hz). APCI-MS Found: [M]<sup>+</sup> 1019.96; 'C<sub>44</sub>H<sub>9</sub>F<sub>20</sub>N<sub>5</sub>O<sub>2</sub>' requires [M]<sup>+</sup> 1019.54.

2-Nitro-5,10,15,20-*tetrakis*[4-(trifluoromethyl)phenyl]porphyrin (**19**) [57] (387 mg, yield 83%). UV-Vis (CH<sub>2</sub>Cl<sub>2</sub>)  $\lambda_{\max}$ , ( $\epsilon \times 10^{-3}$ ) nm: 428 (183), 525 (14.1), 564 (3.49), 602 (4.03), 660 (6.75). IR (KBr)  $\nu_{\max}$ , cm<sup>-1</sup>: 3336 (NH), 1530 (NO<sub>2</sub>), 1324 (CF). <sup>1</sup>H NMR,  $\delta_{\text{H}}$  (CDCl<sub>3</sub>, 400 MHz), ppm: -2.64 (s, 2H, NH), 7.99 (d, 2H, *J* = 7.9 Hz, Ph), 8.09 (d, 6H, *J* = 7.6 Hz, Ph), 8.36 (d, 8 H, *J* = 7.3 Hz, Ph), 8.72 (dd, 2H, *J* = 7.9, 4.8 Hz,  $\beta$ -H), 8.92 (dd, 2H, *J* = 8.9, 5.1 Hz,  $\beta$ -H), 8.98 (dd, 2H, *J* = 11.4, 5.1 Hz,  $\beta$ -H), 9.04 (s, 1H,  $\beta$ -H). <sup>19</sup>F NMR,  $\delta_{\text{F}}$  (CDCl<sub>3</sub>, 376 MHz), ppm: -62.2 (s, 3F), -62.1 (d, 9F, *J* = 16.5 Hz). APCI-MS Found: [M]<sup>+</sup> 932.22; 'C<sub>48</sub>H<sub>25</sub>F<sub>12</sub>N<sub>5</sub>O<sub>2</sub>' requires [M]<sup>+</sup> 931.73.

### 3.1.5. General procedure for preparation of 2-amino-5,10,15,20-tetraarylporphyrins (**20-24**).

To a mixture of the corresponding 2-nitro-substituted porphyrin (0.3 mmol) and 10% palladium on activated charcoal (30 mg) in dichloromethane – methanol (2:1) system (30 ml) sodium borohydride (1.5 mmol) was added under argon atmosphere in the dark. The reaction mixture was stirred at room temperature for 30 min. After completion of the reaction (TLC control) the reaction mass was filtered, and the organic phase was washed with water and dried over Na<sub>2</sub>SO<sub>4</sub>. The solvent was removed under reduced pressure. The residue was purified by column chromatography using CH<sub>2</sub>Cl<sub>2</sub>-hexane system (2:3) as an eluent to afford the appropriate 2-amino-5,10,15,20-tetraarylporphyrin.

2-Amino-5,10,15,20-tetraphenylporphyrin (**20**) [61] (149 mg, yield 79 %). UV-Vis (CH<sub>2</sub>Cl<sub>2</sub>)  $\lambda_{\max}$ , ( $\epsilon \times 10^{-3}$ ) nm: 424 (76.3), 523 (8.8), 560 (3.6), 596 (3.9), 650 (4.4). IR (KBr)  $\nu_{\max}$ , cm<sup>-1</sup>: 3460 (NH). <sup>1</sup>H NMR,  $\delta_{\text{H}}$  (CDCl<sub>3</sub>, 400 MHz), ppm: -2.73 (br s, 2H, NH), 4.47 (br s, 2H, NH<sub>2</sub>), 7.75 (d, 10H, *J* = 5.4 Hz, Ph), 7.81 (d, 2H, *J* = 7.9 Hz, Ph), 8.14 (m, 4H, Ph), 8.22 (d, 4H, *J* = 6.4 Hz, Ph), 8.53 (d, 1H, *J* = 3.8 Hz,  $\beta$ -H), 8.59 (br s, 1H,  $\beta$ -H), 8.71 (br s, 1H,  $\beta$ -H), 8.75 (d, 1H, *J* = 3.8 Hz,  $\beta$ -H), 8.80 (br s, 3H,  $\beta$ -H). MALDI-MS Found: [M]<sup>+</sup> 630.65; 'C<sub>44</sub>H<sub>31</sub>N<sub>5</sub>' requires [M]<sup>+</sup> 629.75.

2-Amino-5,10,15,20-*tetrakis*(pentafluorophenyl)porphyrin (**21**) [32] (211 mg, yield 71%). UV-Vis (CH<sub>2</sub>Cl<sub>2</sub>)  $\lambda_{\max}$ , ( $\epsilon \times 10^{-3}$ ) nm: 420 (100), 516 (7.71), 557 (3.1), 591 (3.86), 656 (2.29). IR (KBr)  $\nu_{\max}$ , cm<sup>-1</sup>: 3314 (NH), 1498 (CF), 1150 (CF). <sup>1</sup>H NMR,  $\delta_{\text{H}}$  (CDCl<sub>3</sub>, 400 MHz), ppm: -2.60 (br s, 2H, NH), 4.70 (br s, 2H, NH<sub>2</sub>), 7.87 (br s, 1H,  $\beta$ -H), 8.66 (d, 1H, *J* = 4.8 Hz,  $\beta$ -H), 8.79 (d, 1H, *J* = 4.5 Hz,  $\beta$ -H), 8.85 (dd, 3H, *J* = 10.0, 4.5 Hz,  $\beta$ -H), 8.89 (d, 1H, *J* = 4.2 Hz,  $\beta$ -H). <sup>19</sup>F NMR,  $\delta_{\text{F}}$  (CDCl<sub>3</sub>, 376 MHz), ppm: -135.5 (d, 2F, *J* = 17.1 Hz), -136.6 (d, 6F, *J* = 21.3 Hz), -149.8 (d, 1F, *J* = 21.3 Hz), -151.5 (d, 2F, *J* = 21.3 Hz), -152.0 (d, 1F, *J* = 21.3 Hz), -159.6 (dd, 2F, *J* = 36.3, 17.1 Hz), -161.6 (d, 6F, *J* = 21.3 Hz). APCI-MS Found: [M+H]<sup>+</sup> 991.19; 'C<sub>44</sub>H<sub>12</sub>F<sub>20</sub>N<sub>5</sub>' requires [M+H]<sup>+</sup> 990.56.

2-Amino-5,10,15,20-*tetrakis*[4-(trifluoromethyl)phenyl]porphyrin (**22**) (198 mg, yield 73%, purple solid). UV-Vis (CH<sub>2</sub>Cl<sub>2</sub>)  $\lambda_{\max}$ , ( $\epsilon \times 10^{-3}$ ) nm: 424 (87.2), 523 (11.4), 558 (5.11), 595 (5.36), 651 (5.55). IR (KBr)  $\nu_{\max}$ , cm<sup>-1</sup>: 3403 (NH), 3313 (NH<sub>2</sub>), 1325 (CF). <sup>1</sup>H NMR,  $\delta_{\text{H}}$  (CDCl<sub>3</sub>, 400 MHz), ppm: -2.70 (br s, 2H, NH), 4.43 (br s, 2H, NH<sub>2</sub>), 7.72 (s, 1H,  $\beta$ -H), 8.03 (dd, 6H,  $J = 7.9, 3.8$  Hz, Ph), 8.10 (d, 2H,  $J = 7.9$  Hz, Ph), 8.31 (dd, 8 H,  $J = 11.8, 8.0$  Hz, Ph), 8.46 (d, 1H,  $J = 4.8$  Hz,  $\beta$ -H), 8.69 (dd, 2H,  $J = 12.3, 4.7$  Hz,  $\beta$ -H), 8.77 (s, 1H,  $\beta$ -H), 8.78 (dd, 2H,  $J = 10.5, 4.8$  Hz,  $\beta$ -H). <sup>19</sup>F NMR,  $\delta_{\text{F}}$  (CDCl<sub>3</sub>, 376 MHz), ppm: -62.2 (s, 3F), -62.0 (s, 9F). APCI-MS Found: [M+H]<sup>+</sup> 902.91; 'C<sub>48</sub>H<sub>28</sub>F<sub>12</sub>N<sub>5</sub>' requires [M+H]<sup>+</sup> 902.74.

[2-Amino-5,10,15,20-tetraphenylporphyrinato]copper (II) (**23**) [62] (160 mg, yield 77%). UV-Vis (CH<sub>2</sub>Cl<sub>2</sub>)  $\lambda_{\max}$ , ( $\epsilon \times 10^{-3}$ ) nm: 423 (147), 548 (12.4), 596 (7.6). IR (KBr)  $\nu_{\max}$ , cm<sup>-1</sup>: 3371 (NH). APCI-MS Found: [M]<sup>+</sup> 691.08; 'C<sub>44</sub>H<sub>29</sub>CuN<sub>5</sub>' requires [M]<sup>+</sup> 691.28.

[2-Amino-5,10,15,20-*tetrakis*(pentafluorophenyl)porphyrinato]zinc (II) (**24**) [59] (237 mg, yield 75%, green solid). UV-Vis (CH<sub>2</sub>Cl<sub>2</sub>)  $\lambda_{\max}$ , ( $\epsilon \times 10^{-3}$ ) nm: 409 (109), 556 (10.3), 605 (8.85). IR (KBr)  $\nu_{\max}$ , cm<sup>-1</sup>: 3392 (NH), 1492 (CF), 1338 (CF). <sup>1</sup>H NMR,  $\delta_{\text{H}}$  (CDCl<sub>3</sub>, 400 MHz), ppm: 4.57 (br s, 2H, NH<sub>2</sub>), 7.88 (s, 1H,  $\beta$ -H), 8.75 (d, 1H,  $J = 4.5$  Hz,  $\beta$ -H), 8.93 (m, 5H,  $\beta$ -H). <sup>19</sup>F NMR,  $\delta_{\text{F}}$  (CDCl<sub>3</sub>, 376 MHz), ppm: -136.0 (dd, 2F,  $J = 24.7, 5.5$  Hz), -136.9 (d, 6F,  $J = 19.2$  Hz), -150.6 (t, 1F,  $J = 19.2$  Hz), -152.3 (q, 2F,  $J = 24.0$  Hz), -152.7 (t, 1F,  $J = 22.0$  Hz), -160.0 (d, 2F,  $J = 35.7$  Hz), -161.9 (m, 6F,  $J = 44.0, 13.7$  Hz). APCI-MS Found: [M]<sup>+</sup> 1052.35; 'C<sub>44</sub>H<sub>9</sub>F<sub>20</sub>N<sub>5</sub>Zn' requires [M]<sup>+</sup> 1052.92.

### 3.1.6. Preparation of maleinoylamino-substituted porphyrins (**25**, **26**, **28**).

To 2-aminosubstituted porphyrin (0.2 mmol) in glacial acetic acid (15 mL) maleic anhydride (59 mg, 0.6 mmol) was added, and the reaction was stirred under argon for 50 h at room temperature. The solution was evaporated, the resulting solid was dissolved in dichloromethane (20 mL), washed with water and dried over Na<sub>2</sub>SO<sub>4</sub>. After removal of the solvent *in vacuo*, the residue was purified by column chromatography on silica gel using CH<sub>2</sub>Cl<sub>2</sub>-MeOH system (9:1) as an eluent.

2-(Maleinoylamino)-5,10,15,20-tetraphenylporphyrin (**25**) (120 mg, yield 82%). UV-Vis (CH<sub>2</sub>Cl<sub>2</sub>)  $\lambda_{\max}$ , ( $\epsilon \times 10^{-3}$ ) nm: 424 (166), 520 (20), 555 (5.8), 593 (6.6), 651 (4.1). IR (KBr)  $\nu_{\max}$ , cm<sup>-1</sup>: 3328 (NH), 2853.26 (CH), 1720 (C=O), 1610 (amide I), 1596 (C=C), 1539 (amide II). <sup>1</sup>H NMR,  $\delta_{\text{H}}$  (CDCl<sub>3</sub>, 400 MHz), ppm: -2.80 (br s, 2H, NH), 5.42 (d, 1H,  $J = 12.4$  Hz, CH=CH), 6.34 (d, 1H,  $J = 12.4$  Hz, CH=CH), 7.79 (s, 9H, Ph), 7.89 (t, 2H,  $J = 7.0$  Hz, Ph), 7.96 (d, 1H,  $J = 6.7$  Hz, Ph), 8.21 (br s, 8H, Ph), 8.68 (d, 1H,  $J = 4.5$  Hz,  $\beta$ -H), 8.80 (br s, 3H,  $\beta$ -H), 8.91 (d, 3H,  $J = 9.9$  Hz,  $\beta$ -H), 9.34 (br s, 1H, NHCO). APCI-MS Found: [M+H]<sup>+</sup> 728.51; 'C<sub>48</sub>H<sub>34</sub>N<sub>5</sub>O<sub>3</sub>' requires [M+H]<sup>+</sup> 728.81.

2-(Maleinoylamino)-5,10,15,20-*tetrakis*(pentafluorophenyl)porphyrin (**26**) (43 mg, yield 20%). UV-Vis (CH<sub>2</sub>Cl<sub>2</sub>)  $\lambda_{\max}$ , ( $\epsilon \times 10^{-3}$ ) nm: 424 (166), 520 (20), 555 (5.8), 593 (6.6), 651 (4.1). IR (KBr)  $\nu_{\max}$ , cm<sup>-1</sup>: 3341 (NH), 1723 (C=O), 1612 (amide I), 1591 (C=C), 1532 (amide II). <sup>1</sup>H NMR,  $\delta_{\text{H}}$  (CDCl<sub>3</sub>, 400 MHz), ppm: -2.72 (br s, 2H, NH), 4.87 (d, 1H,  $J = 6.0$  Hz, CH=CH), 5.70 (d, 1H,  $J = 2.9$  Hz, CH=CH), 8.63 (d, 2H,  $J = 4.1$  Hz,  $\beta$ -H), 8.82 (s, 3H,  $\beta$ -H), 9.00 (d, 2H,  $J = 4.8$  Hz,  $\beta$ -H), 9.12 (br s, 1H, NHCO). <sup>19</sup>F NMR,  $\delta_{\text{F}}$  (CDCl<sub>3</sub>, 376 MHz), ppm: -136.1 (d, 1F,  $J = 16.5$  Hz), -136.5 (d, 6F,  $J = 16.5$  Hz), -137.4 (d, 1F,  $J = 16.5$  Hz), -148.6 (d, 1F,  $J = 19.2$  Hz), -150.6 (t, 3F,  $J = 22.0$  Hz), -159.1 (d, 1F,  $J = 16.5$  Hz), -160.9 (d, 6F,  $J = 22.0$  Hz), -162.0 (d, 1F,  $J = 8.3$  Hz). APCI-MS Found: [M]<sup>+</sup> 1088.22; 'C<sub>48</sub>H<sub>13</sub>F<sub>20</sub>N<sub>5</sub>O<sub>3</sub>' requires [M]<sup>+</sup> 1087.62.

[2-(Maleinoylamino)-5,10,15,20-tetraphenylporphyrinato]copper (II) (**28**) (123 mg, yield 78%). UV-Vis (CH<sub>2</sub>Cl<sub>2</sub>)  $\lambda_{\max}$ , ( $\epsilon \times 10^{-3}$ ) nm: 424 (97), 546 (10.8), 580 (4.7). IR (KBr)  $\nu_{\max}$ , cm<sup>-1</sup>: 3381 (NH), 1722 (C=O), 1610 (amide I), 1539 (amide II). APCI-MS Found: [M]<sup>+</sup> 789.18; 'C<sub>48</sub>H<sub>31</sub>CuN<sub>5</sub>O<sub>3</sub>' requires [M]<sup>+</sup> 789.34.

### 3.1.8. Preparation of maleinoylamino-substituted porphyrins (**27**, **29**).

To a solution of the corresponding 2-amino-substituted porphyrin (0.2 mmol) in MeCN (15mL) maleic anhydride (59 mg, 0.6 mmol) was added, and reaction was refluxed for 11 h under argon. The mixture was poured into water (80 mL), extracted with dichloromethane and dried over Na<sub>2</sub>SO<sub>4</sub>. After removal of the solvent *in vacuo*, the residue was purified by column chromatography on silica gel using CH<sub>2</sub>Cl<sub>2</sub>-MeOH system (95:5) as an eluent.

2-(Maleinoylamino)-5,10,15,20-*tetrakis*[4-(trifluoromethyl)phenyl]porphyrin (**27**) (152 mg, yield 76%). UV-Vis (CH<sub>2</sub>Cl<sub>2</sub>)  $\lambda_{\max}$ , ( $\epsilon \times 10^{-3}$ ) nm: 428 (93.8), 526 (10.5), 565 (2.90), 601 (4.81), 656 (3.10). IR (KBr)  $\nu_{\max}$ , cm<sup>-1</sup>: 3397 (NH), 1726 (C=O), 1616 (amide I), 1531 (amide II), 1325 (CF). <sup>1</sup>H NMR,  $\delta_{\text{H}}$  ((CD<sub>3</sub>)<sub>2</sub>CO, 400 MHz), ppm: -2.51 (br s, 2H, NH), 4.85 (dd, 1H,  $J = 2.9, 9.7$  Hz, CH=CH), 5.78 (dd, 1H,  $J = 4.6, 2.0$  Hz, CH=CH), 8.03 (m, 6H, Ph), 8.18 (d, 2H,  $J = 6.5$  Hz, Ph), 8.32 (m, 6H, Ph), 8.49 (d, 2H,  $J = 8.4$  Hz, Ph), 8.93 (m, 7H,  $\beta$ -H). <sup>19</sup>F NMR,  $\delta_{\text{F}}$  ((CD<sub>3</sub>)<sub>2</sub>CO, 376 MHz), ppm: -62.9 (s, 3F), -62.6 (t, 9F,  $J = 4.5$  Hz). APCI-MS Found: [M]<sup>+</sup> 1000.40; 'C<sub>52</sub>H<sub>29</sub>F<sub>12</sub>N<sub>5</sub>O<sub>3</sub>' requires [M]<sup>+</sup> 999.80.

[2-(Maleinoylamino)-5,10,15,20-*tetrakis*(pentafluorophenyl)porphyrinato]zinc (II) (**29**) (159 mg, yield 69%). UV-Vis (CH<sub>2</sub>Cl<sub>2</sub>)  $\lambda_{\max}$ , ( $\epsilon \times 10^{-3}$ ) nm: 419 (129), 550 (7.58), 628 (6.13). IR (KBr)  $\nu_{\max}$ , cm<sup>-1</sup>: 3340 (NH), 1729 (C=O), 1632 (C=C), 1496 (CF), 1254 (CF). <sup>1</sup>H NMR,  $\delta_{\text{H}}$  (CDCl<sub>3</sub>, 400 MHz), ppm: 5.32 (dd, 1H,  $J = 3.7, 1.4$  Hz, CH=CH), 5.82 (dd, 1H,  $J = 7.5, 4.6$  Hz, CH=CH), 8.76 (d, 1H,  $J = 4.5$  Hz,  $\beta$ -H), 8.81 (s, 1H,  $\beta$ -H), 8.88 (d, 2H,  $J = 4.5$  Hz,  $\beta$ -H), 8.94 (s, 3H,  $\beta$ -H), 9.18 (br s, 1H, NHCO). <sup>19</sup>F NMR,  $\delta_{\text{F}}$  (CDCl<sub>3</sub>, 376 MHz), ppm: -133.1 (d, 1F,  $J = 19.2$  Hz), -134.8 (d, 2F,  $J = 19.2$  Hz), -136.2 (br s, 2F), -136.8 (br s, 4F), -151.9 (dd, 4F,  $J = 52.2,$

33.0 Hz), -160.5 (br s, 1F), -161.5 (br s, 2F), -161.8 (br s, 4F), -161.8 (br s, 1F). APCI-MS Found:  $[M]^+$  1150.12; 'C<sub>48</sub>H<sub>11</sub>F<sub>20</sub>N<sub>5</sub>O<sub>3</sub>Zn' requires  $[M]^+$  1150.98.

*3.1.9. General procedure for preparation of maleimide substituted 5,10,15,20-tetraarylporphyrins (1-5).*

To a solution of maleinoylaminoporphyrin (0.15 mmol) in acetic anhydride (8 mL) NaOAc (10 mg, 0.12 mmol) was added and reaction was heated at 110 °C for 5 h under argon. Then the reaction was treated with water (50 mL), extracted with dichloromethane (2x 25 mL). The combined organic layers were dried over Na<sub>2</sub>SO<sub>4</sub>. After evaporating of the solvent the residue was purified by column chromatography on silica gel using CH<sub>2</sub>Cl<sub>2</sub> as an eluent.

2-(3'-Maleimido)-5,10,15,20-tetraphenylporphyrin (**1**) (82 mg, yield 77%). UV-Vis (CH<sub>2</sub>Cl<sub>2</sub>)  $\lambda_{\max}$ , ( $\epsilon \times 10^{-3}$ ) nm: 420 (559), 518 (22.4), 552 (8.20), 592 (7.08), 648 (8.20). IR (KBr)  $\nu_{\max}$ , cm<sup>-1</sup>: 3323 (NH), 1720 (C=O). <sup>1</sup>H NMR,  $\delta_H$  (CDCl<sub>3</sub>, 400 MHz), ppm: -2.70 (br s, 2H, NH), 6.46 (d, 2H,  $J = 1.9$  Hz, CH=CH), 7.59 (m, 2H, Ph), 7.78 (t, 10H,  $J = 7.1$  Hz, Ph), 8.04 (br s, 2H, Ph), 8.25 (m, 6H, Ph), 8.61 (br s, 1H,  $\beta$ -H), 8.81 (m, 4H,  $\beta$ -H), 8.93 (d, 2H,  $J = 3.2$  Hz,  $\beta$ -H). APCI-MS Found:  $[M+H]^+$  710.84; 'C<sub>48</sub>H<sub>32</sub>N<sub>5</sub>O<sub>2</sub>' requires  $[M+H]^+$  710.79.

2-(3'-Maleimido)-5,10,15,20-tetrakis(pentafluorophenyl)porphyrin (**2**) (114 mg, yield 71%). UV-Vis (CH<sub>2</sub>Cl<sub>2</sub>)  $\lambda_{\max}$ , ( $\epsilon \times 10^{-3}$ ) nm: 415 (169), 510 (12.3), 543 (3.15), 587 (4.72), 641 (1.21). IR (KBr)  $\nu_{\max}$ , cm<sup>-1</sup>: 3331 (NH), 1727 (C=O), 1499 (CF), 1353 (CF). <sup>1</sup>H NMR,  $\delta_H$  (CDCl<sub>3</sub>, 400 MHz), ppm: -2.86 (br s, 2H, NH), 6.98 (s, 2H, CH=CH), 8.83 (s, 2H,  $\beta$ -H), 8.87 (dd, 2H,  $J = 7.0$  Hz,  $J = 4.8$  Hz,  $\beta$ -H), 8.94 (d, 1H,  $J = 5.0$  Hz,  $\beta$ -H), 8.99 (s, 2H,  $\beta$ -H). <sup>19</sup>F NMR,  $\delta_F$  (CDCl<sub>3</sub>, 376 MHz), ppm: -133.6 (dd, 2F,  $J = 22.0, 5.5$  Hz), -135.7 (dd, 2F,  $J = 23.5, 6.5$  Hz), -136.4 (dd, 4F,  $J = 13.8, 8.3$  Hz), -150.8 (m, 3F,  $J = 19.3$  Hz), -151.3 (t, 1F,  $J = 19.3$  Hz), -161.0 (m, 6F), -161.4 (t, 2F,  $J = 19.3$  Hz). APCI-MS Found:  $[M+H]^+$  1070.61; 'C<sub>48</sub>H<sub>11</sub>F<sub>20</sub>N<sub>5</sub>O<sub>2</sub>' requires  $[M+H]^+$  1070.60.

2-(3'-Maleimido)-5,10,15,20-tetrakis[4-(trifluoromethyl)phenyl]porphyrin (**3**) (90 mg, yield 61 %). UV-Vis (CH<sub>2</sub>Cl<sub>2</sub>)  $\lambda_{\max}$ , ( $\epsilon \times 10^{-3}$ ) nm: 418 (256), 517 (18.7), 548 (5.30), 590 (5.85), 648 (4.54). IR (KBr)  $\nu_{\max}$ , cm<sup>-1</sup>: 3323 (NH), 1723 (C=O), 1324 (CF). <sup>1</sup>H NMR,  $\delta_H$  (CDCl<sub>3</sub>, 400 MHz), ppm: -2.79 (s, 2H, NH), 6.55 (s, 2H, CH=CH), 7.91 (d, 2H,  $J = 7.9$  Hz, Ph), 8.06 (m, 6H, Ph), 8.18 (d, 2H,  $J = 7.8$  Hz, Ph), 8.36 (m, 6H, Ph), 8.62 (d, 1H,  $J = 4.8$  Hz,  $\beta$ -H), 8.72 (s, 1H,  $\beta$ -H), 8.75 (m, 2H,  $\beta$ -H), 8.81 (d, 1H,  $J = 4.8$  Hz,  $\beta$ -H), 8.90 (s, 2H,  $\beta$ -H). <sup>19</sup>F NMR,  $\delta_F$  (CDCl<sub>3</sub>, 376 MHz), ppm: -62.7 (s, 3F), -62.1 (s, 3F), -62.0 (s, 6F). APCI-MS Found:  $[M+H]^+$  982.82; 'C<sub>52</sub>H<sub>28</sub>F<sub>12</sub>N<sub>5</sub>O<sub>2</sub>' requires  $[M+H]^+$  982.78.

[2-(3'-Maleimido)-5,10,15,20-tetraphenylporphyrinato]copper (II) (**4**) (102 mg, yield 88%, dark red solid). UV-Vis (CH<sub>2</sub>Cl<sub>2</sub>)  $\lambda_{\max}$ , ( $\epsilon \times 10^{-3}$ ) nm: 416 (214), 542 (10.3), 577 (2.3). IR

(KBr)  $\nu_{\max}$ ,  $\text{cm}^{-1}$ : 3440 (NH), 1719 (C=O). MALDI-MS Found:  $[\text{M}]^+$  771.21; ' $\text{C}_{48}\text{H}_{29}\text{CuN}_5\text{O}_2$ ' requires  $[\text{M}]^+$  771.32.

[2-(3'-Maleimido)-5,10,15,20-tetrakis(pentafluorophenyl)porphyrinato]zinc (II) (**5**) (129 mg, yield 76%). UV-Vis ( $\text{CH}_2\text{Cl}_2$ )  $\lambda_{\max}$ , ( $\epsilon \times 10^{-3}$ ) nm: 421 (523), 553 (22.0), 590 (6.32). IR (KBr)  $\nu_{\max}$ ,  $\text{cm}^{-1}$ : 3440 (NH), 1723 (C=O), 1499 (CF), 1285 (CF).  $^1\text{H}$  NMR,  $\delta_{\text{H}}$  ( $\text{CDCl}_3$ , 400 MHz), ppm: 6.91 (s, 2H, CH=CH), 8.77 (d, 1H,  $J = 4.8$  Hz,  $\beta$ -H), 8.90 (m, 2H,  $\beta$ -H), 8.97 (m, 4H,  $\beta$ -H).  $^{19}\text{F}$  NMR,  $\delta_{\text{F}}$  ( $\text{CDCl}_3$ , 376 MHz), ppm: -135.9 (dd, 2F,  $J = 24.3, 5.5$  Hz), -139.2 (dd, 1F,  $J = 23.0, 5.5$  Hz), -139.6 (dd, 4F,  $J = 16.5, 8.2$  Hz), -155.6 (t, 1F,  $J = 19.2$  Hz), -156.1 (q, 3F,  $J = 19.2$  Hz), -164.9 (dd, 6F,  $J = 46.7, 22.0$  Hz), -165.2 (dd, 2F,  $J = 42.7, 6.2$  Hz). APCI-MS Found:  $[\text{M}]^+$  1133.16; ' $\text{C}_{48}\text{H}_9\text{F}_{20}\text{N}_5\text{O}_2\text{Zn}$ ' requires  $[\text{M}]^+$  1132.97.

3.1.10. Preparation of carborane succinimidyl thioethers of 5,10,15,20-tetraarylporphyrins (**32-35**).

To a solution of maleimidoporphyrin (0.06 mmol) in  $\text{CHCl}_3$  (10 mL) mercaptocarborane (12 mg, 0.07 mmol) and NaOAc (5 mg, 0.06 mmol) were added and reaction mixture was heated at reflux under argon for 8 h. After completion of the reaction (TLC control) the solvent was removed under reduced pressure. The residue was purified by column chromatography on silica gel using  $\text{CH}_2\text{Cl}_2$  as an eluent.

2-{3-[(*o*-Carboran-1'-yl)thio]pyrrolidine-2,5-dione-1-yl}-5,10,15,20-tetraphenylporphyrin (**32**) (44 mg, yield 83%). UV-Vis ( $\text{CH}_2\text{Cl}_2$ )  $\lambda_{\max}$ , ( $\epsilon \times 10^{-3}$ ) nm: 421 (288), 519 (14.8), 553 (4.93), 592 (4.62), 648 (5.06). IR (KBr)  $\nu_{\max}$ ,  $\text{cm}^{-1}$ : 3438 (NH), 3054 (carborane CH), 2581 (BH), 1724 (C=O).  $^1\text{H}$  NMR,  $\delta_{\text{H}}$  ( $\text{CDCl}_3$ , 400 MHz), ppm: -2.72 (br s, 2H, NH), 2.55 (dd, 1H,  $J = 18.8, 6.4$  Hz, CH), 2.99 (dd, 1H,  $J = 18.8, 10.2$  Hz, CH), 3.69 (dd, 1H,  $J = 10.2, 6.4$  Hz, CH), 4.10 (br s, 1H, carborane CH), 7.80 (m, 12H, Ph), 8.24 (m, 8H, Ph), 8.65 (d, 1H,  $J = 4.8$  Hz,  $\beta$ -H), 8.73 (s, 1H,  $\beta$ -H), 8.81 (m, 2H,  $\beta$ -H), 8.88 (d, 1H,  $J = 5.1$  Hz,  $\beta$ -H), 8.95 (dd, 2H,  $J = 6.4, 4.8$  Hz,  $\beta$ -H).  $^{11}\text{B}$  NMR,  $\delta_{\text{B}}$ , ( $\text{CDCl}_3$ , 128 MHz), ppm: -0.8 (d, 1B,  $J = 151$  Hz), -4.4 (d, 1B,  $J = 144$  Hz), -9.2 (d, 4B,  $J = 142$  Hz), -12.3 (d, 4B,  $J = 168$  Hz). MALDI-MS Found:  $[\text{M}]^+$  886.99; ' $\text{C}_{50}\text{H}_{43}\text{B}_{10}\text{N}_5\text{O}_2\text{S}$ ' requires  $[\text{M}]^+$  886.08.

2-{3-[(*m*-Carboran-9'-yl)thio]pyrrolidine-2,5-dione-1-yl}-5,10,15,20-tetraphenylporphyrin (**33**) (47 mg, yield 88%). UV-Vis ( $\text{CH}_2\text{Cl}_2$ )  $\lambda_{\max}$ , ( $\epsilon \times 10^{-3}$ ) nm: 420 (290), 517 (14.5), 556 (4.83), 591 (4.63), 649 (5.02). IR (KBr)  $\nu_{\max}$ ,  $\text{cm}^{-1}$ : 3331 (NH), 3054 (carborane CH), 2603 (BH), 1723 (C=O).  $^1\text{H}$  NMR,  $\delta_{\text{H}}$  ( $\text{CDCl}_3$ , 400 MHz), ppm: -2.72 (br s, 2H, NH), 2.75 (dd, 1H,  $J = 18.8, 5.1$  Hz, CH), 2.91 (dd, 2H,  $J = 18.9, 9.4$  Hz,  $\text{CH}_2$ ), 3.00 (br s, 2H, carborane CH), 7.77 (dd, 12H,  $J = 12.7, 6.8$  Hz, Ph), 8.17 (dd, 2H,  $J = 18.8, 6.4$  Hz, Ph), 8.25 (dd, 6H,  $J = 18.6, 6.8$  Hz, Ph), 8.63 (d, 1H,  $J = 4.5$  Hz,  $\beta$ -H), 8.76 (s, 1H,  $\beta$ -H), 8.83 (dd, 3H,  $J = 17.5, 4.5$  Hz,  $\beta$ -H), 8.87 (d, 1H,  $J = 5.1$  Hz,  $\beta$ -H), 8.94 (s, 2H,  $\beta$ -H).  $^{11}\text{B}$  NMR,  $\delta_{\text{B}}$ , ( $\text{CDCl}_3$ , 128 MHz),

Journal Pre-proof  
ppm: -0.7 (br s, 1B, B<sup>9</sup>), -6.3 (d, 2B,  $J = 135$  Hz), -9.7 (d, 1B,  $J = 147$  Hz), -13.7 (d, 5B,  $J = 159$  Hz), -17.3 (d, 1B,  $J = 180$  Hz). MALDI-MS Found:  $[M]^+$  886.41; 'C<sub>50</sub>H<sub>43</sub>B<sub>10</sub>N<sub>5</sub>O<sub>2</sub>S' requires  $[M]^+$  886.08.

2-{3-[(*m*-Carboran-9'-yl)thio]pyrrolidine-2,5-dione-1-yl}-5,10,15,20-tetrakis[4-(trifluoromethyl)phenyl]porphyrin (**34**) (66 mg, yield 95%). UV-Vis (CH<sub>2</sub>Cl<sub>2</sub>)  $\lambda_{\max}$ , ( $\epsilon \times 10^{-3}$ ) nm: 419 (323), 517 (21.8), 551 (6.17), 592 (7.08), 648 (5.58). IR (KBr)  $\nu_{\max}$ , cm<sup>-1</sup>: 3329 (NH), 3060 (carborane CH), 2606 (BH), 1725 (C=O), 1324 (CF). <sup>1</sup>H NMR,  $\delta_{\text{H}}$  (CDCl<sub>3</sub>, 400 MHz), ppm: -2.74 (br s, 2H, NH), 2.85 (d, 2H,  $J = 6.5$  Hz, CH<sub>2</sub>), 2.98 (s, 1H, CH), 3.08 (br s, 2H, carborane CH), 8.03 (d, 2H,  $J = 8.2$  Hz, Ph), 8.09 (t, 6H,  $J = 7.9$  Hz, Ph), 8.35 (m, 8H, Ph), 8.65 (t, 1H,  $J = 2.5$  Hz,  $\beta$ -H), 8.71 (s, 1H,  $\beta$ -H), 8.77 (m, 2H,  $\beta$ -H), 8.83 (d, 1H,  $J = 5.1$  Hz,  $\beta$ -H), 8.92 (s, 2H,  $\beta$ -H). <sup>11</sup>B NMR,  $\delta_{\text{B}}$ , (CDCl<sub>3</sub>, 128 MHz), ppm: -0.2 (s, 1B, B<sup>9</sup>), -7.1 (d, 2B,  $J = 163$  Hz), -10.8 (d, 1B,  $J = 147$  Hz), -14.0 (d, 2B,  $J = 177$  Hz), -15.4 (d, 2B,  $J = 173$  Hz), -19.0 (d, 1B,  $J = 182$  Hz), -23.0 (d, 1B,  $J = 182$  Hz). <sup>19</sup>F NMR,  $\delta_{\text{F}}$  (CDCl<sub>3</sub>, 376 MHz), ppm: -62.2 (s, 3F), -62.1 (d, 9F,  $J = 4.1$  Hz). MALDI-MS Found:  $[M]^+$  1158.19; 'C<sub>54</sub>H<sub>39</sub>B<sub>10</sub>F<sub>12</sub>N<sub>5</sub>O<sub>2</sub>S' requires  $[M]^+$  1158.08.

[2-{3-[(*m*-Carboran-9'-yl)thio]pyrrolidine-2,5-dione-1-yl}-5,10,15,20-tetrakis(pentafluorophenyl)porphyrinato]zinc (II) (**35**) (61 mg, yield 78%). UV-Vis (CH<sub>2</sub>Cl<sub>2</sub>)  $\lambda_{\max}$ , ( $\epsilon \times 10^{-3}$ ) nm: 422 (336), 553 (17.0), 590 (4.56). IR (KBr)  $\nu_{\max}$ , cm<sup>-1</sup>: 3435 (NH), 3067 (carborane CH), 2607 (BH), 1729 (C=O), 1494 (CF). <sup>1</sup>H NMR,  $\delta_{\text{H}}$  (CDCl<sub>3</sub>, 400 MHz), ppm: 2.83 (dd, 2H,  $J = 13.7, 6.7$  Hz CH<sub>2</sub>), 3.63 (dd, 1H,  $J = 14.3, 6.3$  Hz, CH), 3.08 (br s, 2H, carborane CH), 9.10 (t, 1H,  $J = 4.9$  Hz,  $\beta$ -H), 9.24 (d, 1H,  $J = 4.7$  Hz,  $\beta$ -H), 9.30 (d, 5H,  $J = 4.9$  Hz,  $\beta$ -H). <sup>11</sup>B NMR,  $\delta_{\text{B}}$ , (CDCl<sub>3</sub>, 128 MHz), ppm: -0.5 (br s, 1B, B<sup>9</sup>), -6.4 (d, 2B,  $J = 161$  Hz), -9.8 (d, 1B,  $J = 149$  Hz), -13.7 (m, 5B,  $J = 156$  Hz), -17.1 (d, 1B,  $J = 179$  Hz). <sup>19</sup>F NMR,  $\delta_{\text{F}}$  (CDCl<sub>3</sub>, 376 MHz), ppm: -134.8 (d, 1F,  $J = 19.2$  Hz), -135.7 (d, 1F,  $J = 19.2$  Hz), -136.0 (d, 2F,  $J = 22.0$  Hz), -136.8 (t, 3F,  $J = 24.7$  Hz), -136.9 (d, 1F,  $J = 19.2$  Hz), -148.9 (t, 1F,  $J = 22.0$  Hz), -151.9 (quin, 3F,  $J = 19.2$  Hz), -157.6 (t, 1F,  $J = 19.2$  Hz), -161.7 (d, 6F,  $J = 19.2$  Hz), -163.4 (t, 1F,  $J = 16.2$  Hz). MALDI-MS Found:  $[M]^+$  1309.03; 'C<sub>50</sub>H<sub>21</sub>B<sub>10</sub>F<sub>20</sub>N<sub>5</sub>O<sub>2</sub>SZn' requires  $[M]^+$  1309.26.

### 3.1.11. Demetallation of porphyrin **35**.

To a solution of porphyrin **35** (40 mg 0.03 mmol) in CH<sub>2</sub>Cl<sub>2</sub> (8.0 mL) CF<sub>3</sub>COOH (1.0 mL) was added and the reaction mixture was stirred for 2 min at room temperature. After demetallation (TLC monitoring, CHCl<sub>3</sub>-hexane 2:1) the mixture was treated with water (30 mL), extracted with CH<sub>2</sub>Cl<sub>2</sub> (10 mL), and the organic solution was dried over anhydrous Na<sub>2</sub>SO<sub>4</sub>. After removal of the solvent under reduced pressure, the residue was washed with hexane to give porphyrin **36** (34 mg, yield 91%) as a dark violet solid. UV-Vis (CH<sub>2</sub>Cl<sub>2</sub>)  $\lambda_{\max}$ , ( $\epsilon \times 10^{-3}$ ) nm: 417 (313), 511 (15.7), 549 (3.81), 586 (4.63), 647 (2.02). IR (KBr)  $\nu_{\max}$ , cm<sup>-1</sup>: 3331 (NH), 3065

Journal Pre-proof  
(carborane CH), 2609 (BH), 1715 (C=O), 1499 (CF).  $^1\text{H}$  NMR,  $\delta_{\text{H}}$  ( $\text{CDCl}_3$ , 400 MHz), ppm: –2.89 (brs, 2H, NH), 2.63 (dd, 2H,  $J = 18.8, 5.6$  Hz,  $\text{CH}_2$ ), 3.68 (dd, 1H,  $J = 18.8, 9.6$  Hz, CH), 3.87 (br s, 2H, carborane CH), 9.19 (s, 1H,  $\beta$ -H), 9.32 (br s, 3H,  $\beta$ -H), 9.46 (d, 1H,  $J = 4.3$  Hz,  $\beta$ -H), 9.50 (br s, 2H,  $\beta$ -H).  $^{11}\text{B}$  NMR,  $\delta_{\text{B}}$ , ( $\text{CDCl}_3$ , 128 MHz), ppm: –2.3 (br s, 1B,  $\text{B}^{\text{9}}$ ), –5.8 (d, 2B,  $J = 165$  Hz), –8.9 (d, 1B,  $J = 154$  Hz), –12.5 (d, 2B,  $J = 168$  Hz), –13.8 (d, 2B,  $J = 168$  Hz), –17.5 (d, 1B,  $J = 182$  Hz), –20.6 (d, 1B,  $J = 182$  Hz).  $^{19}\text{F}$  NMR,  $\delta_{\text{F}}$  ( $\text{CDCl}_3$ , 376 MHz), ppm: –136.9 (dd, 1F,  $J = 22.9, 6.5$  Hz), –137.5 (dd, 1F,  $J = 22.9, 6.5$  Hz), –139.2 (ddd, 2F,  $J = 50.5, 22.9, 6.2$  Hz), –139.9 (dd, 4F,  $J = 24.8, 6.2$  Hz), –151.5 (t, 1F,  $J = 20.6$  Hz), –154.9 (t, 1F,  $J = 20.6$  Hz), –155.3 (ddd, 2F,  $J = 20.5, 19.6, 5.1$  Hz), –159.7 (td, 1F,  $J = 22.7, 6.2$  Hz), –164.1 (m, 2F), –164.3 (dd, 2F,  $J = 16.5, 8.3$  Hz), –164.5 (dd, 2F,  $J = 20.6, 8.3$  Hz), –165.5 (ddd, 1F,  $J = 22.9, 20.6, 8.2$  Hz). MALDI-MS Found:  $[\text{M}]^+$  1245.23; ‘ $\text{C}_{50}\text{H}_{23}\text{B}_{10}\text{F}_{20}\text{N}_5\text{O}_2\text{S}$ ’ requires  $[\text{M}]^+$  1245.89.

### 3.1.12. Reaction of cysteine with porphyrins **3**, **4**. General procedure.

To a solution (0.03 mmol) of maleimideporphyrins **3** or **4** in 5 ml THF- $\text{H}_2\text{O}$  (3:2) system L-cysteine methyl ester hydrochloride (6.0 mg, 0.04 mmol) was added and reaction was stirred at room temperature for 8 h under argon. After completion of reaction (TLC control), the reaction mixture was treated with water (20 mL) and  $\text{Et}_3\text{N}$  (0.2 mL), extracted with  $\text{CHCl}_3$  (2x10 mL), dried over anhydrous  $\text{Na}_2\text{SO}_4$  and concentrated *in vacuo* to give the desired compounds.

2-[3-(S-Cysteinyl)pyrrolidine-2,5-dione-1-yl]-5,10,15,20-tetrakis[4-(trifluoromethyl)phenyl]porphyrin (**38**) (31 mg, yield 93%). UV-Vis ( $\text{CH}_2\text{Cl}_2$ )  $\lambda_{\text{max}}$ , ( $\epsilon \times 10^{-3}$ ) nm: 419 (269), 518 (14.0), 549 (4.47), 592(5.03), 647(4.47) IR (KBr)  $\nu_{\text{max}}$ ,  $\text{cm}^{-1}$ : 3331(NH), 1724 (C=O), 1324 (CF).  $^1\text{H}$  NMR,  $\delta_{\text{H}}$  ( $\text{CDCl}_3$ , 400 MHz), ppm: –2.81 (brs, 2H, NH), 2.68 (dd, 2H,  $J = 19.1, 10.4$  Hz,  $\text{NH}_2$ ), 3.16 (d, 2H,  $J = 13.3$  Hz,  $\text{CH}_2$ ), 3.27 (d, 2H,  $J = 13.1$  Hz,  $\text{CH}_2$ ), 3.77 (t, 3H,  $J = 9.0$  Hz,  $\text{CH}_3$ ), 3.97 (t, 1H,  $J = 6.9$  Hz, CH), 4.37 (t, 1H,  $J = 6.9$  Hz, CH), 8.07 (t, 8H,  $J = 6.4$  Hz, Ph), 8.30 (m, 8H, Ph), 8.63 (d, 1H,  $J = 3.1$  Hz,  $\beta$ -H), 8.70 (d, 1H,  $J = 3.1$  Hz,  $\beta$ -H), 8.74 (d, 2H,  $J = 4.4$  Hz,  $\beta$ -H), 8.81 (br s, 1H,  $\beta$ -H), 8.89 (br s, 2H,  $\beta$ -H).  $^{19}\text{F}$  NMR,  $\delta_{\text{F}}$  ( $\text{CDCl}_3$ , 376 MHz), ppm: –62.3 (d, 2F,  $J = 11.2$  Hz), –62.1 (br s, 9F), –61.90 (d, 1F,  $J = 14.0$  Hz). APSI-MS Found:  $[\text{M}+\text{H}]^+$  1118.1; ‘ $\text{C}_{56}\text{H}_{37}\text{F}_{12}\text{N}_6\text{O}_4\text{S}$ ’ requires  $[\text{M}+\text{H}]^+$  1117.97.

{2-[3-(S-Cysteinyl)pyrrolidine-2,5-dione-1-yl]-5,10,15,20-tetraphenylporphyrinato} copper (II) (**39**) (26 mg, yield 96%). UV-Vis ( $\text{CH}_2\text{Cl}_2$ )  $\lambda_{\text{max}}$ , ( $\epsilon \times 10^{-3}$ ) nm: 417 (208), 541 (11.0), 577 (2.88). IR (KBr)  $\nu_{\text{max}}$ ,  $\text{cm}^{-1}$ : 3448 (NH), 1721 (C=O). APSI-MS Found:  $[\text{M}]^+$  906.14; ‘ $\text{C}_{52}\text{H}_{38}\text{CuN}_6\text{O}_4\text{S}$ ’ requires  $[\text{M}]^+$  906.51.

### 3.2. UV-visible and fluorescence spectroscopy

Electronic absorption spectra were recorded for new compounds (5  $\mu\text{M}$  solutions in DMSO) on a UV-3101PC spectrophotometer (Shimadzu, Japan) in the range of 300–800

nm in a quartz cuvette with the optical path length 1 cm at room temperature. Molar extinction coefficients were determined on a Vibra AF-R220E, Shinko Denshi, Japan). Results of repetitive measurements varied within 7% ( $\epsilon_{440} = 2 \times 10^5 \text{ M}^{-1} \text{ cm}^{-1}$ ). A Beer-Lambert function was observed for all tested compounds at 1-10  $\mu\text{M}$ . Fluorescence spectra were obtained by analyzing the diluted solutions (absorbance values  $< 0.1$  at the excitation wavelength) using a FluoTime 300 fluorimeter (PicoQuant GmbH, Germany) with sampling interval 1 nm for fluorescence and 2 nm for phosphorescence measurements. A Solea supercontinuum laser (2.5 MHz, bandwidth 5 nm,  $1 \times 1$  cm quartz cuvette) was used as an excitation source.

### 3.3. Measurement of fluorescence quantum yield

Fluorescence quantum yields of **1-3**, **5**, **32**, **34** in ethanol were measured with rhodamine 6G as a standard ( $Q=0.94$  in ethanol) and calculated using the equation (1) [63,64]:

$$Q = Q_r \times (I \times OD_r \times n^2 / I_r \times OD \times n_r^2) \quad (1),$$

where  $Q$  is the quantum yield,  $I$  is the integrated intensity,  $OD$  is the optical density, and  $n$  is the refractive index.  $R$  refers to rhodamine 6G. The optical density ( $< 0.05$  for all samples to avoid the inner filter effect) was matched for tested compounds and reference. Measurements were performed in a quartz cell cuvette (optical path length 1 cm) at room temperature.

### 3.4. Measurements of steady-state singlet oxygen phosphorescence

Steady-state singlet oxygen phosphorescence measurements were carried out on a FluoTime 300 fluorimeter equipped with NIR PMT Module H10330-45 (Hamamatsu, Japan) coupled to a single photon counter TimeHarp TCSPC (PicoQuant GmbH, Germany). Absorbance of new porphyrins and RB in ethanol (at 530 nm for RB (EtOH); 523 nm for **1**, **32**, **3**; 542 nm for **5**; 515 nm for **2** and **34**) were matched with the reference value  $\Phi_{\Delta} = 0.79$  for RB in methanol [65, 66].  $\text{O}_2(^1\Delta_g)$  phosphorescence was detected at  $90^\circ$  relative to the excitation beam. Corrected emission spectra were recorded with the integration time 5 s between 1230 nm and 1330 nm. Total phosphorescence intensities were calculated by integrating the emission band centered at 1278 nm. Experiments were performed at room temperature.

Singlet oxygen quantum yields ( $\Phi_{\Delta_s}$ ) were determined using the method described in [67] and the equation (2):

$$\Phi_{\Delta_s} = (I_r \times I_{\Delta_s} \times \tau_r / I_s \times I_{\Delta_r} \times \tau_s) \times \Phi_{\Delta_r} \quad (2),$$

where  $I_s$  and  $I_r$  represent the absorbed incident light, and  $I_{\Delta_s}$  and  $I_{\Delta_r}$  are singlet oxygen integrated emission intensities at 1230-1330 nm for tested compound and the reference, respectively.  $\tau_r$  and  $\tau_s$  are the singlet oxygen phosphorescence lifetimes in the reference and the sample solutions;  $\Phi_{\Delta_r}$  is the quantum yield of singlet oxygen of the reference compound. The analysis did not require the calculation of the absorbed incident light  $I_{\text{abs}}$  because the optical

densities of tested and reference compounds at the excitation wavelength were equal.  $\Phi_{\Delta}$  measurements were performed in triplicate (standard deviation <15%).  $T_r$  for  $O_2(^1\Delta_g)$  in MeOH is 10  $\mu$ s and  $\tau_r$  for  $O_2(^1\Delta_g)$  in EtOH is 14.5  $\mu$ s [67]. The value  $\Phi_{\Delta}$  = 0.86 for RB in ethanol is in agreement with  $\Phi_{\Delta}$  = 0.90 obtained in the present study.

### 3.5. Fluorescence lifetime

Fluorescence lifetimes were measured by the time correlated single photon counting using a FluoTime 300 fluorimeter (PicoQuant). Excitation/emission at 515 nm/660 nm for **1**, **3**, **34**; 507 nm/645 nm for **32**, **2**; 553 nm/650 nm for **5** was performed with a Solea™ supercontinuum laser. Excitation pulse frequency was set at 10 MHz for all tested compounds except **5** (40 MHz); excitation/detection bandpass 5 nm/10 nm, bin width 32 ps. In each case, the instrument response function (IRF) was recorded at the excitation wavelength with the Ludox scattering probe. Plots of the residuals showed random distributions in all cases. Fluorescence decays were fitted using a FluoFit software (PicoQuant). Fluorescence lifetimes were estimated by the multi-exponential model according to equation (3):

$$I(t) = \int_{-\infty}^t IRF(t') \sum_{i=1}^n I_i \times \exp((-t-t')/\tau_i) dt' \quad (3),$$

where  $I_i$  is the amplitude,  $\tau_i$  is the lifetime of the  $i$ -th decay component,  $n$  is the number of the decay component. The quality of fit was evaluated by a  $\chi^2$  test (close to 1 for the best fit) as well as by control of residuals and autocorrelation function.

### 3.6. Flash photolysis

The triplet-triplet absorption spectra and kinetics decay of the triplet states were measured using a conventional flash photolysis setup (optical path length 20 cm, excitation was performed through multi-band blue-green optical absorption filters 400-510 nm or 480-560 nm, 80 J/15  $\mu$ s). Signals were recorded by PMT-38 photomultiplier (MELZ, USSR) at 400-760 nm. All solutions were degassed before use.

### 3.7. Binding to HSA

Solutions of porphyrin derivatives and HSA in PBS were mixed and allowed to equilibrate for 1 h before analysis. Binding was monitored at room temperature. The absorption spectra of porphyrins (1  $\mu$ M) in the absence or presence of HSA (duplicate dilutions from 0.2  $\mu$ M to 50  $\mu$ M) were recorded within 300–800 nm range with a 2 nm increment (slit width 2 nm). Values of the dissociation constant ( $K_d$ ) for porphyrin-HSA complexes were calculated from the absorption measurements at 425 nm with GraphPad Prism 6 (non-linear regression, saturation binding: one site specific binding) using equation (4):

$$A = A_{\max} \times [HSA] / (K_d + [HSA]) \quad (4),$$

where [HSA] is HSA concentration,  $A_{\max}$  is the absorption of total bound porphyrin,  $A$  is the absorption at different HSA concentrations. The  $A_{\max}$  values were obtained by hyperbolic extrapolation of experimental data to the higher HSA concentrations.

### 3.8. Cell culture, cytotoxicity and intracellular accumulation assays

The HCT116 human colon carcinoma cell line (American Type Culture Collection, Manassas, VA) was propagated in Dulbecco modified Eagle's medium supplemented with 10% fetal calf serum (HyClone, Logan, UT), 2 mM *L*-glutamine, 100 U/ml penicillin and 100  $\mu$ g/ml streptomycin (PanEco, Russia) (complete medium) at 37°C, 5% CO<sub>2</sub> in a humidified atmosphere. Compounds **1-3**, **5**, **32** and **34** were dissolved as 10 mM stock solutions in DMSO and stored at –20°C. Aqueous dilutions in the complete medium were prepared immediately before the experiments. Dark cytotoxicity of new compounds was assessed in a formazan conversion assay (MTT-test) after a 72 h continuous drug exposure [68]. The cytotoxicity at a given drug concentration was calculated as the percentage of absorbance in wells with drug-treated cells to that of vehicle control cells (100%). The IC<sub>50</sub> (50% growth inhibitory concentration) was defined as the concentration of the compound that inhibited MTT conversion by 50%. To measure light activated cytotoxicity, HCT116 cells (10<sup>4</sup> in 190  $\mu$ l of complete medium, a 96-well format) were treated with **1-3**, **5**, **32** or **34** (0-50  $\mu$ M each, twofold serial dilutions) for 24 h at 37°C, 5% CO<sub>2</sub>. After the completion of cell exposure the compounds were washed off with saline, and cell monolayers were illuminated with either 420 nm (1.5 J/cm<sup>2</sup>) or 650 nm (5 J/cm<sup>2</sup> or 30 J/cm<sup>2</sup>) lasers followed by the addition of fresh medium supplemented with 0.5 mg/ml 3-(4,5-dimethylthiazol-2-yl)-2,5-diphenyltetrazolium bromide (MTT), incubation for 2 h and measurement of absorbance at 540 nm.

For measurement of intracellular accumulation of **1-3**, **5**, **32** and **34** the HCT116 cells (5x10<sup>4</sup> in 60 mm Petri dishes) were treated with 5  $\mu$ M of each compound for 24 h at 37°C, 5% CO<sub>2</sub>. Cells were washed three times with an ice cold saline, detached with trypsin-EDTA solution and immediately analyzed on FACSDiva flow cytometer (BD Biosciences; excitation 405 nm, emission 710 nm and 780 nm). Two emission wavelengths were used for an accurate detection of fluorescence keeping in mind spectral differences (although insignificant) of individual compounds. Ten thousand fluorescent events were collected per each sample. Data were analyzed using FACSDiva software.

### 3.9. Fluorescence microscopy

The HCT116 cells were grown on round glass coverslips for up to 72 h to reach 70% confluence by the day of experiment. The medium was changed for the same medium without serum, and compounds **1**, **2**, **3**, **32** and **34** (1  $\mu$ M each) were added to the cell culture for 1 h, then washed with saline. The complete medium was added. Cell imaging was performed on an

inverted microscope Eclipse Ti-E with the confocal module A1 (Nikon Corp., Japan). The following parameters were used for cell visualization: 512×512 pixel images were registered with an Apo TIRF 60x/Oil DIC N2 objective, fluorescence of porphyrins was excited with a 405 nm diode laser, emission was registered using BS 20/80 filter within 560-570 nm. Wavelengths were chosen based on autofluorescence of **1**, **2**, **3**, **32** and **34** in DMSO. Colocalization of **32** with organelles was detected using LysoTracker Green DND-26 (Invitrogen), MitoTracker GreenFM (Invitrogen) and transferrin-FITC (Nanocs) for lysosomes, mitochondria and endosomes, respectively. Cell staining was performed according to manufacturer's instructions. Fluorescence of LysoTracker Green DND-26, MitoTracker GreenFM and transferrin-FITC was excited with a 488 nm laser, filter BS 525/50 nm. Simultaneous visualization of **32** and organelles was performed by a dual channel analysis of optical planes in a multichannel regimen using a set of dichroic mirrors and filters. Pinholes were set up as recommended by the manufacturer. Images were analyzed with NIS-Elements Nikon software (Nikon).

For detection of superoxide anion radicals and cell viability upon photoactivation of **32**, HCT116 cells were grown in 35 mm Petri dishes with a glass bottom at 37<sup>0</sup>C, 5% CO<sub>2</sub> for 48 h. Compound **32** (5 μM) or vehicle (0.05% DMSO) were added for another 24 h. Then cells were washed with the culture medium and incubated in fresh culture medium for 3 h followed by loading with 5 μM MitoSOX Red, 50 nM MitoTracker Red CMX ROS and 18 μM Hoechst 33342 (all dyes from Thermo Fisher Sci., Waltham, MA) for 10 min at 37°C. Cells were washed three times with saline. For detection of the plasma membrane integrity PI (10 μg/ml) was added to the complete medium 10 min prior to taking images. To photoactivate compound **32** cells were illuminated with a 405 nm laser (39 ps, 40 MHz, 2 mW). Cell morphology was analyzed on a Leica TCS SPE 5 confocal laser scanning microscope (Leica Microsystems GmbH, Germany). Autofluorescence of **32** did not interfere with other dyes.

### **Acknowledgements**

This work was performed with the financial support from Ministry of Science and Higher Education of the Russian Federation using the equipment of Center for molecular composition studies of INEOS RAS.

### **Appendix A. Supplementary data**

Supplementary data to this article can be found online at <https://>

### **References**

- [1] Urbani M, Grätzel M, Nazeeruddin MK, Torres T. *Meso*-substituted porphyrins for dye-sensitized solar cells. *Chem Rev* 2014; 114(24): 12330–96. <https://doi.org/10.1021/cr5001964>.
- [2] Lu F, Feng Y, Wang X, Zhao Y, Yang G, Zhang J, et al. Influence of the additional electron-withdrawing unit in  $\beta$ -functionalized porphyrin sensitizers on the photovoltaic performance of

dye-sensitized solar cells. *Dyes Pigments* 2017; 139: 255–63.

<https://doi.org/10.1016/J.dyepig.2016.12.02710>.

[3] Paolesse R, Nardis S, Monti D, Stefanelli M, Di Natale C. Porphyrinoids for chemical sensor applications. *Chem Rev* 2017; 117(4): 2517–83. <https://doi.org/10.1021/acs.chemrev.6b00361>.

[4] Ishihara S, Labuta J, Van Rossom W, Ishikawa D, Minami K, Hill J-P, et al. Porphyrin-based sensor nanoarchitectonics in diverse physical detection modes. *Phys Chem Chem Phys* 2014; 16(21): 9713–46. <https://doi.org/10.1039/c3cp55431g>.

[5] Jurowa M, Schuckmanb AE, Batteas JD, Drain CM. Porphyrins as molecular electronic components of functional devices. *Coord Chem Rev* 2010; 254(19-20): 2297–310.

<https://doi.org/10.1016/J.ccr.2010.05.014>.

[6] Kalnoor BS, Bisht PB, Jena KC, Velkannan V, Bhyrappa P. Mixed  $\beta$ -pyrrole substituted *meso*-tetraphenylporphyrins and their metal complexes: optical nonlinearity using degenerate four wave mixing technique. *J Phys Chem A* 2013; 117(34): 8216–21.

<https://doi.org/10.1021/Jp404451x>.

[7] Senge MO, Fazekas M, Notaras EGA, Blau WJ, Zawadzka M, Locos OB, et al. Nonlinear optical properties of porphyrins. *Adv Mater* 2007; 19(19): 2737–74.

<https://doi.org/10.1002/adma.200601850>.

[8] Barona-Castaño JC, Carmona-Vargas CC, Brocksom TJ, de Oliveira KT. Porphyrins as catalysts in scalable organic reactions. *Molecules* 2016; 2193: 310–337.

<https://doi.org/10.3390/molecules21030310>.

[9] Huynha E, Zheng G. Porphysome nanotechnology: A paradigm shift in lipid-based supramolecular structures. *NanoToday* 2014; 9: 212–222.

<http://doi.org/10.1016/j.nantod.2014.04.012>.

[10] Allison RR, Mota HC, Bagnato VS, Sibata CH. Bio-nanotechnology and photodynamic therapy-state of the art review. *Photodiagnosis Photodyn Ther* 2008; 5(1): 19–28.

<https://doi.org/10.1016/J.pdpdt.2008.02.001>.

[11] Pandey RK, Zheng G. Porphyrins as photosensitizers in photodynamic therapy. In: Kadish KM, Smith KM, Guilly R, editors. *The porphyrin handbook*. vol 6, San Diego: Academic Press; 2000, p. 157–230.

[12] Macdonald IJ, Dougherty TJ. Basic principles of photodynamic therapy. *J Porphyr Phthalocyanines* 2001; 05: 105–29. <https://doi.org/10.1002/jpp.328>.

[13] Agostinis P, Berg K, Cengel KA, Foster TH, Girotti AW, Gollnick SO, et al. Photodynamic therapy of cancer: an update. *CA. Cancer J Clin* 2011; 61(4): 250–81.

<https://doi.org/10.3322/caac.20114>.

- [14] Ol'shevskaya VA, Zaitsev AV, Shtil AA. Carborane derivatives of porphyrins and chlorines for photodynamic and boron neutron capture therapies: synthetic strategies. In: Hey-Hawkins E, Viñas Teixidor C, editors. Boron-based compounds: potential and emerging applications in medicine, Hoboken: Wiley; 2018, p. 343-370. <https://doi.org/10.1002/9781119275602.ch3.3>.
- [15] Berezin DB. The macrocyclic effect and structural chemistry of porphyrins. Moscow: Krasand; 2010. (in Russ.)
- [16] Alonso CMA, Palumbo A, Bullous AJ, Pretto F, Neri D, Boyle RW. Site-specific and stoichiometric conjugation of cationic porphyrins to antiangiogenic monoclonal antibodies. *Bioconjug Chem* 2010; 21(2): 302–13. <https://doi.org/10.1021/bc9003537>.
- [17] Giuntini F, Alonso CMA, Boyle RW. Synthetic approaches for the conjugation of porphyrins and related macrocycles to peptides and proteins. *Photochem Photobiol Sci* 2011; 10(5): 759-91. <https://doi.org/10.1039/c0pp00366b>.
- [18] Aksenova AA, Sebyakin YL, Mironov AF. Conjugates of porphyrins with carbohydrates. *Russ J Bioorg Chem* 2003; 29(3): 201–19. <https://doi.org/10.1023/A:1023924213863>.
- [19] Zheng X, Pandey RK. Porphyrin-carbohydrate conjugates: impact of carbohydrate moieties in photodynamic therapy (PDT). *Anti-Cancer Agents Med Chem* 2008; 8(3): 241–68. <https://doi.org/10.2174/187152008783961897>.
- [20] Acherar S, Colombeau L, Frochot C, Vanderesse R. Synthesis of porphyrin, chlorin and phthalocyanine derivatives by azide-alkyne click chemistry. *Curr Med Chem* 2015; 22(28): 3217-54. <https://doi.org/10.2174/0929867322666150716115832>.
- [21] Schneider R, Tirand L, Frochot C, Vanderesse R, Thomas N, Gravier J, et al. Recent improvements in the use of synthetic peptides for a selective photodynamic therapy. *Anti-Cancer Agents Med Chem* 2006; 6(5): 469–488. <https://doi.org/10.2174/187152006778226503>.
- [22] Sussman D, Westendorf L, Meyer DW, Leiske CI, Anderson M, Okeley NM, et al. Engineered cysteine antibodies: an improved antibody-drug conjugate platform with a novel mechanism of drug-linker stability. *Protein Eng Des Sel* 2018; 31(2): 47-54. <https://doi.org/10.1093/protein/gzx067>.
- [23] Lyon RP, Setter JR, Bovee TD, Doronina SO, Hunter JH, Anderson ME, et al. Self-hydrolyzing maleimides improve the stability and pharmacological properties of antibody-drug conjugates. *Nature Biotechnol* 2014; 32:1059–62. <https://doi.org/10.1038/nbt.2968>.
- [24] St Amant AH, Lemen D, Florinas S, Mao S, Fazenbaker C, Zhong H, et al. Tuning the Diels-Alder reaction for bioconjugation to maleimide drug-linkers. *Bioconjug Chem* 2018; 29(7): 2406–14. <https://doi.org/10.1021/acs.bioconjchem.8b00320>.

- [25] Ravasco JMJM, Faustino H, Trindade A, Gois PMP. Bioconjugation with maleimides: a useful tool for chemical biology. *Chem Eur J* 2019; 25: 43–59.  
<https://doi.org/10.1002/chem.201803174>.
- [26] Tavares-Carreón F, Ruan X, Ford A, Valvano MA. Sulfhydryl labeling as a tool to investigate the topology of membrane proteins involved in lipopolysaccharide biosynthesis. *Methods Mol Biol* 2019; 1954: 203–13. [https://doi.org/10.1007/978-1-4939-9154-9\\_16](https://doi.org/10.1007/978-1-4939-9154-9_16).
- [27] Lorenzer C, Streußnig S, Tot E, Winkler AM, Merten H, Brandl F, et al. Targeted delivery and endosomal cellular uptake of DARPin-siRNA bioconjugates: Influence of linker stability on gene silencing. *Eur J Pharm Biopharm* 2019; 141: 37–50.  
<https://doi.org/10.1016/j.ejpb.2019.05.015>.
- [28] Gunnoo SB, Madder A. Chemical protein modification through cysteine. *Chembiochem* 2016; 17(7): 529–53. <https://doi.org/10.1002/cbic.201500667>.
- [29] Chen Y, Parr T, Holmes AE, Nakanishi K. Porphyrinmaleimides: towards thiol probes for cysteine residues in proteins. *Bioconjug Chem* 2008; 19(1): 5–9.  
<https://doi.org/10.1021/bc700267f>.
- [30] Bhyrappa P. Recent advances in mixed  $\beta$ -pyrrole substituted *meso*-tetraphenylporphyrins. *Tetrahedron Lett* 2016; 57(47): 5150–67. <https://doi.org/10.1016/J.tetlet.2016.10.010>.
- [31] Cerqueira AFR, Moura NMM, Vaz Serra V, Faustino MAF, Tomé AC, Cavaleiro JAS, et al.  $\beta$ -Formyl- and  $\beta$ -vinylporphyrins: magic building blocks for novel porphyrin derivatives. *Molecules* 2017; 22(8): 1269–313. <https://doi.org/10.3390/molecules22081269>.
- [32] Abdulaeva IA, Birin KP, Michalak J, Romieu A, Stern C, Bessmertnykh-Lemeune A, et al. On the synthesis of functionalized porphyrins and porphyrin conjugates via  $\beta$ -aminoporphyrins. *New J Chem* 2016; 40(7): 5758–74. <https://doi.org/10.1039/c5nJ03247d>.
- [33] Sunaina S, Aggarwal A, Bhupathiraju NVDK, Arianna G, Tiwari K, Drain C. M. Glycosylated porphyrins, phthalocyanines, and other porphyrinoids for diagnostics and therapeutics. *Chem Rev* 2015; 115(18): 10261–306 and references therein.  
<https://doi.org/10.1021/acs.chemrev.5b00244>.
- [34] Moisenovich MM, Ol'shevskaya VA, Rokitskaya TI, Ramonova AA, Nikitina RG, Savchenko AN, et al. Novel photosensitizers trigger rapid death of malignant human cells and rodent tumor transplants via lipid photodamage and membrane permeabilization. *PLoS One* 2010; 5(9): e12717. <https://doi.org/10.1371/journal.pone.0012717>.
- [35] Hanakova A, Bogdanova K, Tomankova K, Pizova K, Malohlava J, Binder S, et al. The application of antimicrobial photodynamic therapy on *S. aureus* and *E. coli* using porphyrin photosensitizers bound to cyclodextrin. *Microbiol Res* 2014;169(2-3):163–70.  
<https://doi.org/10.1016/j.micres.2013.07.005>.

- [36] Olshevskaya VA, Zaytsev AV, Savchenko AN, Shtil AA, Seong C-S, Kalinin VN. Boronated porphyrins and chlorins as potential anticancer drugs. *Bull Korean Chem Soc* 2007; 28(11): 1910–16. <https://doi.org/10.5012/bkcs.2007.28.11.1910>.
- [37] Bhupathiraju NVSDK, Vicente MGH. Synthesis of carborane-containing porphyrin derivatives for the boron neutron capture therapy of tumors. In: Paolesse R, Ed. *Applications of Porphyrinoids*, Berlin: Springer; 2014, p. 31-52. [https://doi.org/10.1007/7081\\_2013\\_111](https://doi.org/10.1007/7081_2013_111).
- [38] Adler AD, Longo FR, Finarelli JD, Goldmacher J, Assour, J, Korsakoff LJ. Simplified synthesis for *meso*-tetraphenylporphine. *Org Chem* 1967; 32(15): 476. <https://doi.org/10.1021/Jo01288a053>.
- [39] Lindsey JS, Schreiman IC, Hsu HC, Kearney PC, Marguerettaz AM. Rothmund and Adler-Longo reactions revisited: synthesis of tetraphenylporphyrins under equilibrium conditions. *J Org Chem* 1987; 52(5): 827-36. <https://doi.org/10.1021/Jo00381a022>.
- [40] Giraudeau A, Callot HJ, Jordan J, Ezhar I, Gross M. Substituent effects in the electroreduction of porphyrins and metalloporphyrins. *J Am Chem Soc* 1979; 101(14): 3857–62. <https://doi.org/10.1021/Ja00508a024>.
- [41] Wyřębek P, Ostrowski S. Synthesis of some  $\beta$ -nitro-*meso*-tetraphenylporphyrin derivatives. *J Porphyr Phthalocyanines* 2007; 11(11): 822-28. <https://doi.org/10.1142/S1088424607000941>.
- [42] Baldwin JE, Crossley MJ, DeBernardis J. Efficient peripheral functionalization of porphyrins. *Tetrahedron* 1982; 38(5): 685–92. [https://doi.org/10.1016/0040-4020\(82\)80211-1](https://doi.org/10.1016/0040-4020(82)80211-1).
- [43] Promarak V, Burn PL. A new synthetic approach to porphyrin- $\alpha$ -diones and a -2,3,12,13-tetraone: building blocks for laterally conjugated porphyrin arrays. *J Chem Soc, Perkin Trans 1* 2001; 1: 14–20. <https://doi.org/10.1039/b007389J>.
- [44] Zakharkin LI, Zhigareva GG. Synthesis and some reactions of mercapto derivatives of barenes. *Bull Acad Sci USSR Div Chem Sci (Engl. Transl.)* 1967; 16(6): 1308-10.
- [45] Pleřek J, Janousek Z, Heřmánek S. Chemistry of 9-mercapto-1,7-dicarba-*closo*-dodecaborane. *Collection Czechoslov Chem Commun* 1976; 43: 1332-34.
- [46] Gouterman M. Optical Spectra and electronic structure of porphyrins and related rings. In: Dolphin D, editor. *The Porphyrins, Volume III: Physical Chemistry, Part A*, New York: Academic Press; 1978, p. 1-165. <https://doi.org/10.1016/B978-0-12-220103-5.50008-8>.
- [47] Gouterman M, Rentzepis PM, Straub KD. *Porphyrins. Excited states and dynamics*. Washington: ACS Symposium Series, Amer Chemical Society; 1986. <https://doi.org/10.1021/bk-1986-0321>.
- [48] Quimby DJ, Longo FR. Luminescence studies on several tetraarylporphyrins and their zinc derivatives. *J Am Chem Soc* 1975; 97(18): 5111-17. <https://doi.org/10.1021/ja00851a015>.

- [49] Uttamlal M, Holmes-Smith AS. The excitation wavelength dependent fluorescence of porphyrins. *Chem Phys Lett* 2008; 454(4-6): 223-28.  
<https://doi.org/10.1016/j.cplett.2008.02.012>.
- [50] Dąbrowski JM, Pucelik B, Regiel-Futyra A, Brindell M, Mazuryk O, Kyzioł A et al. Engineering of relevant photodynamic processes through structural modifications of metallotetrapyrrolic photosensitizers. *Coord Chem Rev* 2016; 325: 67-101.  
<https://doi.org/10.1016/j.ccr.2016.06.007>.
- [51] Figueiredo TLC, Johnstone RA, Sørensen AMS, Burget D, Jacques P. Determination of fluorescence yields, singlet lifetimes and singlet oxygen yields of water-insoluble porphyrins and metalloporphyrins in organic solvents and in aqueous media. *J Photochem Photobiol* 1999; 69(5): 517-28. <https://doi.org/10.1111/j.1751-1097.1999.tb03322.x>.
- [52] Haniman A, Hosie RJ. Luminescence of porphyrins and metalloporphyrins. Part 4.— Fluorescence of substituted tetraphenylporphyrins. *J Chem Soc, Faraday Trans 2* 1981; 77: 1695-702. <https://doi.org/10.1039/F2981770169510>.
- [53] Golovina GV, Rychkov GN, Ol'shevskaya VA, Zaitsev AV, Kalinin VN, Kuzmin VA, et al. Differential binding preference of methylpheophorbide a and its diboronated derivatives to albumin and low density lipoproteins. *Anticancer Agents Med Chem* 2013; 13(4): 639-646.  
<https://doi.org/10.2174/1871520611313040012>.
- [54] Zhang Y, Chen X, Gueydan C, Han J. Plasma membrane changes during programmed cell deaths. *Cell Res* 2018; 28(1): 9–21. <https://doi.org/10.1038/cr.2017.133>.
- [55] Pearson RJ, Blake DG, Mezna M, Fischer PM, Westwood NJ, McInnes C. The Meisenheimer complex as a paradigm in drug discovery: reversible covalent inhibition through C67 of the ATP binding site of PLK1. *Cell Chem Biol*. 2018; 25: 1107–16.  
<https://doi.org/10.1016/j.chembiol.2018.06.001>.
- [56] Ha-Thi M-H, Shafizadeh N, Poisson L, Soep B. An efficient indirect mechanism for the ultrafast intersystem crossing in copper porphyrins. *J Phys Chem A* 2013; 117(34), 8111–18.  
<https://doi.org/10.1021/Jp4008015>.
- [57] Sobotta L, Sniechowska J, Ziental D, Długaszewska J, Potrzebowski MJ. Chlorins with (trifluoromethyl)phenyl substituents – Synthesis, lipid formulation and photodynamic activity against bacteria. *Dyes Pigments* 2019; 160: 292–300.  
<https://doi.org/10.1016/J.dyepig.2018.08.004>.
- [58] Ostrowski S, Szerszeń D, Ryszczuk M. Electrophilic nitration of *meso*-tetraarylporphyrin complexes at the  $\beta$ -pyrrolic position. *Synthesis* 2005; 5: 819–23. <https://doi.org/10.1055/s-2005-861853>.

- [59] Lipińska ME, Teixeira DMD, Laia CAT, Silva AMG, Rebelo SLH, Freire C.  $\beta$ -Functionalized zinc(II)aminoporphyrins by direct catalytic hydrogenation. *Tetrahedron Lett* 2013; 54(1): 110–113. <https://doi.org/10.1016/J.tetlet.2012.10>.
- [60] Das SK, Song B, Mahler A, Nesterov VN, Wilson AK, Ito O, D'Souza F. Electron transfer studies of high potential zinc porphyrin–fullerene supramolecular dyads. *J Phys Chem C* 2014; 118(8): 3994–4006. <https://doi.org/10.1021/Jp4118166>.
- [61] Blom M, Norrehed S, Andersson C-H, Huang H, Light M, Bergquist J et al. Synthesis and properties of bis-porphyrin molecular tweezers: effects of spacer flexibility on binding and supramolecular chirogenesis. *Molecules* 2015; 21(1): 16–40. <https://doi.org/10.3390/molecules21010016>.
- [62] Singh DK, Nath M. Synthesis and spectroscopic properties of  $\beta$ -triazoloporphyrin–xanthone dyads. *Beilstein J Org Chem* 2015; 11: 1434–40. <https://doi.org/10.3762/bJoc.11.155>.
- [63] Lakowicz JR. *Principles of fluorescence spectroscopy*. 3rd ed. New York: Springer; 2006. <https://doi.org/10.1007/978-0-387-46312-4>.
- [64] Brouwer AM. Standards for photoluminescence quantum yield measurements in solution (IUPAC Technical Report). *Pure Appl Chem* 2011; 83(12): 2213–28. <https://doi.org/10.1351/PAC-REP-10-09-31>.
- [65] Wilkinson F, Helman WP, Ross AB. Rate constants for the decay and reactions of the lowest electronically excited singlet state of molecular oxygen in solution. An expanded and revised compilation. *J Chem Ref Data* 1995; 24(2): 663–77. <https://doi.org/10.1063/1.555965>.
- [66] Mathai S, Smith TA, Ghiggino KP. Singlet oxygen quantum yields of potential porphyrin-based photosensitisers for photodynamic therapy. *Photochem Photobiol Sci* 2007; 6(9): 995–1002. <https://doi.org/10.1039/b705853e>.
- [67] Shimizu O, Watanabe J, Imakubo K, Naito S. Absolute quantum yields and lifetimes of photosensitized phosphorescence of singlet oxygen  $O_2 (^1\Delta_g)$  in air-saturated aqueous and organic solutions of phenalenone. *Chem Lett* 1999; 28(1): 67–8. <https://doi.org/10.1246/cl.1999.67>.
- [68] Tikhomirov AS, Lin CY, Volodina YL, Dezhenkova LG, Tatarskiy VV, Schols D, et al. New antitumor anthra[2,3-*b*]furan-3-carboxamides: Synthesis and structure-activity relationship. *Eur J Med Chem* 2018; 148: 128–39. <https://doi.org/10.1016/j.ejmech.2018.02.027>.

**$\beta$ -Maleimide substituted *meso*-arylporphyrins: Synthesis, transformations,  
physico-chemical and antitumor properties**

Valentina A.Ol'shevskaya<sup>a</sup>, Viktoriya M. Alpatova<sup>a,b</sup>, Alexandra S. Radchenko<sup>c</sup>,  
Alla A. Ramonova<sup>d</sup>, Albina S. Petrova<sup>e</sup>, Victor V. Tatarskiy<sup>f,g,h</sup>, Andrei V. Zaitsev<sup>a</sup>,  
Elena G. Kononova<sup>a</sup>, Nikolay S. Ikonnikov<sup>a</sup>, Alexey A. Kostyukov<sup>c</sup>, Anton E. Egorov<sup>c</sup>,  
Mikhail M. Moisenovich<sup>d</sup>, Vladimir A. Kuzmin<sup>c</sup>, Natalya A. Bragina<sup>b</sup>, Alexander A. Shtil<sup>f,g</sup>

<sup>a</sup>*A.N.Nesmeyanov Institute of Organoelement Compounds, Russian Academy of Sciences,  
119991 Moscow, Russian Federation*

<sup>b</sup>*MIREA - Russian Technological University, M.V. Lomonosov Institute of Fine Chemical  
Technologies, 119571 Moscow, Russian Federation*

<sup>c</sup>*Emanuel Institute of Biochemical Physics, Russian Academy of Sciences, 119334 Moscow,  
Russian Federation*

<sup>d</sup>*Department of Biology, Moscow State University, 119991 Moscow, Russian Federation*

<sup>e</sup>*RUDN University, 117198 Moscow, Russian Federation*

<sup>f</sup>*Blokhin National Medical Research Center of Oncology, 115478 Moscow, Russian Federation*

<sup>g</sup>*Institute of Gene Biology, Russian Academy of Sciences, 119334 Moscow, Russian Federation*

<sup>h</sup>*National University of Science and Technology "MISIS", 119991 Moscow, Russian Federation*

**Table of contents**

1.	The <sup>1</sup> H NMR of 2-(maleinoylamino)-5,10,15,20-tetraphenylporphyrin ( <b>25</b> )	3
2.	The <sup>1</sup> H, <sup>19</sup> F NMR of 2-(maleinoylamino)-5,10,15,20-tetrakis(pentafluorophenyl)porphyrin ( <b>26</b> )	3
3.	The <sup>1</sup> H, <sup>19</sup> F NMR of 2-(maleinoylamino)-5,10,15,20-tetrakis[4-(trifluoromethyl)phenyl]porphyrin ( <b>27</b> )	4
4.	The <sup>1</sup> H, <sup>19</sup> F NMR of [2-(maleinoylamino)-5,10,15,20-tetrakis(pentafluorophenyl)porphyrinato]zinc (II) ( <b>29</b> )	5
5.	The <sup>1</sup> H NMR of 2-(3'-maleimido)-5,10,15,20-tetraphenylporphyrin ( <b>1</b> )	5
6.	The <sup>1</sup> H, <sup>19</sup> F NMR of 2-(3'-maleimido)-5,10,15,20-tetrakis(pentafluorophenyl)porphyrin ( <b>2</b> )	6

7.	The $^1\text{H}$ , $^{19}\text{F}$ NMR of 2-(3'-maleimido)-5,10,15,20-tetrakis[4-(trifluoromethyl)phenyl]porphyrin ( <b>3</b> )	6
8.	The $^1\text{H}$ , $^{19}\text{F}$ NMR of [2-(3'-maleimido)-5,10,15,20-tetrakis(pentafluorophenyl)porphyrinato]zinc (II) ( <b>5</b> )	7
9.	The $^1\text{H}$ , $^{11}\text{B}$ NMR of 2-{3-[( <i>o</i> -carboran-1'-yl)thio]pyrrolidine-2,5-dione-1-yl}-5,10,15,20-tetraphenylporphyrin ( <b>32</b> )	8
10.	The $^1\text{H}$ , $^{11}\text{B}$ NMR of 2-{3-[( <i>m</i> -carboran-9'-yl)thio]pyrrolidine-2,5-dione-1-yl}-5,10,15,20-tetraphenylporphyrin ( <b>33</b> )	9
11.	The $^1\text{H}$ , $^{11}\text{B}$ , $^{19}\text{F}$ NMR of 2-{3-[( <i>m</i> -carboran-9'-yl)thio]pyrrolidine-2,5-dione-1-yl}-5,10,15,20-tetrakis[4-(trifluoromethyl)phenyl]porphyrin ( <b>34</b> )	9
12.	The $^1\text{H}$ , $^{11}\text{B}$ , $^{19}\text{F}$ NMR of [2-{3-[( <i>m</i> -carboran-9'-yl)thio]pyrrolidine-2,5-dione-1-yl}-5,10,15,20-tetrakis(pentafluorophenyl)porphyrinato]zinc (II) ( <b>35</b> )	10
13.	The $^1\text{H}$ , $^{11}\text{B}$ , $^{19}\text{F}$ NMR of 2-{3-[( <i>m</i> -carboran-9'-yl)thio]pyrrolidine-2,5-dione-1-yl}-5,10,15,20-tetrakis(pentafluorophenyl)porphyrin ( <b>36</b> )	11
14.	Relative quantum efficacy of singlet oxygen generation in DMSO normalized to RB	13
15.	Characterization of stable complexes <b>32</b> :HSA	14
16.	Accumulation of porphyrins <b>1-3</b> , <b>5</b> , <b>32</b> and <b>34</b> in HCT116 cells	15
17.	Intracellular distribution of porphyrins <b>1-3</b> and <b>34</b> in HCT116 cells	16

### 1. The $^1\text{H}$ NMR of 2-(maleinoylamino)-5,10,15,20-tetraphenylporphyrin (**25**)

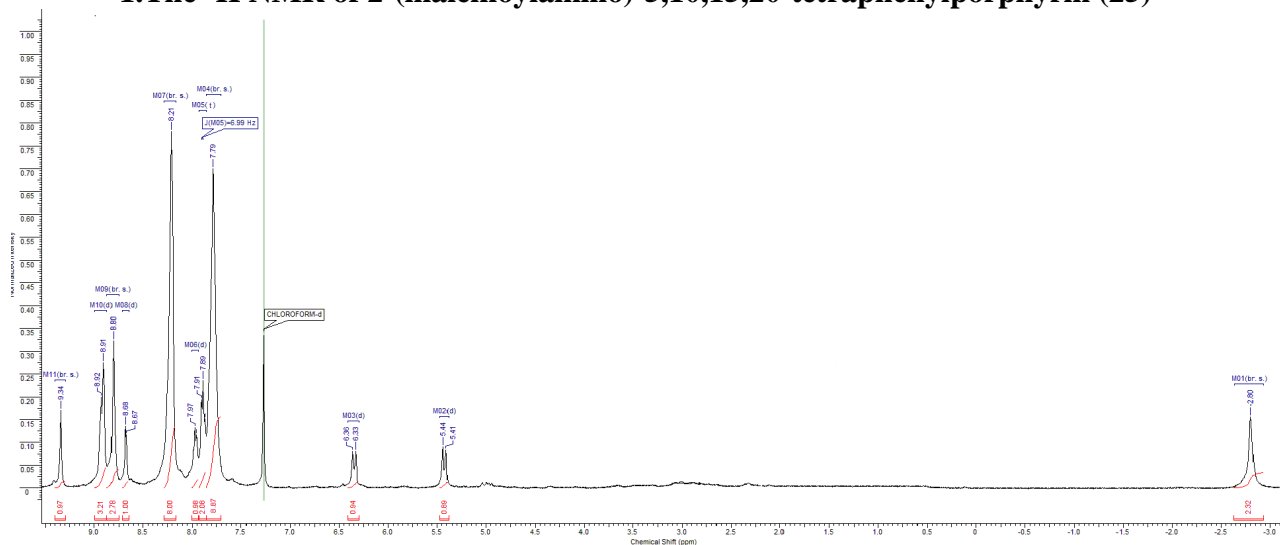


Figure S1. The  $^1\text{H}$  NMR spectrum of porphyrin **25** in  $\text{CDCl}_3$  at  $25^\circ\text{C}$ .

### 2. The $^1\text{H}$ , $^{19}\text{F}$ NMR of 2-(maleinoylamino)-5,10,15,20-tetrakis(pentafluorophenyl)porphyrin (**26**)

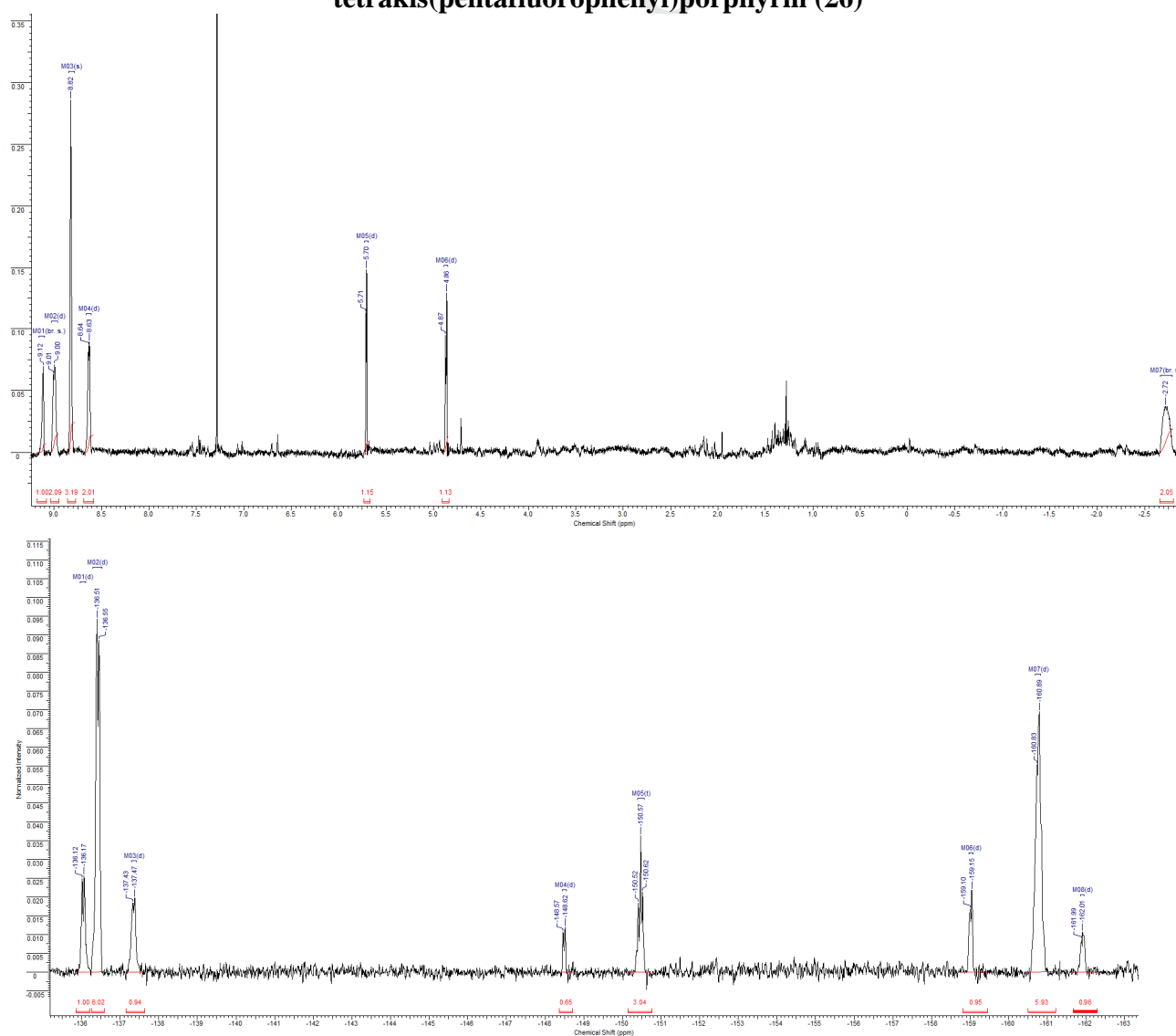
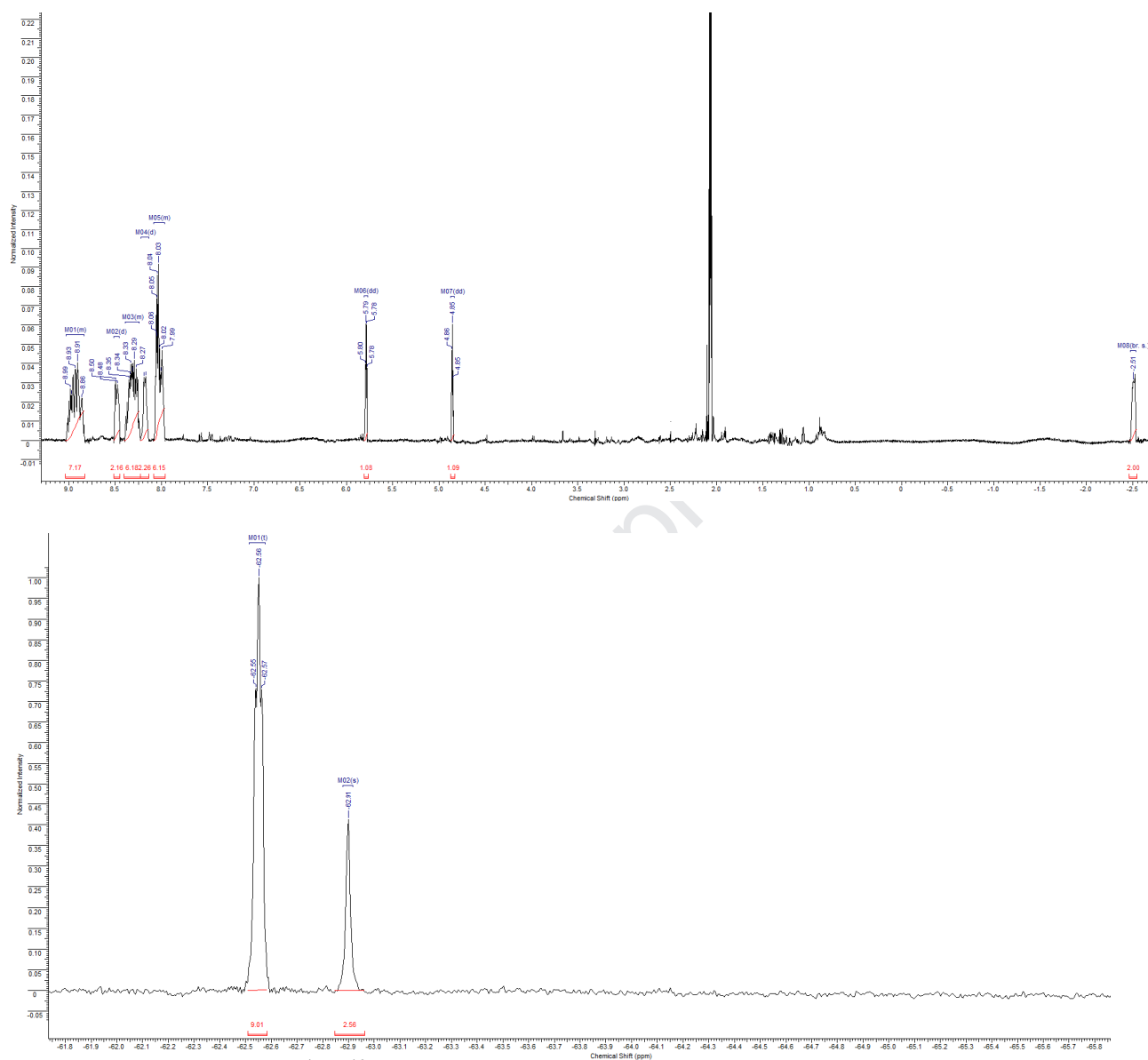


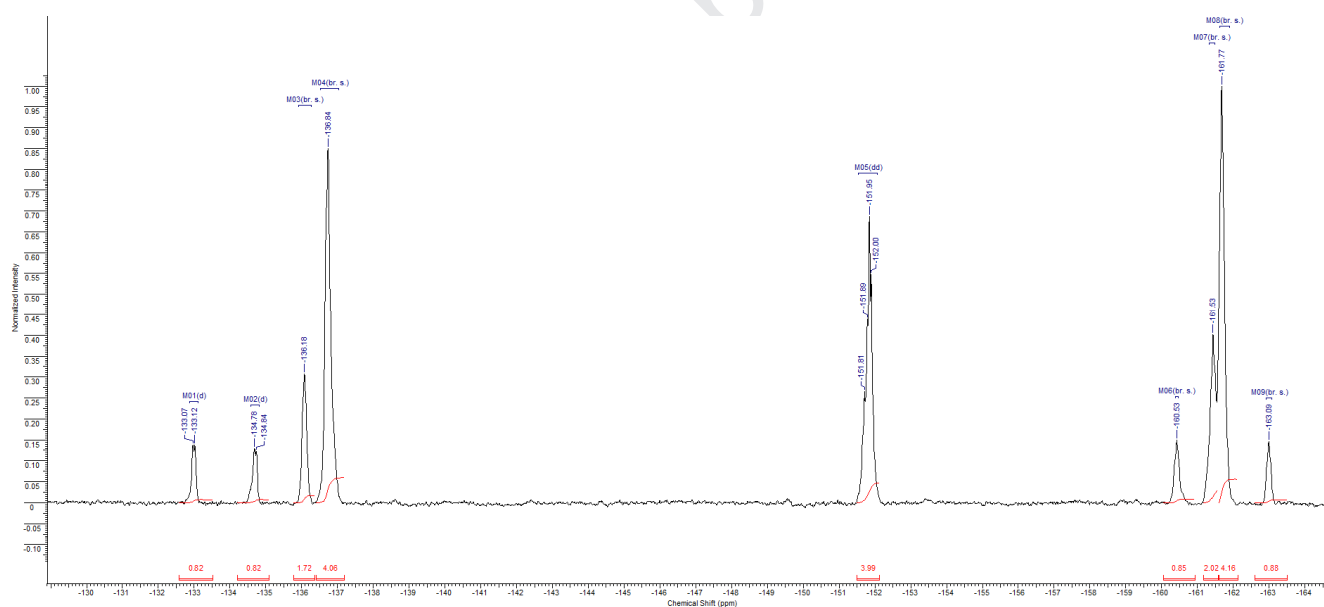
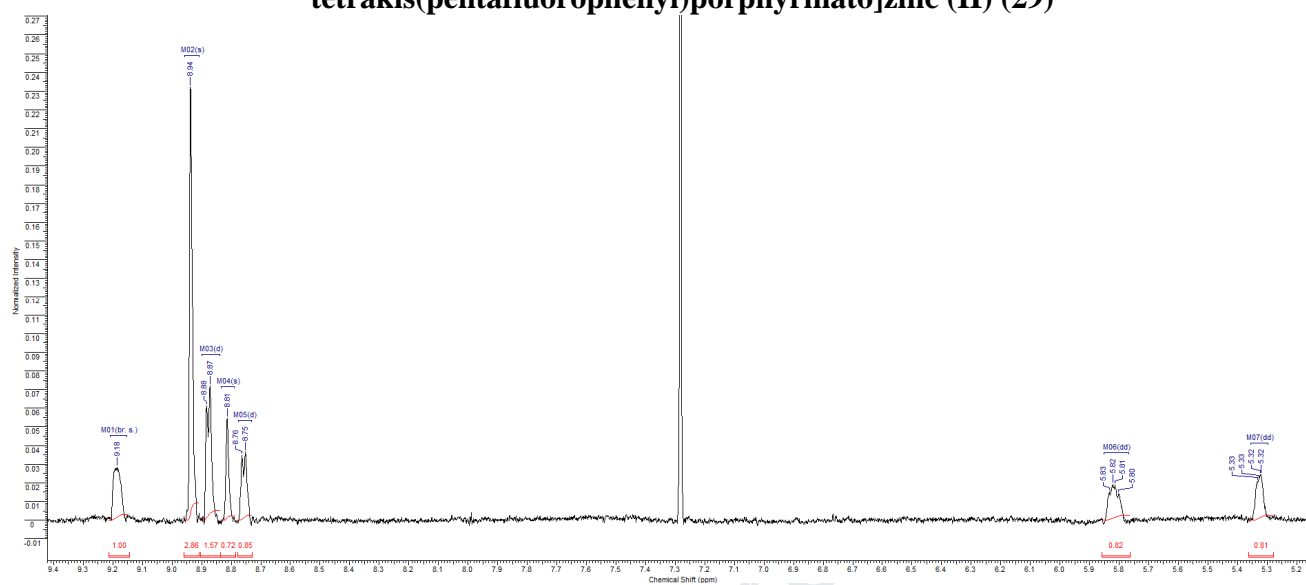
Figure S2. The  $^1\text{H}$ ,  $^{19}\text{F}$  NMR spectrum of porphyrin **26** in  $\text{CDCl}_3$  at  $25^\circ\text{C}$ .

### 3. The $^1\text{H}$ , $^{19}\text{F}$ NMR of 2-(maleinoylamino)-5,10,15,20-tetrakis[4-(trifluoromethyl)phenyl]porphyrin (**27**)



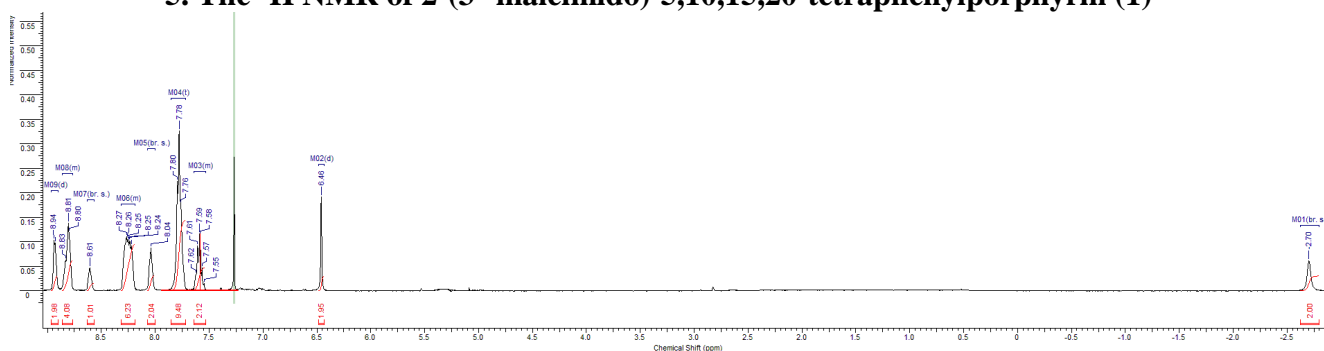
**Figure S3.** The  $^1\text{H}$ ,  $^{19}\text{F}$  NMR spectrum of porphyrin **27** in  $(\text{CD}_3)_2\text{CO}$  at 25 °C.

#### 4. The $^1\text{H}$ , $^{19}\text{F}$ NMR of [2-(maleinoylamino)-5,10,15,20-tetrakis(pentafluorophenyl)porphyrinato]zinc (II) (**29**)



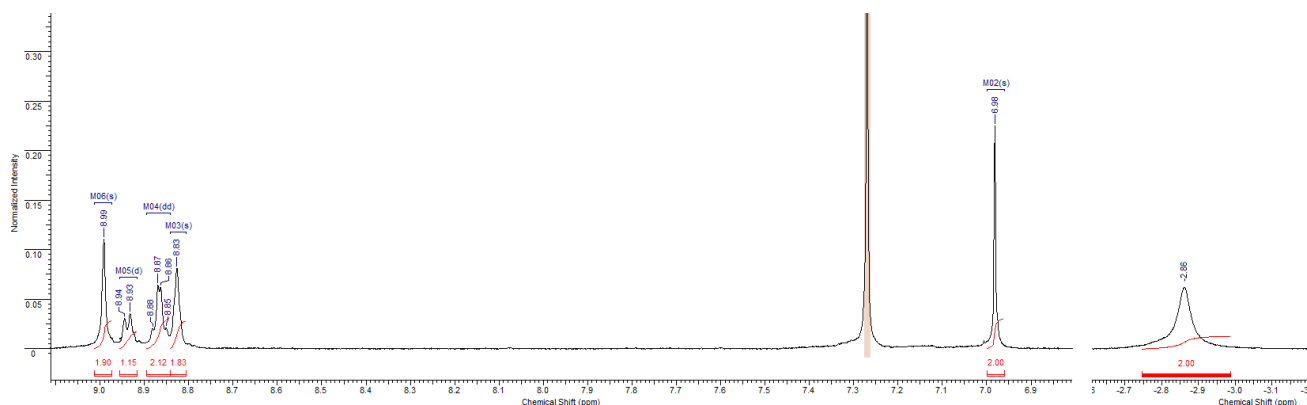
**Figure S4.** The  $^1\text{H}$ ,  $^{19}\text{F}$  NMR spectrum of porphyrin **29** in  $\text{CDCl}_3$  at  $25^\circ\text{C}$ .

#### 5. The $^1\text{H}$ NMR of 2-(3'-maleimido)-5,10,15,20-tetraphenylporphyrin (**1**)



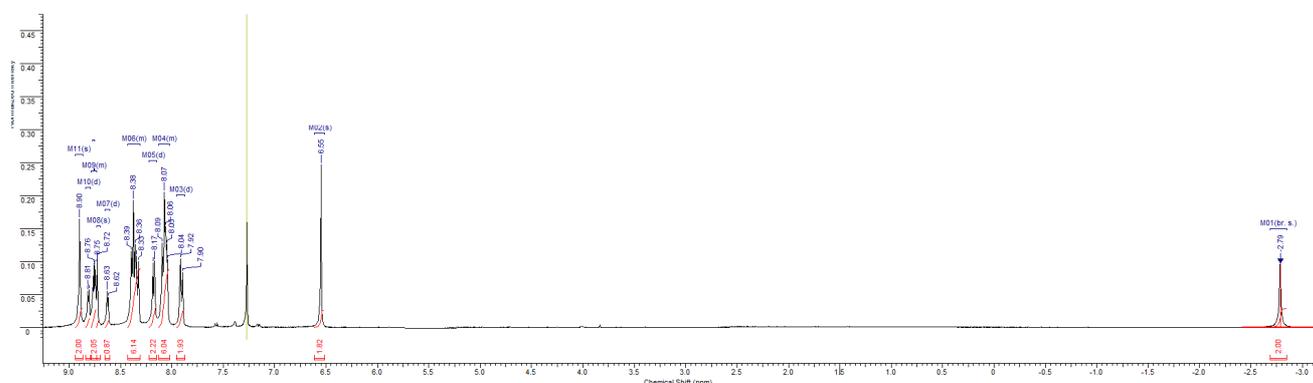
**Figure S5.** The  $^1\text{H}$  NMR spectrum of porphyrin **1** in  $\text{CDCl}_3$  at  $25^\circ\text{C}$ .

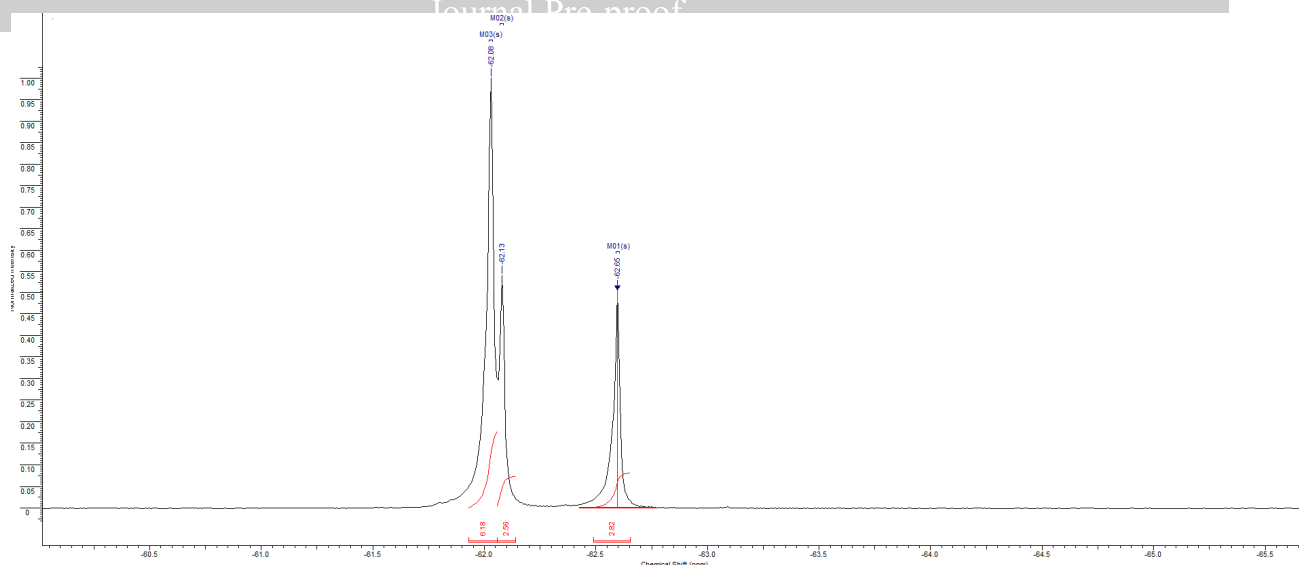
### 6. The $^1\text{H}$ , $^{19}\text{F}$ NMR of 2-(3'-maleimido)-5,10,15,20-tetrakis(pentafluorophenyl)porphyrin (2)



**Figure S6.** The  $^1\text{H}$ ,  $^{19}\text{F}$  NMR spectrum of porphyrin 2 in  $\text{CDCl}_3$  at 25 °C.

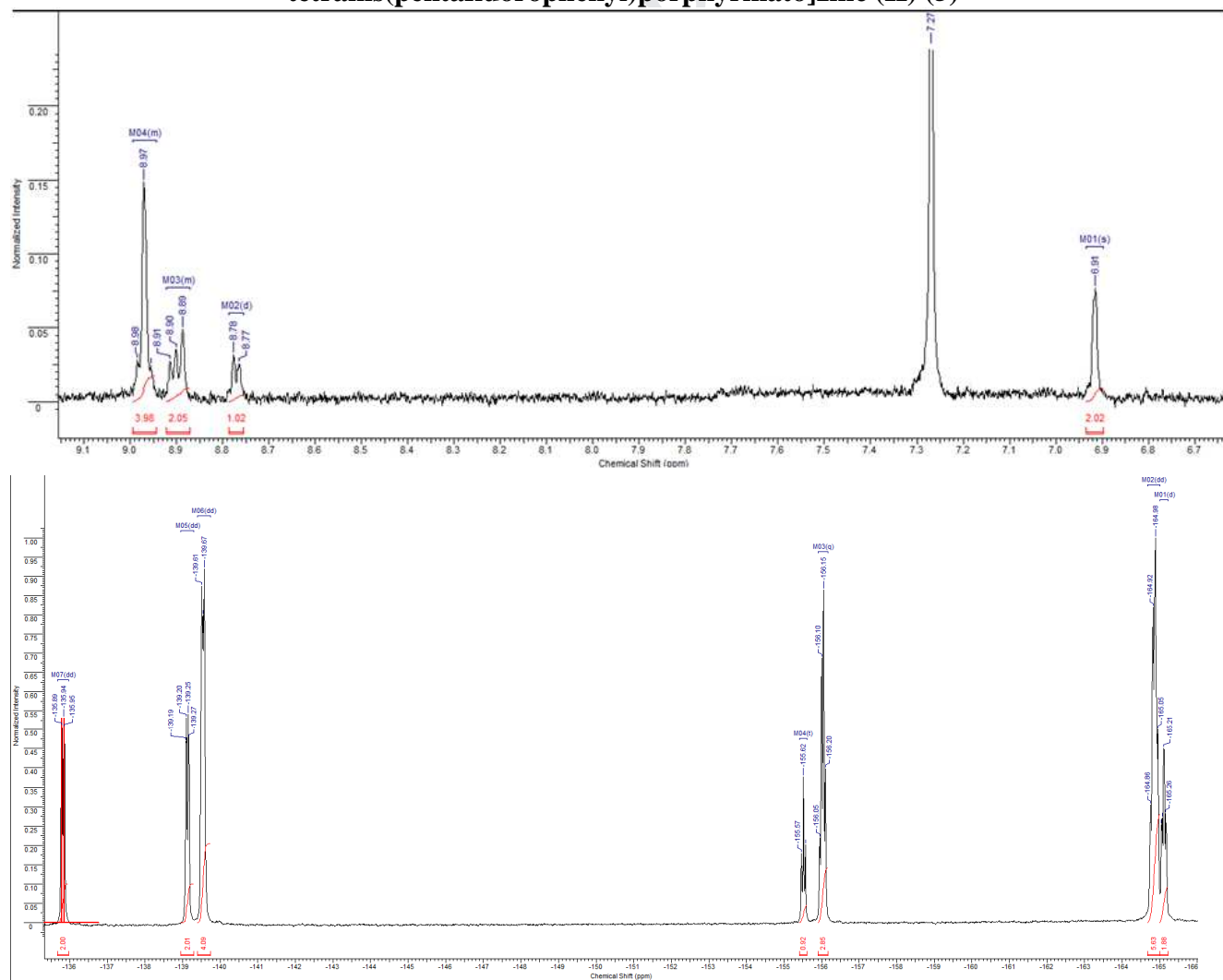
### 7. The $^1\text{H}$ , $^{19}\text{F}$ NMR of 2-(3'-maleimido)-5,10,15,20-tetrakis[4-(trifluoromethyl)phenyl]porphyrin (3)





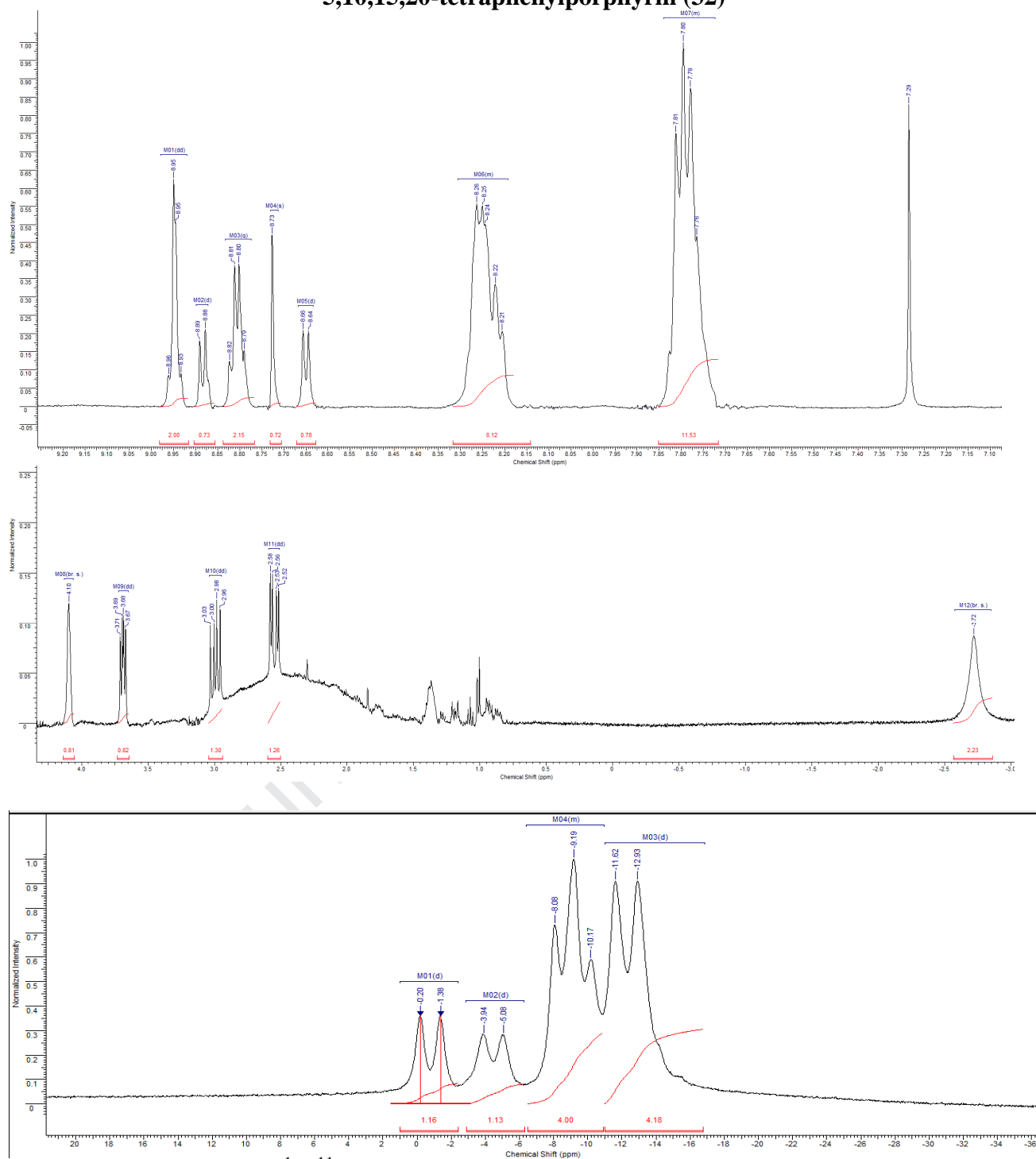
**Figure S7.** The  $^1\text{H}$ ,  $^{19}\text{F}$  NMR spectrum of porphyrin **3** in  $\text{CDCl}_3$  at  $25^\circ\text{C}$ .

### 8. The $^1\text{H}$ , $^{19}\text{F}$ NMR of [2-(3'-maleimido)-5,10,15,20-tetrakis(pentafluorophenyl)porphyrinato]zinc (II) (**5**)



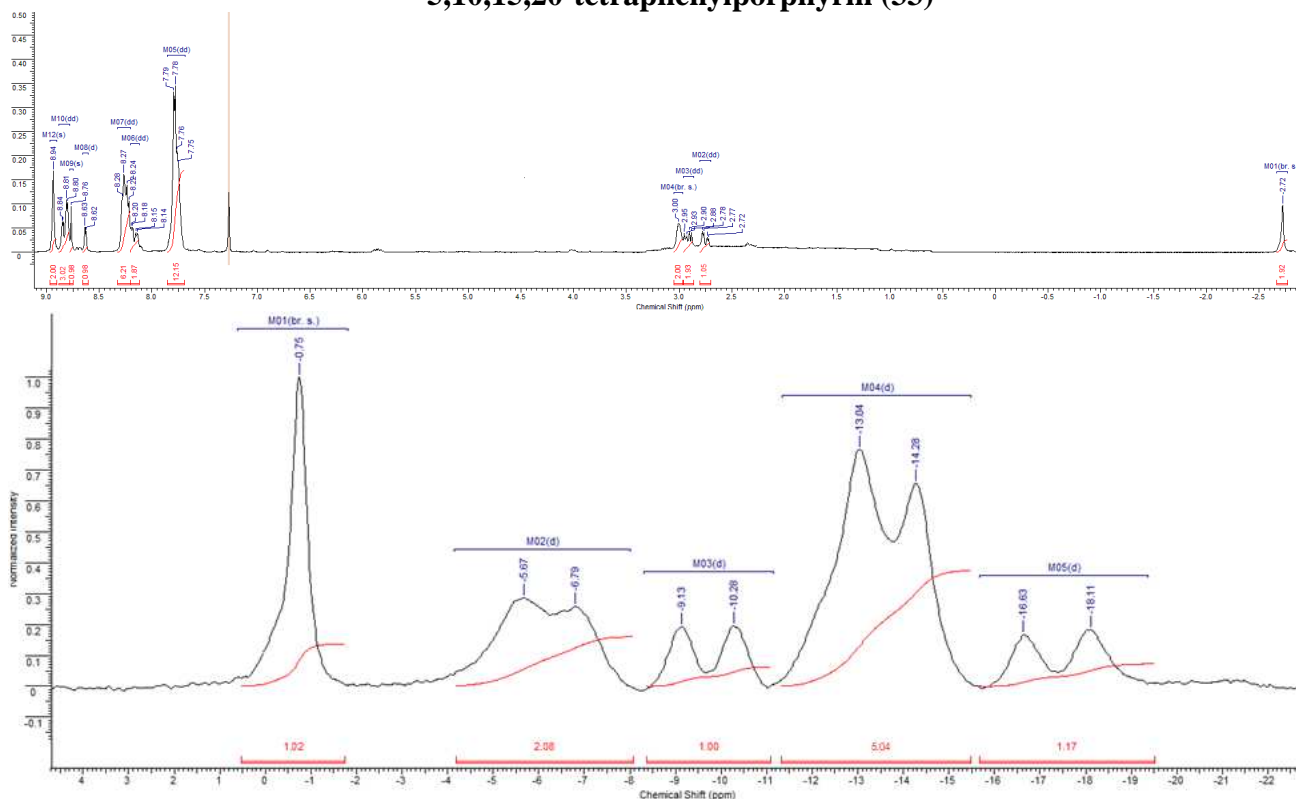
**Figure S8.** The  $^1\text{H}$ ,  $^{19}\text{F}$  NMR spectrum of porphyrin **5** in  $\text{CDCl}_3$  at  $25^\circ\text{C}$ .

**9. The  $^1\text{H}$ ,  $^{11}\text{B}$  NMR of 2-[3-(*o*-carboran-1'-yl)thio]pyrrolidine-2,5-dione-1-yl]-5,10,15,20-tetraphenylporphyrin (32)**



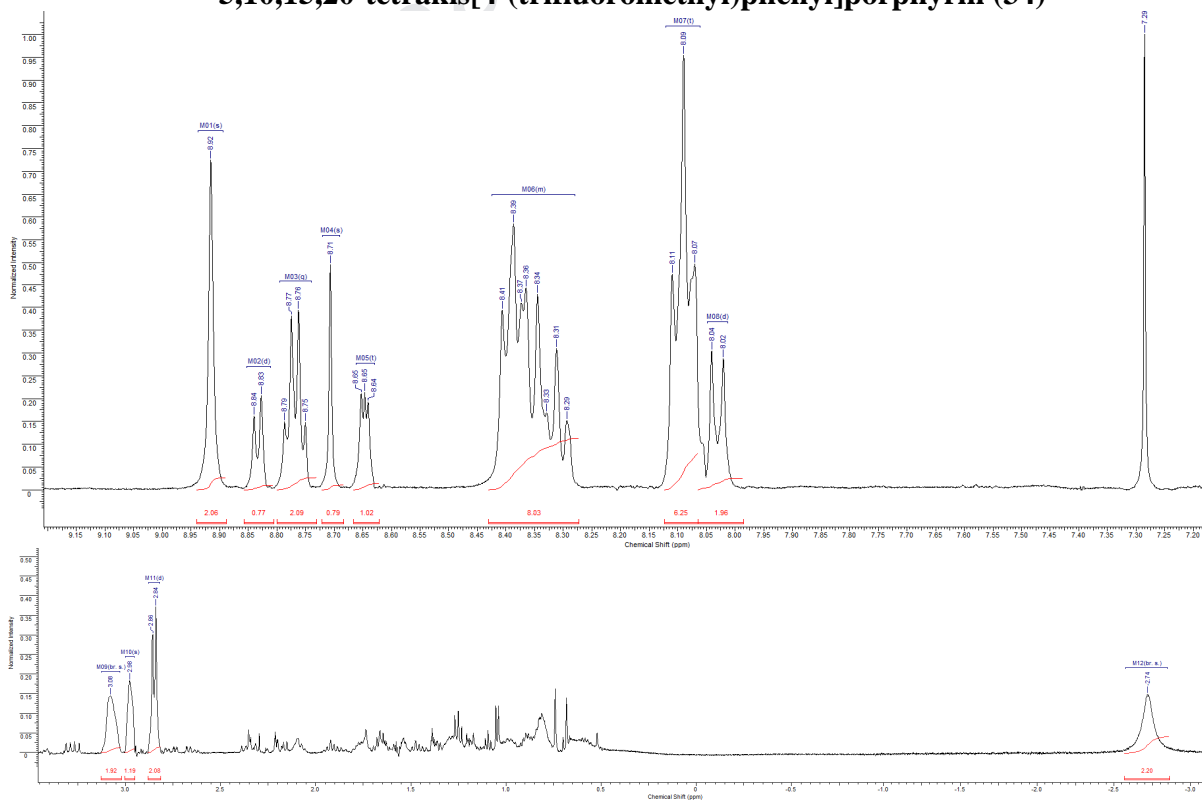
**Figure S9.** The  $^1\text{H}$ ,  $^{11}\text{B}$  NMR spectrum of porphyrin 32 in  $\text{CDCl}_3$  at  $25^\circ\text{C}$ .

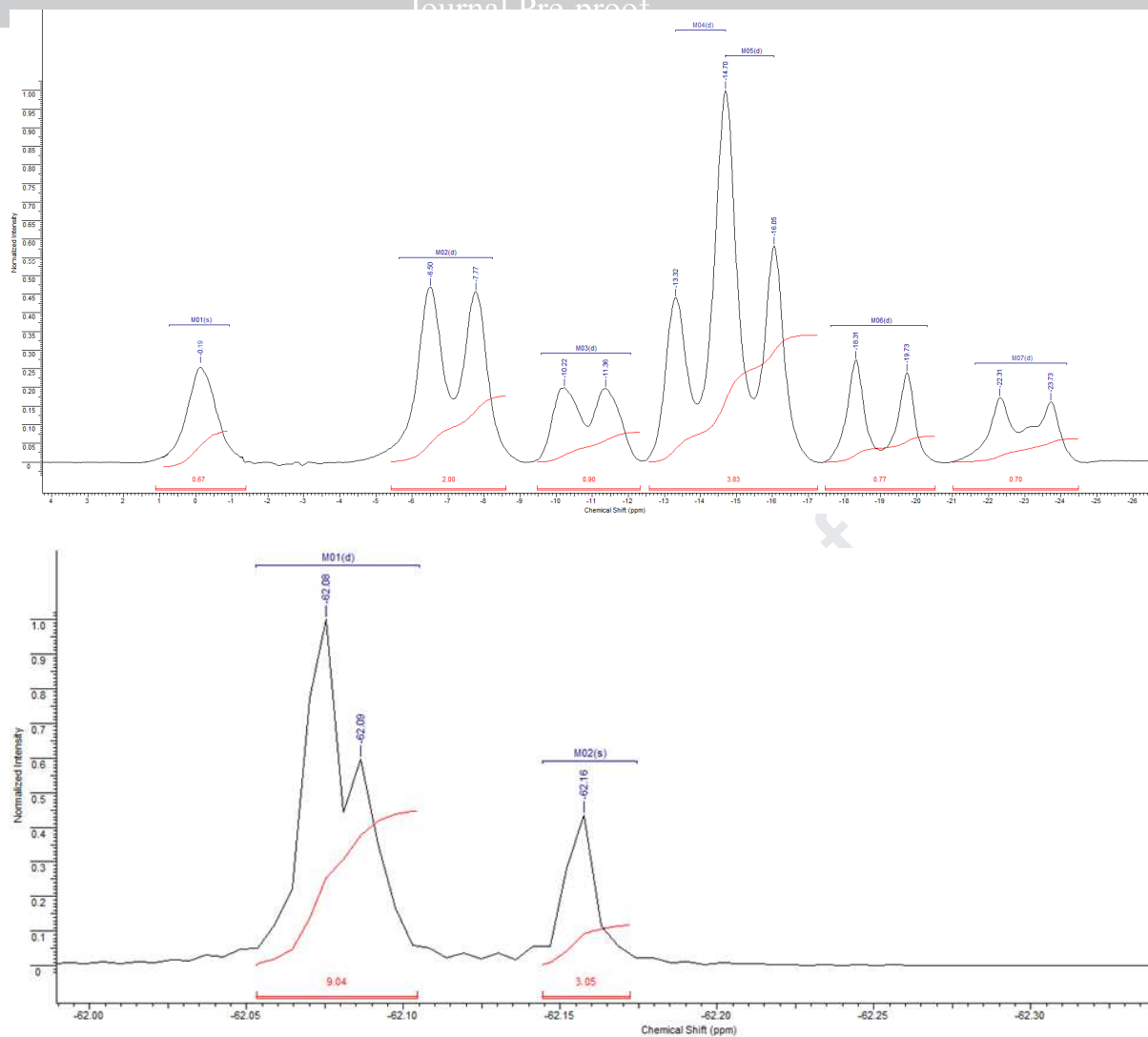
Journal Pre-proof  
**10. The  $^1\text{H}$ ,  $^{11}\text{B}$  NMR of 2-{3-[(*m*-carboran-9'-yl)thio]pyrrolidine-2,5-dione-1-yl}-5,10,15,20-tetraphenylporphyrin (33)**



**Figure S10.** The  $^1\text{H}$ ,  $^{11}\text{B}$  NMR spectrum of porphyrin 33 in  $\text{CDCl}_3$  at 25 °C.

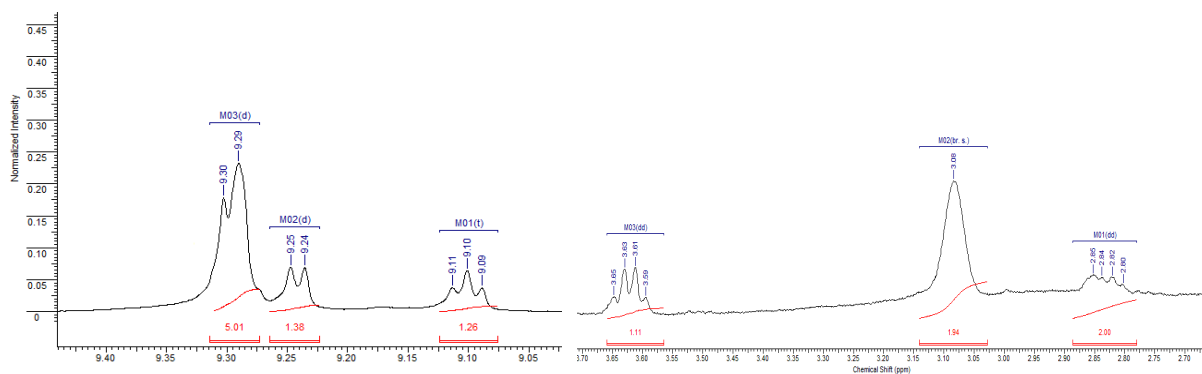
**11. The  $^1\text{H}$ ,  $^{11}\text{B}$ ,  $^{19}\text{F}$  NMR of 2-{3-[(*m*-carboran-9'-yl)thio]pyrrolidine-2,5-dione-1-yl}-5,10,15,20-tetrakis[4-(trifluoromethyl)phenyl]porphyrin (34)**





**Figure S11.** The  $^1\text{H}$ ,  $^{11}\text{B}$ ,  $^{19}\text{F}$  NMR spectrum of porphyrin **34** in  $\text{CDCl}_3$  at  $25^\circ\text{C}$ .

**12. The  $^1\text{H}$ ,  $^{11}\text{B}$ ,  $^{19}\text{F}$  NMR of [2-{3-[(*m*-Carboran-9'-yl)thio]pyrrolidine-2,5-dione-1-yl}-5,10,15,20-tetrakis(pentafluorophenyl)porphyrinato]zinc (II) (**35**)**



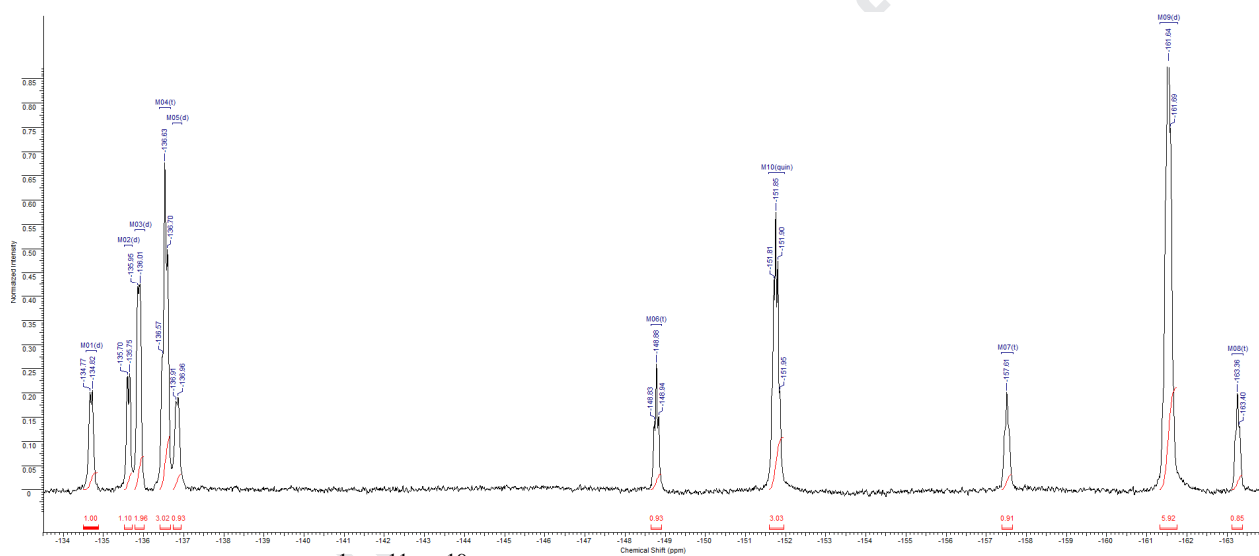
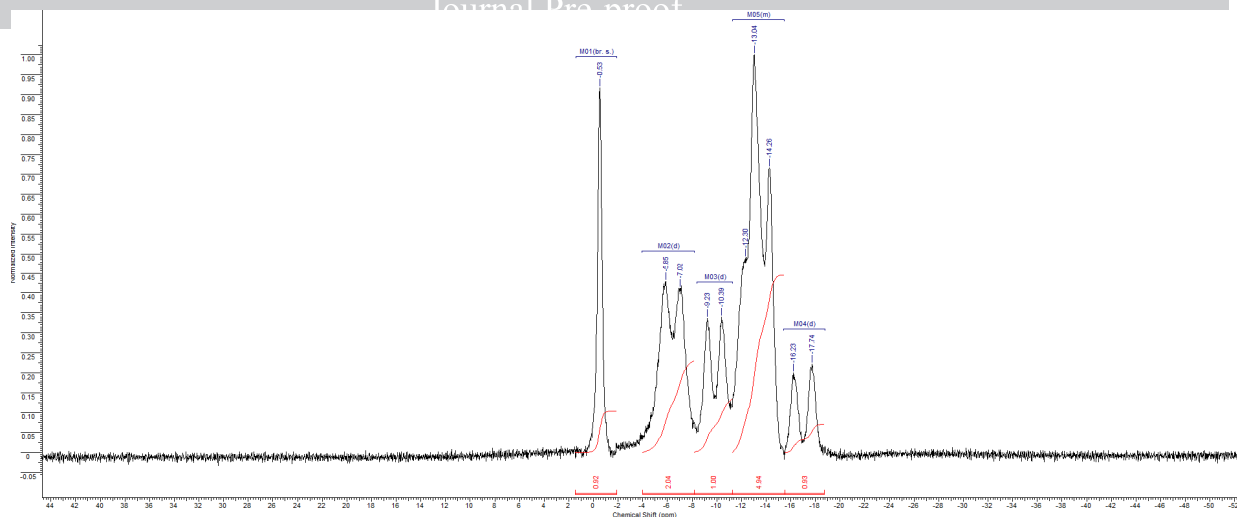
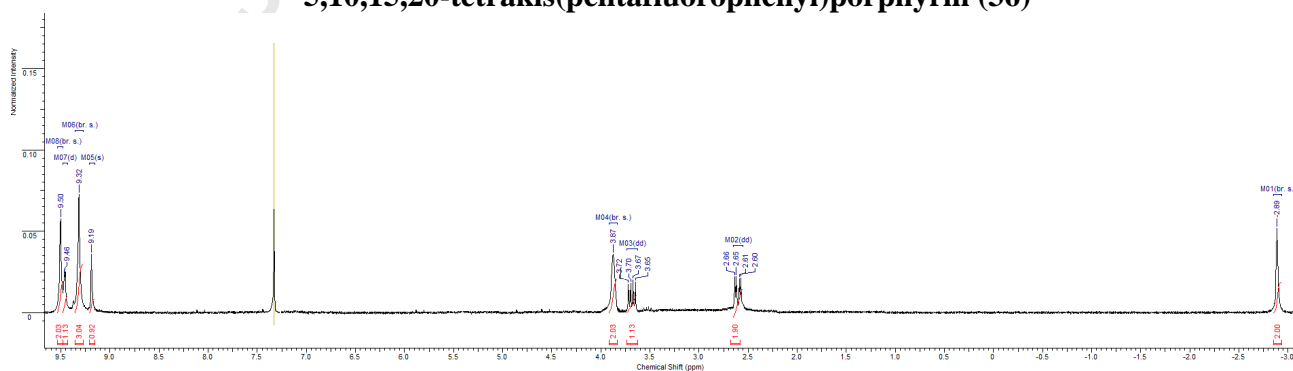


Figure S12. The  $^1\text{H}$ ,  $^{11}\text{B}$ ,  $^{19}\text{F}$  NMR spectrum of porphyrin **35** in  $\text{CDCl}_3$  at  $25^\circ\text{C}$ .

**13. The  $^1\text{H}$ ,  $^{11}\text{B}$ ,  $^{19}\text{F}$  NMR of 2-{3-[(m-carboran-9'-yl)thio]pyrrolidine-2,5-dione-1-yl}-5,10,15,20-tetrakis(pentafluorophenyl)porphyrin (**36**)**



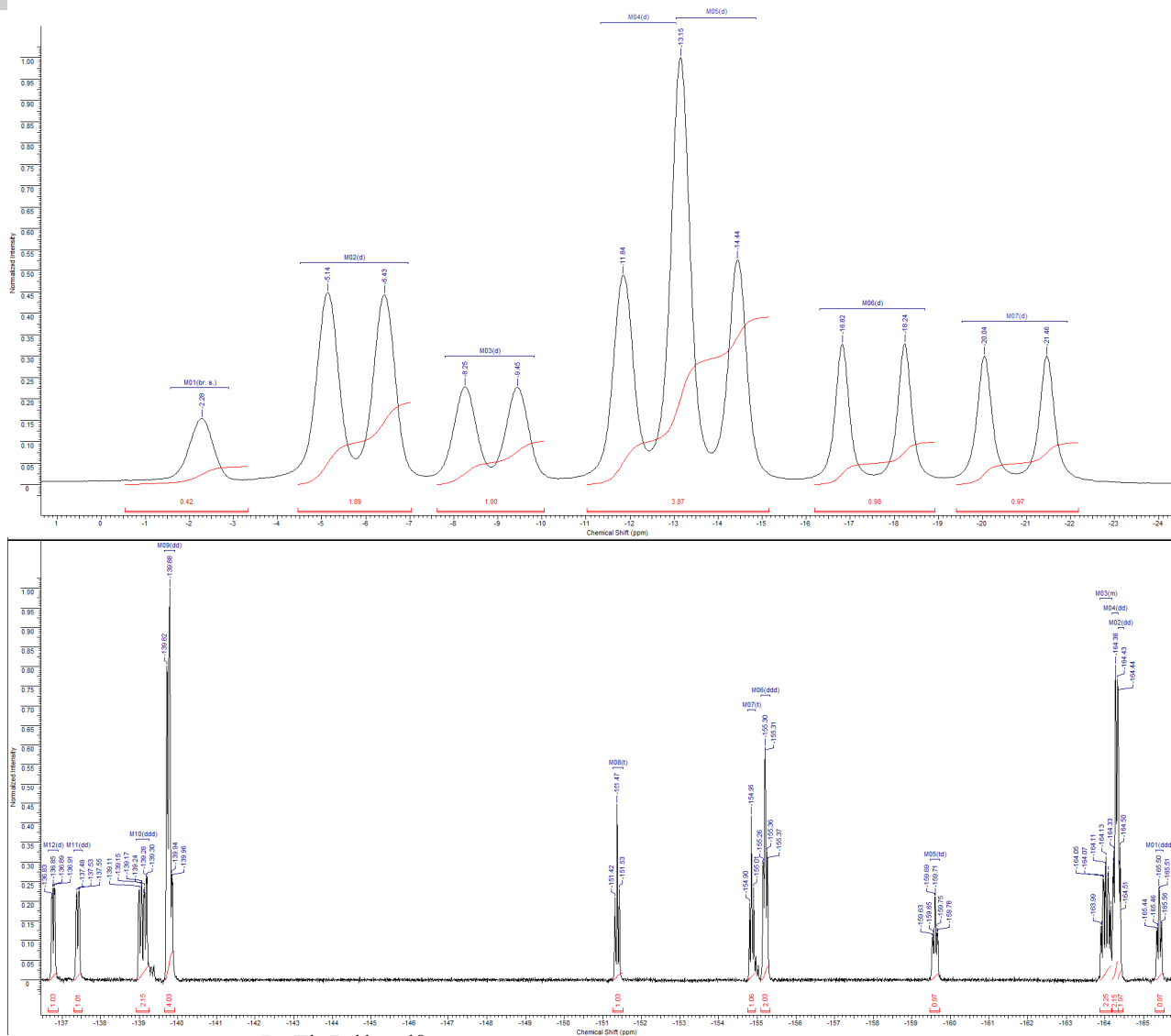
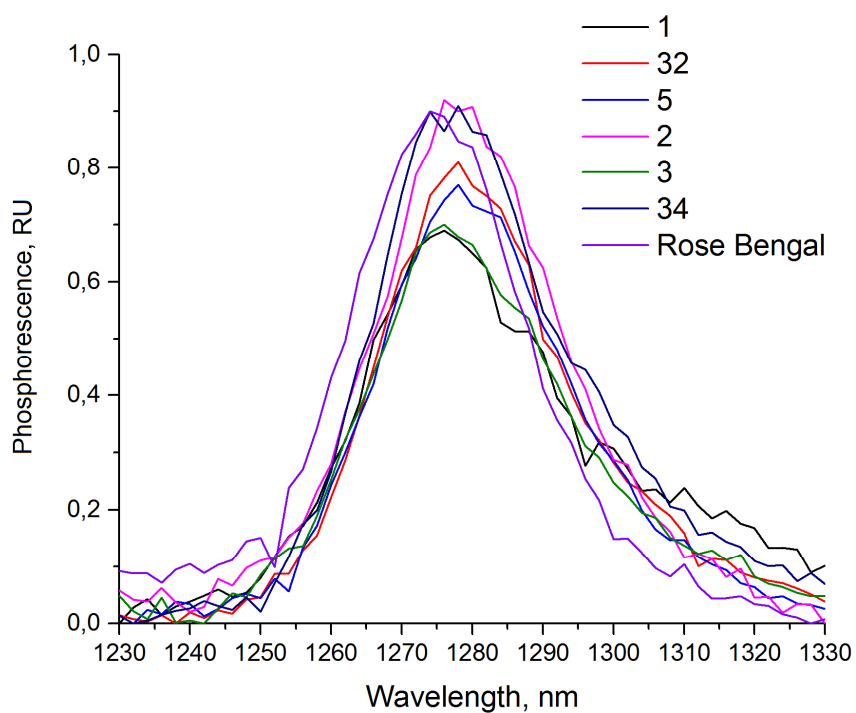
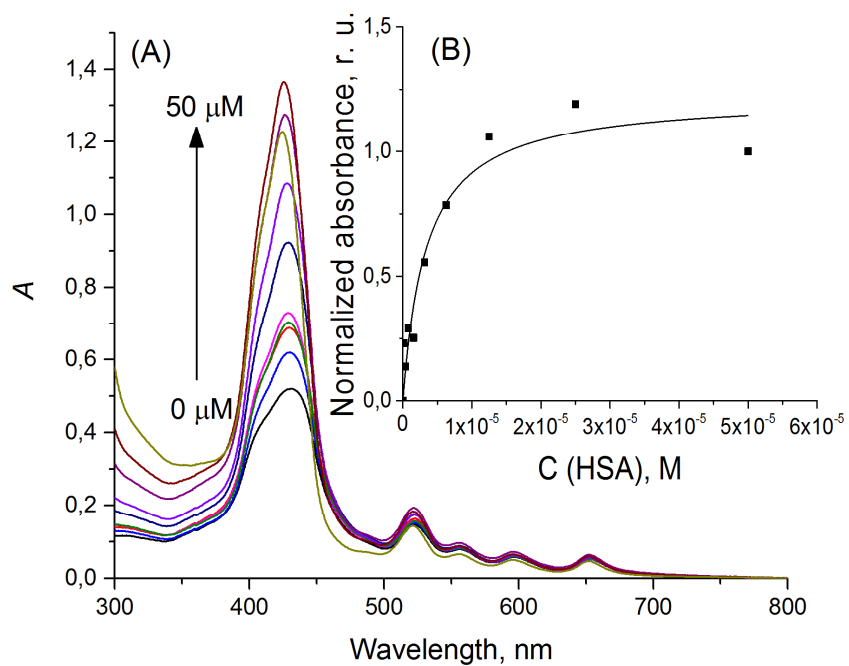


Figure S13. The <sup>1</sup>H, <sup>11</sup>B, <sup>19</sup>F NMR spectrum of porphyrin 36 in CDCl<sub>3</sub> at 25 °C.

**14. Relative quantum efficacy of singlet oxygen generation in DMSO normalized to RB.**

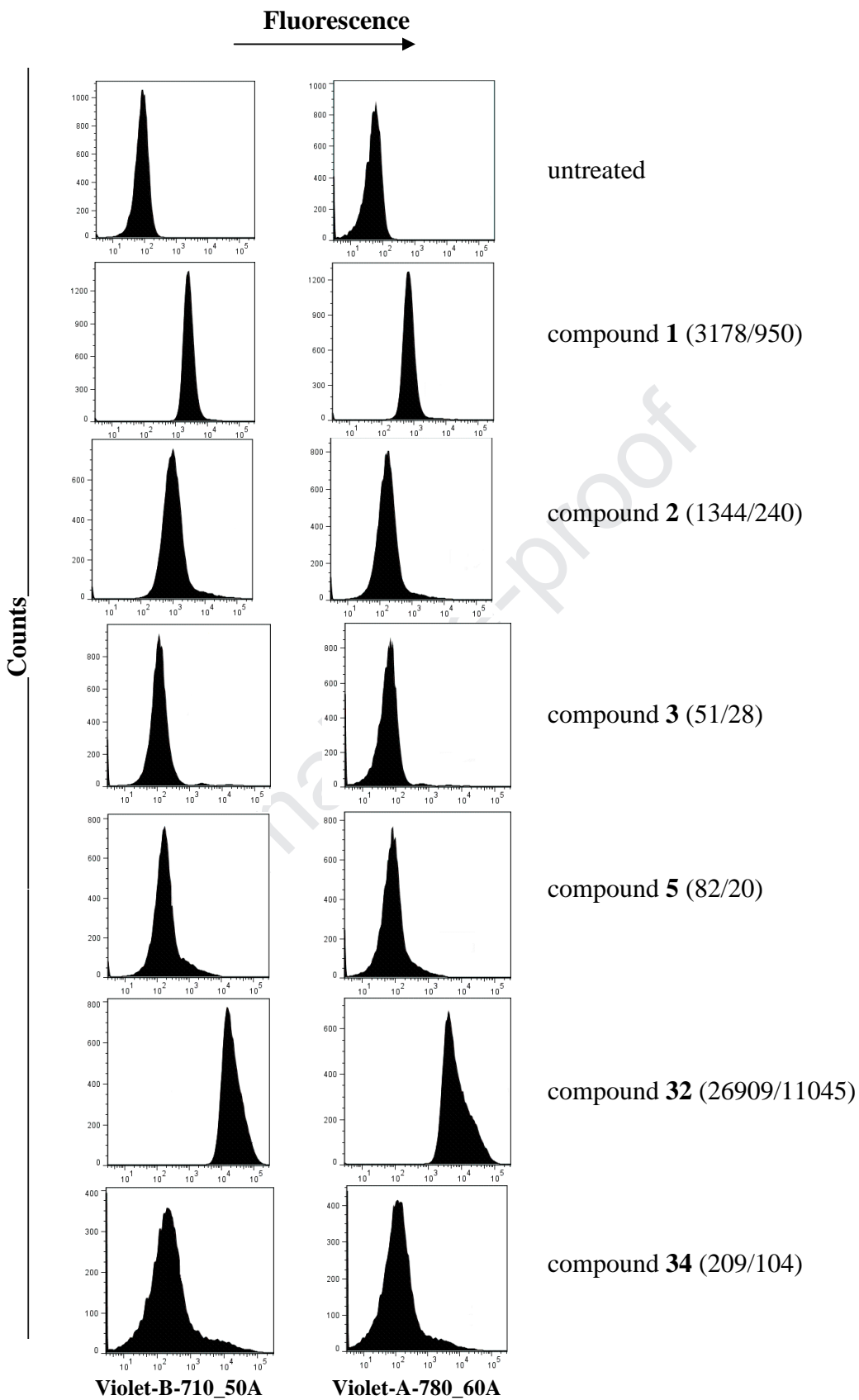
**Figure S14.** Relative quantum efficacy of singlet oxygen generation in DMSO normalized to RB. Shown are spectra of singlet oxygen phosphorescence. RU, relative units.

Journal Pre-proof  
15. Characterization of stable complexes 32:HSA.



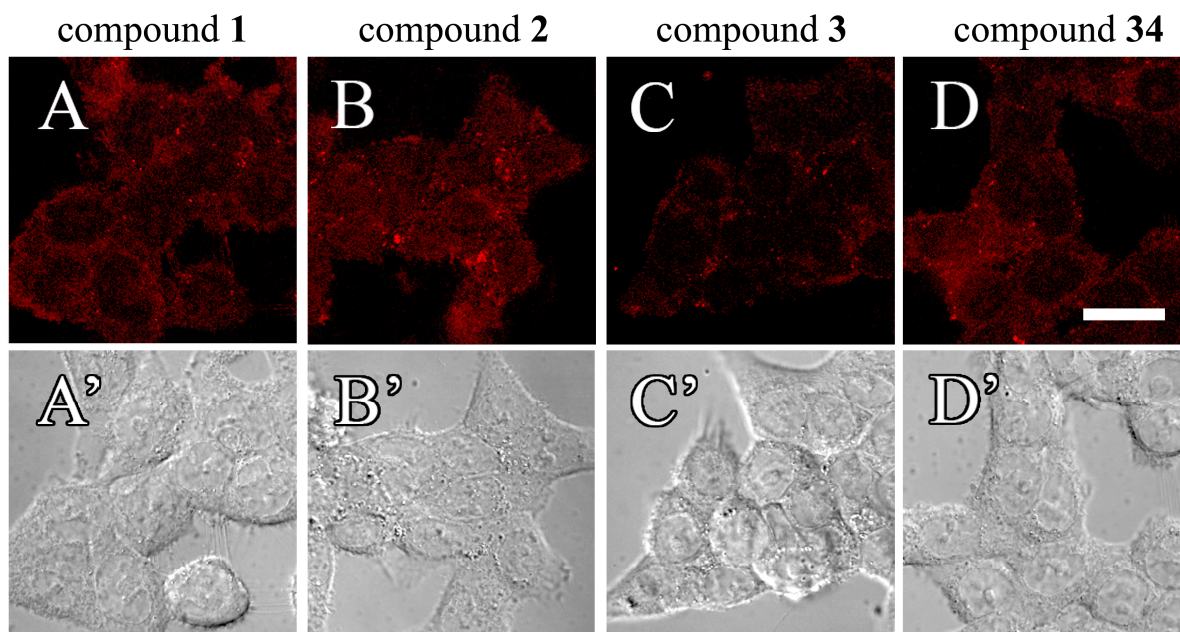
**Figure S15.** Characterization of stable complexes **32**:HSA. A, absorption spectra of **32** at  $\lambda = 425$  nm. B, absorption as a function of [HSA] (serial twofold dilutions down from 50  $\mu$ M).

Journal Pre-proof  
16. Accumulation of porphyrins 1-3, 5, 32 and 34 in HCT116 cells



**Figure S16.** Accumulation of porphyrins 1-3, 5, 32 and 34 in HCT116 cells.

Numbers in parentheses:  $\Delta \text{MFC}_{710} / \Delta \text{MFC}_{780}$ . See *Experimental* for details

**17. Intracellular distribution of porphyrins 1-3 and 34 in HCT116 cells.**

**Figure S17.** Intracellular distribution of porphyrins **1-3** and **34** in HCT116 cells.

Cells were loaded with the respective compound (5  $\mu$ M, 1 h) at 37<sup>0</sup>C, 5% CO<sub>2</sub>. A-D: fluorescence of compounds. A'-D': phase contrast images. Note the cytoplasmic accumulation of  $\beta$ -substituted porphyrins. Bar, 10  $\mu$ m.

**Highlights**

1. A panel of new  $\beta$ -maleimide-substituted *meso*-arylporphyrins was synthesized.
2. Reactivity of porphyrin maleimides towards S-nucleophiles was studied.
3. Flash photolysis showed the ability of new compounds to generate ROS.
4. Complexes with albumin were determined for maleimide and succinimide porphyrins.
5. Selected compounds induced rapid photonecrosis in colon carcinoma cells.

Journal Pre-proof